Cross-compartment signal propagation in the Mitotic Exit Network.

Xiaoxue Zhou[1,*], Wenxue Li[2], Yansheng Liu[2], Angelika Amon[1,*]

[1]David H. Koch Institute for Integrative Cancer Research, Howard Hughes Medical Institute, Massachusetts Institute of Technology, Cambridge, MA 02139, USA

[2]Yale Cancer Biology Institute, Department of Pharmacology, Yale University, West Haven, CT 06516, USA

[*]Correspondence to: xiaoxue@mit.edu and angelika@mit.edu

ABSTRACT (150 words)

In budding yeast, the Mitotic Exit Network (MEN), a GTPase signaling cascade integrates spatial and temporal cues to promote exit from mitosis. This signal integration requires transmission of a signal generated on the cytoplasmic face of spindle pole bodies (SPBs; yeast equivalent of centrosomes) to the nucleolus, where the MEN effector protein Cdc14 resides. Here, we show that the MEN activating signal at SPBs is relayed to Cdc14 in the nucleolus through the dynamic localization of its terminal kinase complex Dbf2-Mob1. Cdc15, the protein kinase that activates Dbf2-Mob1 at SPBs, also regulates its nuclear access. Once in the nucleus, priming phosphorylation of Cfi1/Net1, the nucleolar anchor of Cdc14, by the Polo-like kinase Cdc5 targets Dbf2-Mob1 to the nucleolus. Nucleolar Dbf2-Mob1 then phosphorylates Cfi1/Net1 and Cdc14, activating Cdc14. The kinase-primed transmission of the MEN signal from the cytoplasm to the nucleolus exemplifies how signaling cascades can bridge distant inputs and responses.

15 **INTRODUCTION**

16 In cellular signaling, the sensing of signals (e.g. binding of signaling molecules at cell surface)
17 and the response (e.g. transcription in the nucleus) often occur in different cellular
18 compartments. Determining how signals are transmitted across compartments is thus essential
19 for understanding signal transmission. The Mitotic Exit Network (MEN), a Ras-like GTPase
20 kinase signaling cascade and budding yeast homolog of the Hippo pathway (Hergovich and
21 Hemmings, 2012), represents such an example for signaling across cellular compartments. The
22 MEN-activating signal is sensed and processed at the cytoplasmic face of spindle pole bodies
23 (SPBs; yeast functional equivalent of the centrosomes), whereas the MEN effector protein Cdc14
24 resides in the nucleolus (Figure 1A). Because budding yeast undergo a closed mitosis without
25 disassembling the nuclear envelope and nucleolus, the MEN must transmit a signal generated at
26 the cytoplasmic face of SPBs, across the nuclear envelope and into the nucleolus to activate its
27 effector Cdc14. The molecular mechanisms governing this cross-compartment signaling process
28 remain largely unknown.

29 The central function of the MEN is to couple the final cell cycle transition, exit from
30 mitosis (when the mitotic spindle is disassembled, chromosomes decondense and cytokinesis
31 ensues), to nuclear/spindle position. In many organisms including budding yeast, fission yeast
32 and some plant species, the site of cytokinesis/division plane (i.e. the bud neck) is determined
33 prior to mitosis (Guertin et al., 2002). Thus, the mitotic spindle must be positioned appropriately
34 to ensure accurate genome partitioning between the daughter cells. In addition, these organisms
35 have evolved surveillance mechanisms to monitor spindle position and regulate cell cycle
36 progression in response. This surveillance mechanism is best understood in budding yeast where
37 spindle position controls the activity of the MEN.

38 The MEN senses spindle position through a Ras-like GTPase Tem1. Tem1 is activated
39 when a SPB enters the bud (Bardin et al., 2000; Pereira et al., 2000). Together with the Polo-like
40 kinase Cdc5, Tem1 activates its effector, the Hippo-like protein kinase Cdc15, presumably by
41 recruiting Cdc15 to the SPBs (Rock and Amon, 2011) (Figure 1A). Cdc15 then activates the
42 LATS/NDR kinase Dbf2-Mob1 via a two-step process (Rock et al., 2013). Cdc15 first
43 phosphorylates the MEN scaffold Nud1, a core component of the SPB outer plaque. This
44 phosphorylation creates a docking site for Dbf2-Mob1 on Nud1, facilitating phosphorylation and
45 activation of Dbf2-Mob1 by Cdc15 (Mah et al., 2001; Rock et al., 2013).
46 In addition to sensing spindle position, the MEN also integrates cues of cell cycle
47 progression through the downstream kinases Cdc15 and Dbf2-Mob1 (Campbell et al., 2019).
48 Two cell cycle events are sensed by the MEN: (1) Activity of the Polo-like kinase Cdc5:
49 activation of Cdc15 depends on Cdc5 activity (Rock and Amon, 2011) which occurs only in
50 mitosis (Cheng et al., 1998); (2) Initiation of anaphase: cyclin-dependent kinases (CDKs)
51 phosphorylate Cdc15 and Mob1 thereby inhibiting their activity (Jaspersen and Morgan, 2000;
52 König et al., 2010). At the onset of anaphase, CDK activity declines due to cyclin degradation,
53 which lifts this inhibition. This loss of inhibition by CDKs creates a state whereby the MEN is
54 poised for activation.
55 Once activated, the MEN promotes exit from mitosis by activating the phosphatase
56 Cdc14. As an antagonist of CDKs, Cdc14 reverses CDK-dependent phosphorylation and
57 promotes mitotic CDK inactivation thereby returning the cell to a G1 state (reviewed in
58 Stegmeier and Amon, 2004). Given the central role of Cdc14 in promoting mitotic exit, it is not
59 surprising that the phosphatase is tightly regulated. Cdc14 is sequestered in the nucleolus by its
60 inhibitor Cfi1/Net1 from G1 until the onset of anaphase (Shou et al., 1999; Visintin et al., 1999).

61 During anaphase, Cdc14 is released from its inhibitor and spreads throughout the nucleus and
62 cytoplasm to dephosphorylate its targets.

63 Two pathways, the Cdc fourteen early anaphase release (FEAR) network and the MEN
64 promote the dissociation of Cdc14 from its inhibitor during anaphase. Upon anaphase entry,
65 Cdc14 is transiently released from the nucleolus by the FEAR network (reviewed in Rock and
66 Amon, 2009). The FEAR network promotes dissociation of Cdc14 from Cfi1/Net1 by facilitating
67 phosphorylation of Cfi1/Net1 by mitotic CDKs (Azzam, 2004; Queralt et al., 2006). This
68 transient release, although not essential for exit from mitosis, is crucial for the timely execution
69 of several anaphase events such as segregation of the nucleolus (D'Amours et al., 2004; Sullivan
70 et al., 2004; Torres-Rosell et al., 2004) and MEN activation by counteracting CDK inhibition of
71 MEN kinases (Campbell et al., 2019; Jaspersen and Morgan, 2000; König et al., 2010). In late
72 anaphase, the activated MEN drives a more sustained and complete release of Cdc14 from the
73 nucleolus which ultimately results in exit from mitosis. In the absence of MEN activity, Cdc14,
74 after a transient FEAR network-mediated release from the nucleolus during early anaphase, is re-
75 sequestered in the nucleolus and cells arrest in late anaphase.

76 Despite our extensive knowledge of the MEN and Cdc14, how the MEN promotes the
77 sustained release of Cdc14 from its inhibitor in the nucleolus is not well understood. One
78 contributing mechanism involves the phosphorylation of the nuclear localization signal (NLS)
79 sequence in the C-terminus of Cdc14 by the MEN kinase Dbf2-Mob1 (Mohl et al., 2009).
80 Inactivation of the NLS by the MEN promotes redistribution of Cdc14 via its nuclear export
81 signal (NES) from the nucleus to the cytoplasm. However, retention of Cdc14 in the cytoplasm is
82 not required for mitotic exit (Bembenek et al., 2005; Kuilman et al., 2015; Mohl et al., 2009).
83 Furthermore, a Cdc14 mutant lacking the Dbf2 phosphorylation sites within its NLS is still

84 released from the nucleolus in late anaphase (Mohl et al., 2009). These results suggest that MEN-
85 mediated cytoplasmic retention of Cdc14 is not the main mechanism whereby the MEN activates
86 Cdc14. Rather, the MEN must also disrupt the interaction between Cdc14 and its inhibitor
87 Cfi1/Net1 in the nucleolus.

88 How does the MEN, activated at the outer plaque of SPBs in the cytosol, liberate Cdc14
89 from its inhibitor in the nucleolus? Proteome array screens for Dbf2-Mob1, the terminal kinase
90 in the MEN, have identified Cfi1/Net1 as a potential Dbf2 substrate *in vitro* (Mah et al., 2001;
91 Ptacek et al., 2005) suggesting that the MEN might liberate Cdc14 from Cfi1/Net1 through
92 phosphorylating Cfi1/Net1. However, given that Dbf2-Mob1 and Cfi1/Net1 normally reside in
93 different cellular compartments, whether this phosphorylation occurs *in vivo* and contributes to
94 Cdc14 activation is unclear. In addition, the Polo-like kinase Cdc5, an important regulator of
95 mitotic exit and essential for Cdc14 activation, has also been shown to phosphorylate Cfi1/Net1
96 (Loughrey Chen et al., 2002; Shou et al., 2002; Yoshida and Toh-e, 2002). Whether and how this
97 phosphorylation contributes to MEN-mediated Cdc14 release is not understood.

98 Here, we demonstrate that Dbf2-Mob1 serves as a molecular messenger traveling
99 between the SPBs and the nucleolus to release Cdc14 from its inhibitor. We show that Dbf2-
100 Mob1, normally kept out of the nucleus by Crm1, gains access to the nucleus following
101 activation by Cdc15. We further demonstrate that Dbf2-Mob1 utilizes a nucleolar docking site
102 created by Cdc5 to phosphorylate Cfi1/Net1, resulting in Cdc14 liberation. These findings define
103 the molecular mechanisms of cross-compartment signal transmission in the MEN and provide a
104 novel paradigm for how signaling can occur across organelle boundaries.
105

106 **RESULTS**

107 ***Dbf2-Mob1 dynamically associates with SPBs.***

108 When the MEN is activated in anaphase, Dbf2-Mob1 is recruited to the outer plaque of SPBs by
109 binding to Cdc15-phosphorylated Nud1 (Rock et al., 2013). However, immobilizing Dbf2-Mob1
110 at SPBs by fusing Mob1 to Nud1 disrupts MEN activity (Rock et al., 2013), suggesting that
111 Dbf2-Mob1 is likely needed away from the SPBs for the MEN to function. Additionally, a small
112 fraction of Dbf2-Mob1 was found to enter mitotic nuclei (Stoepel et al., 2005). Thus, we
113 hypothesized that the MEN liberates Cdc14 from its nucleolar inhibitor through the dynamic
114 shuttling of Dbf2-Mob1 between the outer plaque of the SPB and the nucleolus. We reasoned
115 that as a messenger between the SPB and nucleolus, Dbf2-Mob1 needs to be mobile at the SPB.
116 To test this hypothesis, we performed fluorescence recovery after photobleaching (FRAP)
117 analysis on eGFP tagged Mob1 in anaphase cells (Figure 1B). We observed a rapid recovery of
118 fluorescence with a half-recovery time of 4.6 ± 0.7 s (mean ± std, n = 6 cells) after
119 photobleaching of Mob1-eGFP fluorescence either at the daughter (dSPB) or the mother (mSPB)
120 SPB. This fast turnover rate (~1/500 of the total duration for Dbf2-Mob1's SPB localization in
121 anaphase) indicates that localization of Dbf2-Mob1 to SPBs is highly dynamic.

122

123 ***Dbf2-Mob1 transiently localizes to the nucleolus during anaphase.***

124 We next investigated whether Dbf2-Mob1 localizes to the nucleolus by live-cell fluorescence
125 microscopy. Although subtle, we observed transient localization of Mob1-eGFP to the nucleolus
126 in some cells as judged by co-localization with the nucleolar protein Cfi1/Net1. Importantly, this
127 nucleolar localization was only observed in late anaphase cells after nucleolar segregation, when
128 the MEN is normally active (Figure 1C).

129 It was reported previously that two N-terminally truncated Mob1 mutant proteins,
130 Mob1Δ78 and Mob1Δ132 (Mob1 missing the first 78 and 132 amino acids, respectively),
131 localize more prominently to the nucleus (Stoepel et al., 2005). We found that they also
132 displayed increased nucleolar localization (Figure 1D-F). We hypothesize that the N-terminus of
133 Mob1 harbors auto-inhibitory sequences that prevent access of the protein to the nucleolus.
134 Hence, deleting these sequences ought to cause hyperactivation of Dbf2-Mob1. Indeed, we found
135 that N-terminal truncation mutants of Mob1 partially suppressed temperature sensitive alleles of
136 upstream MEN components (*cdc15-2* and *tem1-3*; Figure 1-figure supplement 1A). This
137 suppression was not a result of elevated Mob1 protein levels because overexpression of Mob1
138 from the *GPD* promoter did not suppress the growth defect of *cdc15-2* or *tem1-3* mutants (Figure
139 1-figure supplement 1A-B), nor did it increase Mob1's nucleolar localization (Figure 1-figure
140 supplement 1C-D). We conclude that N-terminal truncations result in enhanced nucleolar
141 localization and hyperactivation of Mob1.
142 To further characterize the cellular localization of Dbf2-Mob1, we quantified the relative
143 enrichment of full-length and truncated GFP-Mob1 at SPBs and in the nucleolus during the cell
144 cycle (Figure 1E). Full-length Mob1 localized to SPBs and the nucleolus during anaphase.
145 Localization of Mob1Δ78 and Mob1Δ132 to SPBs was similar to that of full-length Mob1. The
146 nucleolar localization of Mob1 and truncated Mob1 (Figure 1E) correlated with MEN activation,
147 as judged by Mob1 association with SPBs, translocation of the MEN activity reporter NLS_{Cdc14}
148 (Campbell et al., 2019) into the cytoplasm, and MEN-mediated Cdc14 release from the nucleolus
149 (Figure 1-figure supplement 2). Consistent with earlier observations, the Mob1 truncations
150 displayed significantly greater nucleolar enrichment relative to full-length Mob1 in anaphase
151 (~30% and 120% increase on average for Mob1Δ78 and Mob1Δ132 respectively, Figure 1F).

152 Mob1Δ78 localization to the nucleolus was, like full-length Mob1, restricted to anaphase but
153 accumulated in the nucleolus to higher levels. In contrast, Mob1Δ132 displayed both greater and
154 earlier nucleolar enrichment, evident already in metaphase. We conclude that Dbf2-Mob1
155 localizes to the nucleolus during anaphase when the MEN is active. N-terminal truncation
156 mutants of Mob1 exhibit enhanced nucleolar localization and are hypermorphic. Given that the
157 nucleolar localization of full-length Mob1 is quite subtle, we used the Mob1 truncation mutants
158 as tools to study Dbf2-Mob1's nucleolar localization.
159
160 ***Dbf2-Mob1 localizes to the nucleolus through interacting with Cfi1/Net1.***
161 To validate the nucleolar localization of Mob1 we observed by microscopy and to identify the
162 potential nucleolar receptor for Dbf2-Mob1, we performed TurboID proximity-based labeling
163 (Branon et al., 2018). We fused the promiscuous biotin ligase TurboID to the MEN components
164 Mob1, Dbf2, Tem1 and Cdc15, and identified their protein interactors by streptavidin pull-down
165 followed by mass spectrometry (MS) (Figure 2-figure supplement 1A). In this experiment, we
166 identified the nucleolar protein Cfi1/Net1 as the top hit for Mob1- and Dbf2-TurboID labeling
167 (Figure 2A, Figure 2-figure supplement 1B, Table S3). Biotinylation of Cfi1/Net1 by Mob1-
168 TurboID was further confirmed by the detection of a biotinylated peptide of Cfi1/Net1 (Figure 2-
169 figure supplement 1C). Importantly, Cfi1/Net1 was only detected in the labeling experiments
170 where Mob1 or Dbf2 were tagged with TurboID but not when Tem1 or Cdc15 were used as baits
171 (Figure 2A). In contrast, Nud1, the MEN scaffold protein at SPBs, was detected in the TurboID
172 labeling experiments for all MEN proteins (Figure 2A).
173 We validated these MS findings using streptavidin gel-shift assays (Fairhead and
174 Howarth, 2015; Housley et al., 2014). To monitor whether a target protein was biotinylated by

175 the TurboID-tagged bait protein *in vivo*, we treated the denatured cell lysates with excess
176 streptavidin prior to immunoblotting. Biotinylated form(s) of the target protein will migrate more
177 slowly in SDS-PAGE due to binding of streptavidin, with each added biotin molecule causing a
178 theoretical size increase of up to 53 kD, the size of a streptavidin tetramer (Figure 2-figure
179 supplement 1D). Using this assay, we observed a slower migrating form of Nud1 in cell lysates
180 from cells expressing all TurboID-tagged MEN proteins (Figure 2B). Slower migrating forms of
181 Cfi1/Net1 were only observed in lysates obtained from cells expressing Mob1-TurboID (Figure
182 2B).

183 To determine whether Cfi1/Net1 was the sole receptor for Mob1 in the nucleolus, we
184 characterized the localization of Mob1Δ78 and Mob1Δ132 in cells lacking *CFI1/NET1*. While
185 still localized to SPBs, Mob1Δ78 and Mob1Δ132 no longer accumulated in the nucleolus during
186 anaphase in *cfi1/net1Δ* cells (Figure 2C-D). Furthermore, when we overexpressed *CFI1/NET1*
187 from the strong galactose-inducible *GAL1-10* promoter, nucleolar localization of both full-length
188 and N-terminal truncation mutants of Mob1 was increased by at least 50% (full-length) and up to
189 300% (truncations) (Figure 2E-F). It is worth noting that the observed decrease in Mob1's dSPB
190 localization with *CFI1/NET1* overexpression (Figure 2F) is likely the result of Cdc14 inhibition
191 by Cfi1/Net1 (Visintin et al., 1999) leading to reduced MEN activation. We conclude that Dbf2-
192 Mob1 localization in the nucleolus during anaphase is mediated by interactions with Cfi1/Net1.
193

194 ***Nucleolar localization of Dbf2-Mob1 depends on MEN activation.***

195 The localization pattern of Dbf2-Mob1 leads to the model in which Dbf2-Mob1 is activated by
196 Cdc15 at SPBs. Active Dbf2-Mob1 then binds to and phosphorylates Cfi1/Net1, promoting the
197 dissociation of Cdc14 from its inhibitor to carry out mitotic exit. This model predicts that the

198 nucleolar localization of Dbf2-Mob1 depends on MEN activity. To test this prediction, we
199 employed an analog-sensitive allele of *CDC15*, *cdc15-as1* (Bishop et al., 2000; D'Aquino et al.,
200 2005). As expected, inhibition of *cdc15-as1* (through addition of the analog 1-NA-PP1)
201 prevented localization of Mob1 to SPBs and translocation of the MEN activity reporter NLS_{Cdc14}
202 into the cytoplasm (Figure 3A). Nucleolar localization of full-length Mob1 was also significantly
203 reduced (Figure 3A). Nucleolar localization of the N-terminally truncated Mob1Δ78 and
204 Mob1Δ132 mutants, on the other hand, was only moderately reduced (Figure 3A), which is
205 consistent with the finding that these alleles partially suppress the temperature sensitive growth
206 defect of *cdc15-2* cells (Figure 1-figure supplement 1B). We conclude that Mob1 localization to
207 the nucleolus depends on MEN activity. The N-terminal hyperactive truncation mutations in
208 Mob1 are less reliant on upstream MEN kinases for their nucleolar localization.
209
210 ***Cdc15 regulates nuclear access of Dbf2-Mob1.***
211 How does Cdc15 cause Dbf2-Mob1 to localize to the nucleolus? To reach the nucleolus, Dbf2-
212 Mob1 must first enter the nucleus. Considering that the size of the complex (102 kD) is above
213 the passive diffusion limit of the nuclear envelope (~40-60 kD) (Knockenhauer and Schwartz,
214 2016), we hypothesized that nuclear access of Dbf2-Mob1 is regulated. We explored this
215 possibility using the PhyB-PIF based light-inducible organelle targeting system (Yang et al.,
216 2013) (Figure 3-figure supplement 1A). We fused Mob1-eGFP to the PIF protein, which binds
217 PhyB upon exposure to red light (650 nm). Using this system, we successfully recruited Mob1-
218 eGFP-PIF to various subcellular locations such as SPBs or the outer mitochondrial membrane
219 (Figure 3-figure supplement 1B).

220 To gauge Dbf2-Mob1's nuclear access in different cell cycle stages, we created a trap for
221 nuclear Dbf2-Mob1 using nucleolar-anchored PhyB (PhyB-Sik1, Figure 3B). If Dbf2-Mob1 was
222 shuttling between the nucleus and cytoplasm, PhyB-Sik1 would capture nuclear Mob1-eGFP-PIF
223 when activated by light. Interestingly, in pre-anaphase cells, we were not able to capture a
224 notable amount of nuclear Dbf2-Mob1 after 2 minutes of red-light activation. In contrast, in
225 anaphase cells in which the MEN is active, Dbf2-Mob1 was readily recruited to the nucleolus
226 within 2 minutes (Figure 3C). We obtained similar results with a Dbf2-PIF fusion (Figure 3-
227 figure supplement 1C). Furthermore, when we activated PhyB every 15 minutes for 2 minutes to
228 recruit Mob1 to the nucleolus in cells progressing through the cell cycle, Mob1 was only
229 recruited to the nucleolus by light during anaphase when the protein was also present at SPBs
230 (Figure 3-figure supplement 1D). By comparison, we were not able to recruit the upstream
231 kinase Cdc15 to the nucleolus in any cell cycle stage (Figure 3-figure supplement 1C). Given
232 that (1) Dbf2-Mob1 protein levels do not fluctuate considerably during the cell cycle (Visintin
233 and Amon, 2001), that (2) the interaction between other PIF fusions and PhyB-Sik1 are not cell
234 cycle regulated (Yang et al., 2013), and that (3) Mob1 can be recruited to cytoplasmic targets
235 throughout the cell cycle (Figure 3-figure supplement 1B), we conclude that nuclear access of
236 Dbf2-Mob1 is cell cycle regulated.
237 Because nuclear access of Dbf2-Mob1 correlates with MEN activation, we next tested
238 whether it was regulated by the MEN by quantifying the relative enrichment of Mob1 in the
239 nucleolus as a function of PhyB activation time (exposure to 650 nm light) in *CDC15* or *cdc15-2*
240 cells. In cells with wild-type *CDC15*, light-induced nucleolar recruitment of Mob1 was higher in
241 anaphase than pre-anaphase cells. In contrast, in *cdc15-2* cells this difference was abolished
242 (Figure 3D). We conclude that in addition to activating Dbf2's kinase activity (Mah et al., 2001),

243 Cdc15 regulates Dbf2-Mob1's nuclear access. Consistent with this notion, we find that
244 Mob1Δ78, which partially suppresses the temperature sensitivity of the *cdc15-2* allele, displayed
245 increased nuclear access in all cell cycle stages (Figure 3-figure supplement 1E).
246
247 ***Dbf2-Mob1 is exported from the nucleus by Crm1.***
248 Dbf2-Mob1 is a substrate of the nuclear exportin Crm1 *in vitro* (Kırlı et al., 2015). To
249 determine whether Crm1 plays a role in controlling Dbf2-Mob1 localization *in vivo*, we
250 quantified the nucleolar localization of full-length and truncated Mob1 in cells carrying an allele
251 of *CRM1* (*crm1T539C*) that is sensitive to the nuclear export inhibitor leptomycin B (LMB)
252 (Neville, 1999). Treatment of *crm1T539C* cells with LMB led to an increase in nucleolar
253 localization of both full-length and N-terminally truncated Mob1 (Figure 3-figure supplement
254 2A), suggesting that Crm1 controls nuclear export of Dbf2-Mob1.
255 Crm1 recognizes substrates with a leucine-rich nuclear export signal (NES). To test
256 whether there was a functional NES in Dbf2 or Mob1, we overexpressed Dbf2 or Mob1 from the
257 galactose-inducible *GAL1-10* promotor. Overexpressed Mob1 was enriched in the nucleus
258 (Figure 3-figure supplement 2B) similar to what we observed for *pGPD-GFP-MOB1* (Figure 1-
259 figure supplement 1C). In contrast, when we overexpressed Mob1 together with Dbf2, Mob1 was
260 no longer nuclear enriched, suggesting that Dbf2 not Mob1 harbors a NES. Consistently, when
261 overexpressed on its own, Dbf2 exhibited diffuse localization but inhibition of *crm1T539C* with
262 LMB led to accumulation of Dbf2 in the nucleus (Figure 3-figure supplement 2C).
263 Sequence analysis identified a putative NES sequence in the N-terminus of Dbf2
264 beginning with L12 (Figure 3-figure supplement 2D). Incidentally, we noticed that this leucine
265 was mutated to methionine in a previously isolated hyperactive allele of *DBF2* (*DBF2-*

266 *HyA*)(Geymonat et al., 2009). Dbf2-HyA, when overexpressed, was nuclear enriched (Figure 3-
267 figure supplement 2E). Inspired by this observation, we overexpressed *DBF2* mutants where L12
268 had been mutated to either methionine (*dbf2-L12M*) or alanine (*dbf2-L12A*). Both mutants
269 accumulated in the nucleus (Figure 3-figure supplement 2E). Furthermore, we found that the first
270 23 amino acids of Dbf2 were sufficient to drive nuclear export of eGFP (Figure 3-figure
271 supplement 2E, G). To test whether the NES in Dbf2 influences Dbf2-Mob1's nucleolar
272 localization in anaphase under normal expression level, we characterized Mob1's cellular
273 localization in *dbf2-L12A* and observed an increase in nucleolar localization by at least 40% for
274 both full-length and N-terminally truncated Mob1(Figure 3E).
275 A previous phosphoproteomic study reported that S17 and S20 within the NES of Dbf2
276 are phosphorylated in anaphase-arrested cells (Holt et al., 2009). We found that mutating S17
277 and S20 to phospho-mimetic residues (S17,20D or S17,20E) disrupted the NES whereas
278 mutating these residues to alanine (S17,20A) retained the NES activity of Dbf2 (Figure 3-figure
279 supplement 2F, G). We propose that phosphorylation of S17 and S20 is regulated, possibly by
280 Cdc15, to control nuclear access of Dbf2-Mob1. Nucleolar localization of Mob1, particularly of
281 Mob1Δ78, was reduced in cells harboring the *dbf2-S17,20A* allele compared to cells with wild-
282 type *DBF2* (Figure 3-figure supplement 3A). However, cells carrying the *dbf2-S17,20A* allele,
283 while exhibiting reduced nuclear access of Mob1 during all cell cycle stages, still showed
284 differential nuclear access between pre-anaphase and anaphase, as is observed in *DBF2* cells
285 (Figure 3-figure supplement 3B). This observation suggests that additional regulatory
286 mechanism(s) control Dbf2-Mob1's nuclear access. In contrast, cells harboring the *dbf2-S17,20D*
287 allele exhibited increased nuclear access of Mob1 during all cell cycle stages (Figure 3-figure
288 supplement 3B), confirming that Dbf2-Mob1 is normally kept out of the nucleus through Dbf2's

289 NES. The NES sequence in Dbf2 is well conserved among *Saccharomycetes* (Figure 3-figure
290 supplement 2D) suggesting that regulated nuclear access of Dbf2-Mob1 is conserved at least
291 across this class of fungi.
292
293 ***Nucleolar localization of Dbf2-Mob1 is regulated by Cdc5.***
294 The analysis of nuclear access and nucleolar localization of the N-terminal truncations of Mob1
295 indicated that the MEN is not the only pathway controlling Dbf2-Mob1's nucleolar localization.
296 The truncation mutants localize to the nucleolus in a manner largely independent of the MEN,
297 yet their nucleolar localization is still restricted to metaphase and anaphase (Figure 3A). This
298 restriction of nucleolar localization is not due to limited nuclear access. Truncated Mob1 mutants
299 have increased nuclear access prior to anaphase (Figure 3-figure supplement 1E). These data
300 indicate that nucleolar localization or the interaction between Dbf2-Mob1 with Cfi1/Net1 is
301 regulated by additional factors.
302 An obvious candidate for this additional regulator is the Polo-like kinase Cdc5, which is
303 active throughout mitosis and plays multiple essential roles in mitotic exit (Lee et al., 2005). As
304 part of both the FEAR network (Rock and Amon, 2009; Stegmeier et al., 2002) and the MEN,
305 Cdc5 is indispensable for Cdc14's nucleolar release. However, the exact role(s) of Cdc5 during
306 this process is not fully understood. To determine whether Cdc5 regulates binding of Dbf2-Mob1
307 to Cfi1/Net1, we examined the consequences of inhibiting Cdc5's kinase activity on nucleolar
308 localization of Dbf2-Mob1 using an analog-sensitive allele of *CDC5* (*cdc5-as1*). Consistent with
309 the known functions of Cdc5 in MEN activation, we observed loss of Mob1's SPB localization
310 and Dbf2-Mob1's kinase activity as monitored by translocation of the NLS_{Cdc14} reporter into the
311 cytoplasm when Cdc5 was inhibited (Figure 4A). Nucleolar localization of Mob1, Mob1Δ78 and

312 Mob1Δ132 was also lost in cells lacking Cdc5 activity (Figure 4A). This is in direct contrast to
313 Cdc15 inhibition, where the nucleolar localization of N-terminal Mob1 truncation mutants
314 particularly Mob1Δ132 was only partially reduced (Figure 3A). These results suggested that
315 Cdc5 regulates Dbf2-Mob1's nucleolar localization independently of its role in activating Cdc15.
316 To directly determine whether *CDC5* regulated Dbf2-Mob1's nucleolar localization
317 independently of the MEN, we took advantage of a hyperactive *CDC15* allele, *GAL-CDC15(1-*
318 *750)* (Bardin et al., 2003), which is active even in the absence of *CDC5* (Rock and Amon, 2011).
319 When *GAL-CDC15(1-750)* was expressed, Mob1's SPB localization and Dbf2-Mob1's kinase
320 activity was no longer restricted to anaphase but rather was high throughout the cell cycle as a
321 result of MEN hyper-activation (Figure 4B). Interestingly, *GAL-CDC15(1-750)* did not abolish
322 cell-cycle regulation of Mob1's nucleolar localization but rather advanced it to early anaphase
323 and metaphase (Figure 4B). In cells expressing *GAL-CDC15(1-750),* inactivation of *CDC5* still
324 abolished nucleolar localization of both full-length and the hyperactive N-terminally truncated
325 Mob1 while Mob1 binding to SPBs was unaffected (Figure 4B). These results demonstrate that
326 nucleolar localization of Dbf2-Mob1 directly depends on Cdc5 independently of its role in MEN
327 activation.
328 Could *CDC5* regulate the nucleolar localization of Dbf2-Mob1 through its role in the
329 FEAR network? To test this, we quantified Mob1's nucleolar localization in cells lacking the
330 FEAR network component *SLK19* (*slk19*Δ). MEN activation (as determined by Mob1
331 localization to the dSPB and nuclear release of the NLS_{Cdc14} reporter) and as a result mitotic exit
332 were considerably delayed and more variable in *slk19*Δ cells (Figure 4-figure supplement 1A).
333 Consistent with a delay in MEN activation, nucleolar localization of Mob1 and Mob1Δ78 but not
334 Mob1Δ132 was also delayed. Importantly, maximum enrichment of Mob1 in the nucleolus was

335 not reduced in *slk19*Δ cells for all three forms of Mob1 (Figure 4-figure supplement 1B). We
336 conclude that Cdc5 regulates Dbf2-Mob1's nucleolar localization through mechanisms in
337 addition to its role in the MEN and the FEAR network.
338
339 ***Cdc5 and Dbf2-Mob1 phosphorylate Cfi1/Net1 at distinct sites.***
340 Our results suggest a model where Cdc5 promotes the interaction between Dbf2-Mob1 and its
341 nucleolar receptor Cfi1/Net1, likely through phosphorylating Cfi1/Net1. This interaction then
342 facilitates phosphorylation of Cfi1/Net1 by Dbf2-Mob1 to bring about the release of Cdc14 from
343 Cfi1/Net1. Cfi1/Net1 is a highly phosphorylated protein with 64 known phosphorylation sites *in*
344 *vivo* (Holt et al., 2009; Swaney et al., 2013). About one fifth of these sites were identified as
345 CDK targets (Holt et al., 2009) including six key CDK sites whose phosphorylation is controlled
346 by the FEAR network (Azzam, 2004). To map sites in Cfi1/Net1 that are phosphorylated in a
347 *CDC5* or MEN-dependent manner, we performed phosphoproteomic analyses on wild-type
348 anaphase cells and cells in which Cdc5 or Cdc15 were inhibited using the *cdc5-as1* and *cdc15-*
349 *as1* alleles, respectively (Figure 5-figure supplement 1A). This analysis identified 44 of the 64
350 previously known sites in Cfi1/Net1 and 18 new sites (Table S4). To achieve complete or close
351 to complete coverage of Cfi1/Net1's phosphorylation sites in anaphase, we also performed
352 immunoprecipitation-mass spectrometry (IP-MS) for Cfi1/Net1 in anaphase enriched cultures
353 and identified 9 additional sites (Table S4) resulting in an astonishing total of 91 phosphorylation
354 sites in Cfi1/Net1. These phosphorylation sites appear to cluster in regions of disorder as
355 predicted by the PONDR score (Romero et al., 1997) (Figure 5A).
356 By comparing the peptide signals between wild-type, *cdc15-as1*, and *cdc5-as1* cells in
357 our quantitative phosphoproteomics dataset, we identified phosphorylation sites that depended

358 on Cdc15 or Cdc5 activity or both (Figure 5-figure supplement 1B-E). Among them, we found
359 11 *CDC15*-dependent and 22 *CDC5*-dependent sites in Cfi1/Net1. Six of the *CDC15*-dependent
360 sites fit Dbf2-Mob1's preferred sequence motif RXXS* (* represents the phosphorylation site)
361 (Mah et al., 2005), supporting our model that Dbf2-Mob1 phosphorylates Cfi1/Net1. Given that
362 Cdc5 activates Cdc15, sites that depended on *CDC15* ought to also depend on *CDC5*. This was
363 indeed the case for 10 of the 11 *CDC15*-dependent phosphorylation sites in Cfi1/Net1.
364 To identify sites that only depended on *CDC5* but not *CDC15*, we subtracted *CDC15*-
365 dependent sites from *CDC5*-dependent sites yielding 12 sites (denoted as *CDC5*-only, Figure
366 5A). Based on the distribution of all 91 phosphorylation sites and degree of disorder, we divided
367 Cfi1/Net1 into four zones: residues 31-69 (z1, 7 sites), 160-615 (z2, 53 sites), 676-840 (z3, 12
368 sites) and 1017-1166 (z4, 19 sites) (Figure 5A). *CDC15*-dependent phosphorylation sites were
369 concentrated in zone 2, whereas *CDC5*-dependent sites were also found in zones 1 and 3. In
370 contrast to Cfi1/Net1, all the *CDC5*-dependent phosphorylation sites in Dbf2 and Mob1 were
371 also *CDC15*-dependent (Figure 5-figure supplement 1F). These data indicate that Cdc5 and
372 Dbf2-Mob1 directly phosphorylate Cfi1/Net1. Dbf2-Mob1 on the other hand is a direct substrate
373 of Cdc15 but not Cdc5.
374
375 ***Cdc5 promotes Dbf2-Mob1's nucleolar localization by phosphorylating Cfi1/Net1.***
376 Having identified phosphorylation sites within Cfi1/Net1, we next asked whether they were
377 important for the interaction between Cfi1/Net1 and Dbf2-Mob1. We generated a *CFI1* allele in
378 which all 91 phosphorylation sites were mutated to alanine (*cfi1-91A*). Cells harboring this allele
379 as the sole source of *CFI1/NET1* were viable and progressed through anaphase with only a slight
380 delay in mitotic exit as judged by the timing of Mob1's dissociation from the SPBs (Figure 5B).

381 Interestingly, Mob1Δ132, which showed the most pronounced nucleolar localization among all
382 Mob1 alleles analyzed, still localized to the SPBs during anaphase in *cfi1-91A* cells, but failed to
383 accumulate in the nucleolus (Figure 5B-C, Figure5-figure supplement 2A). We conclude that
384 Cfi1/Net1 phosphorylation is required for interacting with Dbf2-Mob1.

385 Next, we tested whether *CDC5*-dependent phosphorylation of Cfi1/Net1 regulated Dbf2-
386 Mob1's nucleolar localization. We focused our analysis on zone 2 of Cfi1/Net1 because previous
387 studies had shown that the first 621 amino acids of the protein are sufficient to confer Cdc14
388 regulation (Azzam, 2004). We further note that mutating phosphorylation sites in zone 1 and 3 of
389 Cfi1/Net1 did not affect the nucleolar localization of Mob1Δ132 (Figure 5B-C, Figure 5-figure
390 supplement 2A). We generated a *CFI1/NET1* allele with mutated phosphorylation sites in zone 2
391 that were phosphorylated in a *CDC5*-dependent but *CDC15*-independent manner (henceforth
392 *cfi1-Cdc5only(z2)*). For comparison we generated a *CFI1/NET1* allele in which we only mutated
393 sites that were phosphorylated in a *CDC15*- dependent manner (henceforth *cfi1-Cdc15(z2)*).
394 Analysis of Mob1Δ132 localization in these mutants revealed that, similar to inhibition of Cdc5,
395 *cfi1-Cdc5only(z2)* abolished the nucleolar localization of Mob1Δ132, while *cfi1-Cdc15(z2)*
396 slightly increased nucleolar localization of the protein (Figure 5D-E, Figure 5-figure supplement
397 2B). To validate these findings, we performed TurboID labeling experiments followed by
398 Streptavidin gel-shift assays to probe the interaction between TurboID tagged full-length Mob1
399 and 13Myc tagged Cfi1/Net1. The slower migrating form corresponding to biotinylated
400 Cfi1/Net1 was absent in cells expressing *cfi1-Cdc5only(z2)* but present in cells expressing *CFI* or
401 *cfi1-Cdc15(z2)* (Figure 5F). We conclude that phosphorylation of Cfi1/Net1 by Cdc5 is required
402 for Dbf2-Mob1 binding to the protein.

403 Three lines of evidence indicate that Cdc5 directly phosphorylates Cfi1/Net1. First,
404 consistent with the finding that Cdc5 is already active in metaphase, 10 out of 12 *CDC5*-only
405 sites identified in anaphase cells are already phosphorylated in cells arrested in metaphase using
406 the microtubule depolymerizing drug nocodazole (Figure 5-figure supplement 3) with 6 of them
407 also determined to be *CDC5*-dependent in metaphase (Figure 5-figure supplement 3E). Second,
408 we found considerable overlap between *CDC5*-dependent phosphorylation sites *in vivo* and sites
409 identified *in vitro* (Loughrey Chen et al., 2002; Shou et al., 2002). Four out of five *in vivo*
410 Cdc5only sites in region 1-341 were previously found to be phosphorylated by Cdc5 *in vitro*
411 (Table S4). Third, Cdc5 and Cfi1/Net1 interact with each other *in vivo* as determined by TurboID
412 labeling (Figure 5-figure supplement 4A). The biotinylation of Cfi1/Net1 by Cdc5-TurboID was
413 further confirmed by the detection of biotinylated peptides in Cfi1/Net1 as well as the
414 streptavidin gel-shift assay (Figure 5-figure supplement 4B-C). We conclude that Cdc5
415 phosphorylates Cfi1/Net1 at the onset of metaphase which serves as a priming event for Dbf2-
416 Mob1 binding to Cfi1/Net1 in anaphase. We note that these findings also explain why
417 Mob1Δ132's nucleolar localization is already evident in metaphase (Figure 4B).
418 How does phosphorylation of Cfi1/Net1 by Cdc5 promote its binding to Dbf2-Mob1?
419 Dbf2-Mob1 binds to Cdc15-phosphorylated Nud1 through Mob1's phosphoserine-threonine
420 binding domain (Rock et al., 2013). We propose that a similar mechanism might also mediate the
421 interaction between Dbf2-Mob1 and Cdc5-phosphorylated Cfi1/Net1. To test this possibility, we
422 introduced the mutation R253A,R254A,R257A (3RA), shown to abolish Mob1's ability to bind
423 phosphopeptides (Rock et al., 2013), to Mob1Δ132 and compared the localization of Mob1Δ132-
424 eGFP and Mob1Δ132-3RA-eGFP expressed ectopically (Figure 5-figure supplement 5A). The

425 3RA mutation, while retained nuclear access, abolished both the SPB and nucleolar localization
426 of Mob1Δ132 (Figure 5G and Figure 5-figure supplement 5).
427
428 ***Dbf2-Mob1 promotes the release of Cdc14 from the nucleolus through Cdc5-mediated priming***
429 ***of Cfi1/Net1.***
430 To determine whether the *CDC5* and MEN-dependent phosphorylation sites in Cfi1/Net1
431 regulate the interaction between Cfi1/Net1 and Cdc14 as our model predicted, we examined the
432 consequences of disrupting these phosphorylation sites on the release of Cdc14 from the
433 nucleolus. We first determined which region of Cfi1/Net1 was mediating phospho-regulation of
434 this interaction. We mutated all phosphorylation sites in the individual zones as well as in
435 combination and analyzed the effects on Cdc14 release from the nucleolus. This analysis
436 revealed that only phosphorylation in zone 2 controlled Cdc14 release from Cfi1/Net1 (Figure 6-
437 figure supplement 1A-B). It is important to note that mutating the phosphorylation sites in zone 2
438 also affected the ability of Cfi1/Net1 to bind Cdc14, as judged by the lower degree of Cdc14
439 nucleolar sequestration prior to anaphase and localization of Cdc14 to the dSPB prior to
440 anaphase (Figure 6-figure supplement 1C). This finding indicates that the same residues involved
441 in regulating the interaction between Cfi1/Net1 and Cdc14 are also important for forming the
442 complex in the first place and mutating them to alanine weakens this interaction. Alternatively,
443 mutating so many residues at once (53 sites in zone 2) could change the structure of Cfi1/Net1
444 and thus disrupt binding to Cdc14. Nevertheless, the increased level of free Cdc14 in the cell
445 with *cfi1-91A* and the zone 2-phosphomutant explains why such severe defect in Cdc14 release
446 from the nucleolus did not cause a significant anaphase delay as assayed by the kinetics of Cdc14
447 re-sequestration.

448 Next, we examined kinase-specific phospho-mutants in Cfi1/Net1. There are three known
449 kinases that phosphorylate Cfi1/Net1 to regulate binding to Cdc14: mitotic CDKs (mainly Clb2-
450 Cdk1), Cdc5 and Dbf2-Mob1. CDK phosphorylation of Cfi1/Net1 during early anaphase
451 underlies FEAR network-dependent release of Cdc14 from its inhibitor (Azzam, 2004). In FEAR
452 network mutants such as *slk19*Δ, Cdc14 release from the nucleolus and anaphase progression are
453 delayed and are accompanied by increased cell-to-cell variability (Figure 6A). As reported
454 previously (Azzam, 2004), cells harboring a *CFI1/NET1* allele with 6 CDK sites mutated to
455 alanine, *cfi1/net1-6Cdk*, caused Cdc14 release defects similar to those of FEAR network mutants
456 (Figure 6B).
457 Inactivation of the MEN using the *cdc15-as1* allele led to the previously described
458 pattern of Cdc14 localization, where Cdc14 is initially released from the nucleolus by the FEAR
459 network during early anaphase but is then re-sequestered in the nucleolus during later stages of
460 anaphase (Stegmeier et al., 2002) (Figure 6A). Mutating the *CDC15*-dependent phosphorylation
461 sites in zone 2 (*cfi1-Cdc15(z2)*) resulted in a significant reduction of Cdc14 release from the
462 nucleolus but only recapitulated ~50% of the effect of inactivating *CDC15* (compare Figure 6A
463 and B). As previously reported (Visintin et al., 2008), inhibition of the analog sensitive *cdc5-as1*
464 allele caused defects in both FEAR network and MEN-mediated release of Cdc14 from the
465 nucleolus (Figure 6A). Mutating the *CDC5*-only phosphorylation sites in zone 2 (*cfi1-*
466 *Cdc5only(z2)*) resulted in a similar reduction of Cdc14 release from the nucleolus (Figure 6B) as
467 inhibiting Cdc5. Finally, combining *cfi1-Cdc5only(z2)* with *cfi1-Cdc15(z2)* (*cfi1-*
468 *Cdc15&Cdc5(z2)*) caused an even greater defect in Cdc14 release from the nucleolus than either
469 mutant alone (Figure 6B, Figure 6-figure supplement 2). These results confirmed our model
470 where Cdc5, in addition to activating the MEN, directly phosphorylates Cfi1/Net1 to target

471 Dbf2-Mob1 to Cfi1/Net1. Phosphorylation of Cfi1/Net1 by Dbf2-Mob1 then promotes the
472 dissociation of Cdc14 from Cfi1/Net1.
473
474 ***Phosphorylation of Cfi1/Net1 by Cdc5 and Dbf2-Mob1 promotes mitotic exit.***
475 Preventing the dissociation of Cdc14 from its inhibitor during anaphase ought to interfere
476 with mitotic exit. Indeed, we observed a delay in all mutants analyzed (Figure 6C, Figure 6-
477 figure supplement 3). Both *cfi1-Cdc15(z2)* and *cfi1-Cdc5only(z2)* mutant cells exited mitosis
478 with an average delay of ~6 minutes (~25% increase, Figure 6C). In addition, consistent with
479 Cdc5's role in the FEAR network, we observed a significant delay in nucleolar segregation in
480 *cfi1-Cdc5only(z2)* mutant cells (Figure 6C). Surprisingly, *cfi1-Cdc15&Cdc5(z2)* double mutant
481 cells which had the most severe defect in Cdc14 release from the nucleolus exhibited a similar
482 delay in mitotic exit as the *cfi1-Cdc15(z2)* and *cfi1-Cdc5only(z2)* single mutants and a less severe
483 defect in nucleolar segregation compared to *cfi1-Cdc5only(z2)* (Figure 6C). This relatively short
484 delay in mitotic exit is likely due to the fact that Cdc14 was not tightly sequestered in this mutant
485 prior to anaphase. We observed elevated levels of Cdc14 at dSPB, indicating the presence of free
486 Cdc14 not sequestered in the nucleolus, in both *cfi1-Cdc15(z2)* and *cfi1-Cdc15&Cdc5(z2)* cells
487 prior to anaphase (Figure 6D, Figure 6-figure supplement 2). It appears that mutating *CDC15*-
488 dependent sites in Cfi1/Net1 interferes with its ability to bind Cdc14. Nonetheless, the majority
489 (>60%) of Cdc14 was not released during anaphase in cells harboring *cfi1-Cdc15&Cdc5*.
490 One possible explanation for the apparent discrepancy between the severity of the Cdc14
491 release defect and the more subtle delay in mitotic exit is that, in addition to targeting Cfi1/Net1,
492 MEN also promotes cytoplasmic retention of Cdc14 by phosphorylating its NLS (Mohl et al.,
493 2009). To determine the contribution of this MEN function to promoting mitotic exit in

494 *Cfi1/Net1* mutants, we constructed a *CDC14* mutant (*cdc14-3A*) in which all three potential
495 Dbf2-Mob1 phosphorylation sites capable of driving translocation of the NLS_{Cdc14} reporter into
496 the cytoplasm were mutated to alanine (Figure 6-figure supplement 4A). Interestingly, cells
497 expressing *cdc14-3A* instead of *CDC14* exited from mitosis without significant delays (Figure 6-
498 figure supplement 4B) indicating that cytoplasmic retention of Cdc14 does not play a major role
499 in promoting mitotic exit.

500 Another possibility is that some MEN-dependent phosphorylation sites in Cfi1/Net1
501 eluded our MS analysis. However, given that Cdc14 is a potent phosphatase, we favor the idea
502 that, incomplete sequestration of Cdc14 prior to anaphase coupled with FEAR network-mediated
503 nucleolar release of Cdc14 during early anaphase is sufficient to promote exit from mitosis with
504 only a modest delay in the *cfi1-Cdc15&Cdc5* mutant. Consistent with this idea, we found that the
505 *cfi1-Cdc5only(z2)* mutant, which does not display defects in sequestering Cdc14 prior to
506 anaphase, was synthetic lethal with the FEAR network mutants *slk19Δ* and *spo12Δ* (Figure 6E).
507 Furthermore, combining *cfi1-Cdc5only(z2)* with the FEAR mutant *cfi1-6Cdk* resulted in severe
508 defects in both FEAR network and MEN mediated Cdc14 release (Figure 6-figure supplement
509 5A) and ~20-minute delays in both mitotic exit and nucleolar segregation (Figure 6-figure
510 supplement 5B), the strongest defect in all mutants we have characterized. We conclude that
511 *CDC5* and MEN-dependent phosphorylation of Cfi1/Net1 controls the protein's binding to
512 Cdc14 and exit from mitosis.
513

514 **DISCUSSION**

515 As a model system for mitotic exit control and cellular signaling in eukaryotes, the MEN has
516 been studied extensively for decades. Yet, how the MEN activates its effector Cdc14 to promote

517 exit from mitosis has remained an enigma. Furthermore, the spatial aspect of signal transmission
518 in the MEN, namely how a signal generated at the outer plaque of the SPBs in the cytosol
519 reaches its target in the nucleolus, was largely unexplored. Our study provides mechanistic
520 insights into these questions and together with prior observations lead to a model for Cdc14
521 regulation and mitotic exit in budding yeast (Figure 7).
522
523 ***The role of the Polo-like kinase Cdc5 in regulating Cdc14 activation.***
524 The Polo-like kinase Cdc5 is essential for Cdc14 activation and is part of both the FEAR
525 network and the MEN. However, the exact role(s) of Cdc5 in regulating Cdc14's nucleolar
526 release has remained elusive due to its multiple functions in the MEN and the FEAR network.
527 Using an allele that bypasses *CDC5*'s role in MEN activation, we revealed a novel function of
528 Cdc5 as a priming kinase that targets Dbf2-Mob1 to its substrate Cfi1/Net1.
529 It was hypothesized that phosphorylation of Cfi1/Net1 by Cdc5 weakens the interaction
530 between Cfi1/Net1 and Cdc14. Additional phosphorylation by mitotic CDKs or Dbf2-Mob1
531 were thought to further reduce the interaction resulting in the dissociation of Cdc14 from its
532 inhibitor. Our results suggest an alternative model. Instead of, or at least in addition to,
533 weakening the Cfi1/Net1-Cdc14 interaction, Cdc5 phosphorylation targets Dbf2-Mob1 to
534 Cfi1/Net1. Mutating the Cdc5-only phosphorylation sites in Cfi1/Net1 abolished nucleolar
535 enrichment of Dbf2-Mob1 and resulted in a reduction in MEN-mediated dissociation of Cdc14
536 from Cfi1/Net1. Interestingly, this mutation also caused severe defects in the FEAR network
537 mediated release of Cdc14 from Cfi1/Net1. We thus propose that Cdc5 priming phosphorylation
538 is required not only for Dbf2-Mob1 to phosphorylate Cfi1/Net1 but also for mitotic CDKs
539 (Figure 7). Consistent with this hypothesis, we found that most Cdc5 phosphorylation sites in

540 Cfi1/Net1 are already phosphorylated by Cdc5 in metaphase (Figure 5-figure supplement 3E).
541 This observation indicates that the docking site(s) on Cfi1/Net1 for Dbf2-Mob1 (and mitotic
542 CDKs) is already present in metaphase prior to the activation of the FEAR network and the MEN
543 (Figure 7). This model is further supported by the observation that inhibition of Cdc5 eliminates
544 CDK mediated phosphorylation of T212 in Cfi1/Net1 (Azzam, 2004). Cdc5 activity is regulated
545 by the DNA damage checkpoint (Cheng et al., 1998; Sanchez, 1999). We speculate that making
546 FEAR network and MEN-mediated release of Cdc14 from the nucleolus dependent on Cdc5's
547 priming activity ensures that DNA damage has been repaired and the checkpoint silenced prior to
548 exit from mitosis.
549
550 ***The FEAR network and the MEN regulate Cdc14 binding to Cfi1/Net1 by different***
551 ***mechanisms.***
552 Although both mitotic CDKs and Dbf2-Mob1 appear to require *CDC5*-dependent priming
553 phosphorylation of Cfi1/Net1, the mechanism whereby mitotic CDKs and Dbf2-Mob1 disrupt
554 the interaction between Cfi1/Net1 and Cdc14 is quite different. Mitotic CDKs phosphorylate
555 Cfi1/Net1 mainly on S166, T212, S252, T297 and T304; Dbf2-Mob1 targets sites S259, S295,
556 S362, S439 and S497 (Figure 5A, Table S4). Given that mitotic CDKs and Dbf2-Mob1 target
557 different sites, we propose that increasing the acidity of aa160–500 within Cfi1/Net1 rather than
558 site-specific phosphorylation disrupts the interaction between Cdc14 and its inhibitor. Cfi1/Net1
559 is an integral part of the nucleolus, which has recently been described as a phase-separated
560 structure (Feric et al., 2016; Shin and Brangwynne, 2017). Overall phosphorylation rather than
561 phosphorylation of specific sites has been shown to disrupt interactions within such structures

562 (Carpenter et al., 2018; Owen and Shewmaker, 2019). Perhaps extraction of Cdc14 from the
563 nucleolar phase requires a similar mechanism.
564
565 ***The MEN as a model for cross-compartment signaling.***
566 The MEN, most closely related to the Hippo pathway, employs most, if not all, of the principles
567 governing classic receptor tyrosine signaling logic to convey a signal generated at SPBs to the
568 MEN effector Cdc14 in the nucleolus: (1) scaffold assisted signaling (at the SPB), (2) signal
569 transmission across organelle boundaries - from the cytoplasm to the nucleus, and (3) activation
570 of the effector in a sub-compartment (the nucleolus). As such, we believe that the molecular
571 mechanisms governing MEN activity are broadly applicable to intracellular signal transmission
572 in general.
573
574 ***(1) Dynamic scaffold assisted signaling.***
575 Scaffold assisted assembly of signaling complexes is a widespread phenomenon in eukaryotic
576 signal transduction cascades (Good et al., 2011). We find that in the MEN, assembly of Cdc15-
577 (Dbf2-Mob1) signaling complex on the scaffold Nud1 is highly dynamic and this dynamicity is
578 crucial for effector activation. We propose that this dynamicity also serves to amplify the signal.
579 Cdc15 is the limiting enzyme of the pathway: it is the least abundant component of the MEN and
580 hyperactivating Cdc15 increases Dbf2-Mob1's kinase activity by > 40-fold (Rock and Amon,
581 2011). We further hypothesize that the relatively low affinity of Mob1 for phosphorylated-Nud1
582 (K_d = 2.4 μM; note that for an optimal Mob1 binding phosphopeptide the K_d is 174 nM) (Rock et
583 al., 2013) is selected for to facilitate the fast turnover rate of Dbf2-Mob1 at SPBs and thus to
584 promote release of the kinase and signal amplification. In this model, the binding

585 affinity/kinetics of kinases to their signaling scaffolds is an important parameter that cells fine-
586 tune to generate desirable signaling properties of scaffold-assisted signaling pathways.
587
588 ***(2) Regulated compartment access.***
589 Many signals, be they generated outside or within the cell, ultimately, result in a nuclear
590 response. As such, signals have to be propagated from the cytoplasm into the nucleus. Our
591 studies have led to the discovery that in the MEN, this nuclear access is cell cycle regulated.
592 Prior to anaphase, Dbf2-Mob1 is actively exported out of the nucleus by Crm1 through the
593 conserved NES within the N-terminus of Dbf2. Upon MEN activation, nuclear partitioning of
594 Dbf2-Mob1 increases, likely a result of both increased nuclear import through modification of
595 Mob1's inhibitory N-terminus and decreased nuclear export through modification of Dbf2. One
596 potential mechanism for the latter is via phosphorylation of Dbf2's NES at S17 and S20, possibly
597 by Cdc15. Our observation that mutating these two sites exacerbated the temperature sensitivity
598 of *cdc15-2* (Figure 3-figure supplement 3C) is consistent with this possibility.
599 Disrupting the NES resulted in an increase in nuclear/nucleolar localization of Dbf2-
600 Mob1 in all cell cycle stages, interestingly, including anaphase (Figure 3E). This increase of
601 nuclear localization in anaphase suggests that only a small fraction of Dbf2-Mob1 is activated by
602 Cdc15 to enter the nucleus at any given time during anaphase. Active Dbf2-Mob1 is also needed
603 in the cytosol to phosphorylate substrates other than Cfi1/Net1 such as those involved in
604 cytokinesis. We speculate that fine-turning the balance of nuclear versus cytosolic Dbf2-Mob1,
605 possibly through maintaining a dynamic shuttling of active Dbf-Mob1 between the nucleus and
606 cytoplasm, is important for the timing of late cell cycle events. The dynamic shuttling of Dbf2-
607 Mob1 in combination with the relatively small fraction of active Dbf2-Mob1 would also explain

608 the absence of visible nuclear translocation of Dbf2-Mob1 upon activation. Interestingly,
609 mammalian Dbf2, known as LATS and is thought to mainly function in the cytosol (Yu and
610 Guan, 2013), has been found to localize to the nucleus (Britschgi et al., 2017; Li et al., 2014),
611 indicating nuclear shuttling of kinases might play a role in Hippo signaling as well.
612
613 ***(3) Substrate targeting by priming phosphorylation.***
614 Upon entry into the nucleus, Dbf2-Mob1 specifically functions in the nucleolus to promote the
615 dissociation of Cdc14 from its inhibitor Cfi1/Net1. Priming phosphorylation by Cdc5 on
616 Cfi1/Net1 ensures that Dbf2-Mob1 executes this function effectively. Dbf2-Mob1 binds to
617 Cdc15-phosphorylated Nud1 through Mob1's phosphoserine-threonine binding domain (Rock et
618 al., 2013). We demonstrated that a similar mechanism mediates the interaction between Dbf2-
619 Mob1 and Cdc5-phosphorylated Cfi1/Net1 (Figure 5G). Interestingly, during cytokinesis,
620 phosphorylation of Dbf2-Mob1's substrate Hof1 by Cdc5 has also been shown to facilitate the
621 binding of Hof1 to Mob1 (Meitinger et al., 2011; Rock et al., 2013). Based on our observation
622 that a quarter of potential Dbf2-Mob1 substrates are also targets of Cdc5 (Figure 5-figure
623 supplement 1E) we further speculate that priming phosphorylation by Cdc5 is a general
624 mechanism for targeting Dbf2-Mob1 to its substrates.
625 It is worth noting that Cdc5's consensus motif with an acidic residue at the -2 position of
626 the pS/T (Kettenbach et al., 2011; Nakajima et al., 2003) does not fit well with the optimal Mob1
627 binding motif which prefers Y/F at the -2 position of the pS/T (Rock et al., 2013). This is likely
628 beneficial as a low affinity between Dbf2-Mob1 and its substrates would increase substrate
629 turnover and prevent sequestration of active Dbf2-Mob1. This low affinity would also explain
630 the weak and transient localization of Dbf2-Mob1 in the nucleolus that evaded detection

631 previously. Mob1's phosphoserine-threonine binding domain is well conserved from yeast to
632 humans (Rock et al., 2013) suggesting that substrate targeting through priming phosphorylation
633 might occur for LATS-MOB1 in the Hippo pathway as well.

634 Priming phosphorylation is a widely used mechanism to ensure effective kinase action at
635 a particular site in the cell. Perhaps the best studied example for priming is the Polo-like kinases
636 whose polo-box domain directs the kinase to specific subcellular structures and substrates that
637 have been previously phosphorylated by a priming kinase such as CDKs (Elia et al., 2003;
638 Lowery et al., 2005). Although MAP kinases are mainly directed to their substrates through
639 specialized docking motifs (Bardwell, 2006; Cargnello and Roux, 2011) without priming, it has
640 been demonstrated that successive phosphorylation through priming could contribute to the
641 sensing of MAPK signal duration and strength (Murphy et al., 2002). These examples together
642 with our findings for Dbf2-Mob1 underscore the importance of priming phosphorylation as a
643 conserved paradigm for achieving specificity and efficiency in cellular signal transduction.
644

645 **ACKNOWLEDGEMENTS**

646 We thank F. Luca (Philadelphia, USA), R. Deshaies (Caltech, USA), E. Schiebel (ZMBH,
647 Germany), E. Unal (Berkeley, USA) and J. Haber (Waltham, USA) for strains and reagents; R.
648 Schiavoni and the Biopolymers & Proteomics Facility at Koch Institute Swanson Biotechnology
649 Center for processing samples for the TurboID-MS experiments; S. Bell, A. Seshan and
650 members of our laboratory for their critical reading of the manuscript. This work was supported
651 by National Institute of General Medical Science (GM 118066 to A.A.) and the Eunice Kennedy
652 Shriver National Institute of Child Health and Human Development (HD085866 to A.A.). X.Z.
653 was supported by a Helen Hay Whitney postdoctoral fellowship. A.A. is also investigator of the

654 Howard Hughes Medical Institute and the Paul F. Glenn Center for Biology of Aging Research
655 at MIT.
656

657 **AUTHOR CONTRIBUTIONS**

658 X.Z. and A.A. conceived the study. X.Z. performed all experiments. W.L. and Y.L. provided the
659 phosphoproteomic analysis. X.Z. and A.A. wrote the manuscript with input from all coauthors.
660

661 **COMPETING INTERESTS**

662 The authors declare no competing interests.

663 **MATERIALS AND METHODS**

Key Resources Table				
Reagent type (species) or resource	**Designation**	**Source or reference**	**Identifiers**	**Additional information**
gene (*S. cerevisiae*)	See Table S1			
strain, strain background (*S. cerevisiae*)	W303			
genetic reagent (*S. cerevisiae*)	See Table S1			
recombinant DNA reagent	See Table S2			
strain, strain background (*E. coli*)	DH5α	New England Biolabs	Cat# C2987U	Chemical competent cells
antibody	anti-GFP [JL-8] (Mouse monoclonal)	Takara Bio	Cat# 632381; RRID:AB_2313808	WB (1:1000)
antibody	anti-Myc [9E10] (Mouse monoclonal)	Abcam	Cat# ab32; RRID:AB_303599	WB (1:500)
antibody	anti-V5 (Mouse monoclonal)	Invitrogen	Cat# R960-25; RRID:AB_255656	WB (1:2000)
antibody	Rabbit polyclonal anti-Kar2	Gift from Mark Rose	N/A	WB (1:200,000)
antibody	HRP-conjugated anti-mouse IgG	GE	Cat# NA9310; RRID:AB_772193	(1:10,000)

antibody	HRP-conjugated anti-rabbit IgG	GE	Cat# NA934; RRID:AB_772206	(1:10,000)
antibody	anti-tubulin [YOL1/34] (Rat monoclonal)	Abcam	Cat# Ab6161; RRID:AB_305329	IF (1:100)
antibody	FITC-Donkey anti-Rat IgG	Jackson ImmunoResearch	Cat# 712-095-153; RRID:AB_2340652	(1:50)
peptide, recombinant protein	Streptavidin	Sigma-Aldrich	Cat# 189730	
peptide, recombinant protein	α-factor	The Koch Institute Swanson Biotechnology Center – Biopolymers Core Facility	N/A	
commercial assay or kit	Gibson Assembly Master Mix	New England Biolabs	Cat# E2611S	
commercial assay or kit	Q5 Site-Directed Mutagenesis Kit	New England Biolabs	Cat# E05545	
commercial assay or kit	Bradford protein assay	BioRad	Cat# 5000006	
commercial assay or kit	BCA protein assay	Pierce	Cat# 23227	
commercial assay or kit	MyOne Streptavidin C1 dynabeads	Thermo Fisher Scientific	Cat# 65001	
chemical compound, drug	Nocodazole	Sigma-Aldrich	Cat# M1404	

chemical compound, drug	Biotin	Sigma-Aldrich	Cat# B4639	
chemical compound, drug	1-NA-PP1	Cayman Chemical	Cat# 10954	
chemical compound, drug	CMK	MedChem Express	Cat# HY-52101	
chemical compound, drug	Phycocyanobilin (PCB)	Santa Cruz Biotechnology	Cat# sc-396921	
software, algorithm	FIJI (ImageJ)	(Schindelin et al., 2012)	RRID:SCR_002285	
software, algorithm	MATLAB_R2018 b	Mathworks, Inc. (2018)	RRID:SCR_001622	
software, algorithm	SnapGene v4.3	https://www.s napgene.com	RRID:SCR_015052	
software, algorithm	Custom MATLAB codes	This paper	https://github.com/s now-zhou/Dbf2-Mob1	
other	Mini Bead Beater	Biospec Products	N/A	

664

665 ***Construction of Yeast strains and plasmids***

666 All *Saccharomyces cerevisiae* yeast strains used in this study are derivatives of W303 (A2587)
667 and are listed in Table S1. All plasmids used in this study are listed in Table S2. Yeast were
668 cultured in standard YEP media (1% yeast extract, 2% peptone) with 2% D-glucose, or in
669 standard Synthetic Complete media (SC) with either 2% D-glucose or 2% raffinose prior to

670 induction of *GAL1/10* promoters with 1% raffinose + 1% galactose as indicated in the figure
671 legends. Cells were cultured at 25°C unless noted otherwise.
672 C-terminal fusions were constructed using standard PCR-based methods. N-terminal
673 truncation of *MOB1* mutants were made by first constructing the truncations with N-terminal
674 eGFP fusion in plasmids (pA2828-2830) based on pRS305H-*MOB1* (König et al., 2010). PCR
675 products of the fusion with 500bp upstream promoter region and 300bp downstream of the
676 *MOB1* ORF as well as the hphMX6 marker were transformed and integrated at the *MOB1* locus.
677 Correct integration and mutations were confirmed by PCR and sequencing. The NLS_{Cdc14}
678 reporter was made by Gibson assembly. NLS_{Cdc14} (Cdc14aa450-551) from pA2725 (Mohl et al.,
679 2009) and synthesized yeast codon optimized miRFP670 (Shcherbakova and Verkhusha, 2013)
680 (denoted as ymiRFP670) were assembled into the p404TEF1 vector (pA2726) which yielded
681 pA2786 for integration at the *trp1* locus. The PhyB constructs were integrated at the *leu2* locus
682 as single integrants (Yang et al., 2013). The eGFP-PIF C-terminal tagging plasmid (pA2821) was
683 made by replacing the mCitrine in pA2721 with eGFP and correcting the frame shift mutation
684 (missing a G at codon#2) in the *natMx6* coding sequence in the original plasmid acquired from
685 Addgene. The TurboID tagging plasmid (pA2859) was constructed by inserting the TurboID-V5
686 sequence from pA2847 (Branon et al., 2018) into the vector backbone of pA2821 between the
687 linker and natMx6.
688 Point mutations and truncations in the *GAL-DBF2* plasmids were made using Q5 site-
689 directed mutagenesis (NEB). Single point mutation in *DBF2* (*dbf2-L12A*) was introduced at the
690 endogenous locus using Cas9-mediated gene editing based on previously published protocols
691 (Anand et al., 2017) with modifications. Briefly, BplI cut plasmid pA2911 containing Cas9 and
692 gRNA missing the 20 bp target specific complementary sequence was transformed into A2587

693 together with (1) a ~250 bp synthesized double stranded DNA (IDT) containing the 20 bp
694 complementary sequence for *DBF2* (TGCTCATATTGCCTGCCAAG) sandwiched with
695 homologous sequences to the gRNA sequence in plasmid pA2911 for gap repair, and (2) an
696 80mer single strand DNA harboring *dbf2-L12A* mutation as the repair template. Successfully
697 edited clones were checked by sequencing and cured of the Cas9 plasmid. Phospho-mutants of
698 *DBF2* (*dbf2-S17,20A* and *dbf2-S17,20D*) were first constructed in plasmids (pA2948, pA2953
699 and pA2954) by Q5 site-directed mutagenesis. The *DBF2* ORF as well as the *URA3* marker were
700 then PCR amplified and transformed into A32629 to integrate at the *DBF2* locus as the sole copy
701 of *DBF2*. Correct integration and mutations were confirmed by PCR and sequencing.
702 To generate *CFI1/NET1* phospho-mutants, a fusion of wild-type *CFI1/NET1* and
703 mScarlet-I with ~300 bp upstream and downstream regions of *CFI1/NET1* were first Gibson
704 assembled into a single-integration vector backbone to generate plasmid pA2898. *CFI1/NET1*
705 phospho-mutants were synthesized (Twist Bioscience) in two segments (aa25-624 and aa617-
706 1173) and Gibson assembled into the vector backbone of pA2898 to replace wild-type
707 *CFI1/NET1*. These *CFI1/NET1* constructs were integrated into strain A41362 harboring a
708 heterozygous deletion of *CFI1/NET1*and haploid strains with *cfi1Δ* and different phospho-mutant
709 forms of *CFI1/NET1* integrated as a single copy at the *leu2* locus as the sole source of
710 *CFI1/NET1* were obtained through tetrad dissection. We attempted to generate phospho-mimetic
711 mutants of *CFI1/NET1* where either the Cdc15-dependent or Cdc5only sites in zone 2 were
712 replaced with the Asp or Glu to mimic phosphorylation (A41695-A41706). However, as
713 observed with many other proteins such as Cdc15 phosphorylation of Nud1 (Rock et al., 2013),
714 these mutations did not effectively mimic phosphorylation and in the case of Cdc5only sites led
715 to a loss of function with respect to Mob1 localization to the nucleolus.

716 Phospho-mutants in the NLS_{Cdc14} reporter were made by first introducing the point
717 mutations into the integration plasmid (pA2735) with Q5 site-directed mutagenesis and then
718 transformed and integrated at the *ura3* locus. The triple mutants of *CDC14* (S531,537,546A) was
719 introduced at the endogenous locus in A2588 using Cas9-mediated gene editing as described
720 above. The 20 bp complementary sequence for the gRNA used to target *CDC14* was
721 GGAGAGTAACGTCAGGGAGA. Ectopically expressed *mob1Δ132-eGFP* and *mob1Δ132-*
722 *3RA-eGFP* were made by removing the first 132aa of Mob1 from pA2124 and pA2126 (Rock et
723 al., 2013) with Q5 site-directed mutagenesis, generating pA2972 and pA2973. These plasmids
724 were integrated at the *trp1* locus and were expressed under the endogenous *MOB1* promoter in
725 the presence of a wild-type copy of *MOB1*.
726
727 ***FRAP analysis***
728 FRAP analysis was performed on a DeltaVision-OMX Super-Resolution Microscope (Applied
729 Precision, GE Healthcare Bio-Sciences) using a 60x oil objective and a 488 nm laser adjusted to
730 bleach an area of approximately 0.5 μm in radius. Two prebleach images were acquired followed
731 by a laser pulse (100% intensity) of 0.02 s duration and postbleach images were acquired at 1
732 s/frame for 30 s. Images at each time points were maximum projections of 7 *z* stacks with 0.5 μm
733 spacing. Images were analyzed with a custom MATLAB script. After subtracting the
734 background, fluorescence intensities in the cytosol, $I_{cytosol}(t)$, and at the SPB, $I_{SPB}(t)$ were
735 measured after segmenting the cell and SPBs. Photobleaching was corrected by normalizing I_{SPB}
736 (t) with $I_{cytosol}(t)$, $I_{SPB_norm}(t) = I_{SPB}(t) / I_{cytosol}(t)$. Double normalization for FRAP was calculated
737 to scale the photobleaching effect between 0 and 1: $I_{SPB_FRAP}(t) = [I_{SPB_norm}(t) - I_{SPB_norm}(0)] /$
738 $[I_{SPB_norm}(pre) - I_{SPB_norm}(0)]$, where $t = 0$ is the time point (frame) right after photobleaching and

739 *t = pre* is the time point (frame) right before photobleaching. The double normalized FRAP

740 curves were then fitted to a single exponential curve: $y = y_{max}\left(1 - e^{\left(-ln2/t_{1/2}\right)t}\right)$, where y_{max}

741 is the fraction recovered while $t_{1/2}$ is the half-recovery time.

742

743 ***Microscopy and image analysis***

744 For live-cell microscopy, cells were imaged on agarose pads (2% agarose in SC medium + 2%

745 glucose, unless otherwise noted) affixed to a glass slide and covered with a coverslip. Imaging

746 was performed on a DeltaVision Elite platform (GE Healthcare Bio-Sciences) with an InsightSSI

747 solid state light source, an UltimateFocus hardware autofocus system and a model IX-71,

748 Olympus microscope controlled by SoftWoRx software. A 60x Plan APO 1.42NA objective and

749 CoolSNAP HQ2 camera were used for image acquisition. For each time point, 7 *z* sections with

750 1 μm spacing were collect for each channel and were deconvolved. Maximum projections of the

751 deconvolved *z* stack were used for fluorescence quantification.

752 Image analysis was performed with custom scripts in MATLAB. First, yeast cells were

753 segmented and tracked through time using the bright-field image stacks and a previously

754 reported algorism (Ricicova et al., 2013). A few modifications were made for the tracking

755 process. Images were first aligned to correct for drift in the *xy* plane and cell segmentations in the

756 last frame of the time-lapse series were used as the reference for tracking. Next, fluorescence

757 images of cell cycle markers (such as Spc42 and or Cfi1/Net1) were segmented and tracked

758 based on cell segmentation. Appearance of a cell cycle marker in a cell during the acquisition

759 period was used to identify buds (daughter cells) and cell division events. Tracking of the cell

760 cycle markers that migrated into the buds were used to identify the corresponding mother cells.

761 Finally, for each division event identified, localization of Mob1 (or Cdc14) at regions defined by
762 the cell cycle markers was quantified.

763 For Mob1 localization at the SPBs (I_{SPB}), maximum intensity of Mob1 at SPBs (dilated
764 from the SPB area based on segmentation of Spc42) was used given that the size of SPBs (~100
765 nm) is within the diffraction limit of light microscopy. For Mob1 localization in the nucleolus
766 ($I_{nucleolus}$), the median intensity of Mob1 in the nucleolus as segmented by Cfi1/Net1 was used.
767 To calculate the relative enrichment of Mob1 at the SPB or in the nucleolus, Mob1 intensities at
768 these sites as defined above were normalized to the median intensity of Mob1 in the cytosol
769 which was defined as the cell area with cell cycle marker area subtracted ($I_{cytosol}$):
770 $I_{SPB\ or\ nucleolus}/I_{cytosol} - 1$. For the Dbf2-Mob1 kinase activity reporter, NLS_{Cdc14}, its
771 translocation from the nucleus into the cytoplasm was quantified with the coefficient of variation
772 (CV) of the pixel intensities within the dividing cell. CV is defined as the standard deviation
773 divided by the mean.

774 To quantify Cdc14 release from the nucleolus, the ratio of Cdc14 intensity to Cfi1/Net1
775 intensity (I_{Cdc14}/I_{Cfi1}) was calculated for each pixel within the nucleolus as segmented using
776 Cfi1/Net1 and averaged.

777 Single cell traces were aligned based on the timing of anaphase onset or the movement of
778 a SPB into the bud as indicated in figures, and averaged. 95% confidence intervals were
779 calculated as $\mu \pm 1.96 * \sigma/\sqrt{n}$, where μ and σ denote the mean and standard deviation
780 respectively and *n* is the number of cells measured.

781

782 ***Immunoblot analysis***

783 Log-phase cultures of cells grown in YEP + 2% glucose were harvested and treated with
784 5% TCA at 4°C overnight. TCA treated cell pellets were washed with acetone, air dried, and
785 resuspended in lysis buffer (10 mM Tris, 1 mM EDTA, 2.75 mM DTT, pH = 8). Cells were
786 lysed by bead-beating using a Multivortexer (max speed, 20 minutes) and glass beads at 4°C and
787 followed by boiling in SDS PAGE protein loading buffer for 5 minutes. Lysates were clarified
788 by centrifugation and were resolved on a 15-well NuPAGE 4-12% Bis-Tris protein gel (Thermo
789 Fisher Scientific) prior to transfer onto nitrocellulose membranes. GFP-Mob1 and variants were
790 detected using an anti-GFP antibody (Clontech, JL-8) at a 1:1000 dilution. Nud1-13myc and
791 Cfi1/Net1-3myc were detected using an anti-Myc antibody (abcam, 9E10) at a 1:500 dilution.
792 Mob1-V5-TurboID was detected using an anti-V5 antibody (Invitrogen) at a 1:2000 dilution.
793 Kar2 was detected using a rabbit anti-Kar2 antiserum at a 1:200,000 dilution. Secondary
794 antibodies were used at a 1 :10,000 dilution. Blots were imaged using the ECL Plus system (GE
795 Healthcare).
796
797 ***TurboID-MS and streptavidin gel-shift assay***
798 To identify biotinylated proteins as a result of interaction or physical proximity with TurboID
799 tagged bait protein by mass spectrometry (MS), log-phase cells with TurboID tagged bait and
800 untagged control cells were grown in YEP + 2% glucose + 50 μM biotin at room temperature for
801 3.5 h (~ two doublings). ~40 OD of cells were harvested for each sample and were treated with
802 5% trichloroacetic acid (TCA) at 4°C for a minimum of 10 minutes. TCA treated cells were
803 pelleted, washed with 50 mM Tris (pH = 7.5) and acetone, and dried. Dried cell pellets were
804 resuspended in lysis buffer (50 mM Tris, pH 7.5, 1 mM EDTA, 5 mM DTT, 1 mM PMSF, and
805 complete mini protease inhibitor cocktail by Roche) and were lysed by bead-beating with chilled

806 MiniBeadbeater (Biospec) and glass beads for 5 minutes followed by boiling in 1% SDS for 5
807 minutes. Lysates were diluted with RIPA buffer (50 mM Tris, pH 7.5, 150 mM NaCl, 0.1% SDS,
808 0.5% sodium deoxycholate, 1% NP40) and clarified by centrifugation. Protein concentration of
809 the lysates was measured by Bradford assay. 350 µl MyOne streptavidin C1 dynabeads (Thermo
810 Fisher Scientific) were washed twice with RIPA buffer, incubated with clarified lysates
811 containing ~ 3 mg of total protein for each sample with rotation for 1 hour at room temperature,
812 then moved to 4°C and incubated overnight with rotation. On the second day, the supernatants
813 (flow through) were removed and the beads were washed twice with 1 ml of 0.1 M Na_2CO_3,
814 once with 1 ml of 2 M urea in 10 mM Tris (pH = 7.5), and twice with 1 ml RIPA buffer. Bound
815 proteins were eluted by boiling the beads in 30 µl 3x protein loading buffer supplemented with 2
816 mM biotin. Small aliquots of samples were saved along the process to monitor for the
817 enrichment for biotinylated proteins by immunoblotting for V5 (included in the TurboID tagged
818 bait) and biotin.
819 Eluted proteins were resolved on a 10-well NuPAGE 4-12% Bis-Tris protein gel (Thermo
820 Fisher Scientific), stained with Coomassie (Imperial Protein Stain, Thermo Fisher Scientific) and
821 entire gel lanes were excised and cut into 1-mm pieces. Proteins were reduced with 20 mM
822 dithiothreitol (Sigma) for 1 hour at 56°C and then alkylated with 60 mM iodoacetamide (Sigma)
823 for 1 hour at 25°C in the dark. Proteins were then digested with 12.5 ng/uL modified trypsin
824 (Promega) in 50 µL 100 mM ammonium bicarbonate, pH 8.9 at 25°C overnight. Peptides were
825 extracted by incubating the gel pieces with 5% formic acid in 50% acetonitrile then 100 mM
826 ammonium bicarbonate, repeated twice followed by incubating the gel pieces with 100%
827 acetonitrile then 100 mM ammonium bicarbonate, repeated twice. Each fraction was collected,

828 combined, and reduced to near dryness in a vacuum centrifuge. Peptides were desalted using
829 C18 SpinTips (Protea, Morgantown, WV).
830 Peptides were separated by reverse phase HPLC (Thermo Easy nLC1000) using a
831 precolumn (made in house, 6 cm of 10 µm C18) and a self-pack 5 µm tip analytical column (12
832 cm of 5 µm C18, New Objective) over a 140-minute gradient before nanoelectrospray using a
833 QExactive HF-X mass spectrometer (Thermo). Raw mass spectral data files (.raw) were searched
834 using Proteome Discoverer (Thermo) and Mascot version 2.4.1 (Matrix Science). Mascot search
835 parameters were: 10 ppm mass tolerance for precursor ions; 15 mmu for fragment ion mass
836 tolerance; 2 missed cleavages of trypsin; fixed modification was carbamidomethylation of
837 cysteine; variable modifications were methionine oxidation and lysine biotinylation. Only
838 peptides with a Mascot score greater than or equal to 25 and an isolation interference less than or
839 equal to 30 were included in the data analysis.
840 There are several endogenous biotinylated proteins in yeast. To identify specific proteins
841 enriched in the TurboID labeling experiments (hits), total peptides identified for each protein in
842 cells with TurboID tagged bait were compared with the unlabeled control cells to calculate the
843 ratio of enrichment. A threshold of 10 standard deviations above the average ratio of enrichment
844 for all proteins in each sample was used to identify hits (see Figure 2-figure supplement 1B).
845 For the streptavidin gel-shift assays, cell lysates were prepared as for typical
846 immunoblotting experiments. Prior to loading samples onto protein gels, 20 ul of lysates for each
847 sample was incubated with 2 µl of 10 mg/ml streptavidin for 10 min at room temperature with
848 rotation. Treated samples were then resolved by SDS-PAGE gel at 4°C and processed for
849 immunoblotting as described above.
850

851 ***PhyB-PIF based optogenetics***

852 The PhyB-PIF based optogenetics experiments were performed based on previous reports (Jost
853 and Weiner, 2015; Yang et al., 2013). Cells grown to log phase in 1x SC medium + 2% glucose
854 were incubated with 31.25 μM (0.5 μl of 12.5 mM stock in 200 ul culture) Phycocyanobilin
855 (PCB, Santa Cruz Biotechnology) for 2 hours at room temperature in the dark. Cells were then
856 pelleted and resuspended in fresh medium without PCB and were mounted onto an agarose pad
857 with 2x SC medium + 2% glucose for imaging. To apply the light, we attached one 650 nm and
858 one 750 nm light-emitting diode (LED, Light-speed Technologies) onto the microscope
859 condenser. Light was controlled manually during the experiments. For the continuous exposure
860 of 650 nm light during time-course experiments, the light was briefly turned off for each image
861 acquisition. To quantify the relative enrichment of target protein in the PhyB-anchored region,
862 pixel intensities of the target protein (Mob1-eGFP-PIF, I_{PIF}) and PhyB (PhyB-mCherry, I_{PhyB})
863 inside the cell were fitted to a line ($I_{\mathrm{PIF}} = \alpha + \beta I_{\mathrm{PhyB}}$). The slope of the fitted line (β) was used
864 to assess the extent of co-localization or enrichment of the target protein in the PhyB-anchored
865 region. This method is robust against both photobleaching of the target protein during the time-
866 course and difference in the shape and size of the anchored region (the nucleolus) at different cell
867 cycle stages.

868

869 ***Phosphoproteomics***

870 To map phosphorylation events that depend on *CDC5* or *CDC15* (MEN) activity, we used the
871 analog-sensitive alleles of *CDC5* (*cdc5-as1*) or *CDC15* (*cdc15-as1*) and compared
872 phosphopeptides with and without inhibiting the kinase in anaphase (and metaphase for Cdc5)
873 enriched cultures. To enrich for anaphase cells, we first synchronized cells in G1 with α-factor (5

874 μg/ml for 2.5 hours). α-factor arrested cultures were then washed and released into YEP + 2%
875 glucose + inhibitor (5 μM CMK for *CDC5*/*cdc5-as1* or 10 μM 1-NAPP1 for *CDC5*/*cdc5-as1*) at
876 room temperature to progress to anaphase (~ 100 minutes). Synchronization and cell cycle stage
877 were assessed by monitoring budding and spindle length at various time points. Spindles were
878 visualized by immunofluorescence using an anti-tubulin antibody (Abcam ab6161). Cultures
879 collected for the anaphase experiment harbored 74% (*WT* + 1-NA-PP1), 95% (*cdc15-as1*, 1-NA-
880 PP1), 69% (*WT* + CMK), and 94% (*cdc5-as1* + CMK) cells with anaphase spindles.
881 Phosphopeptide preparation was based on previous methods (Holt et al., 2009; Villén and
882 Gygi, 2008). ~25 ODs of cells were harvested for each replicate (6 replicates per samples for the
883 anaphase experiment and 3 replicates per sample for the metaphase experiment) by
884 centrifugation (5 min at 3000 rpm). Cell pellets were washed with cold 50 mM Tris (pH = 7.5)
885 and resuspended in cold lysis buffer containing 8 M urea in 50 mM Tris (pH = 7.5), 75 mM
886 NaCl, 50 mM NaF, 50 mM β-glycerophosphate, 1 mM sodium orthovanadate, 10 mM sodium
887 pyrophosphate and protease inhibitor cocktail (complete mini, EDTA-free, Roche). Cells were
888 lysed under denaturing conditions by bead-beating with a chilled MiniBeadbeater (Biospec, two
889 rounds of 3 cycles of 90 s each) and glass beads. The protein extract was then separated from the
890 beads and insoluble material by centrifugation. Protein concentration of the lysate was
891 determined by BCA protein assay (Pierce).
892 The protein extraction was ultrasonically lysed at 4°C for 2 minutes with six rounds using
893 a VialTweeter device (Hielscher-Ultrasound Technology). The proteins extracted were then
894 processed with a precipitation-based digestion protocol using trypsin (Promega) at a ratio of 1:20
895 as described previously(Collins et al., 2017). About 500 μg of resultant peptides from each
896 sample were subjected for phosphopeptide enrichment, using the High-Select™ Fe-NTA kit

897 (Thermo Scientific, A32992) according to the kit instruction, as described previously(Gao et al.,
898 2019). About 1.5 μg of phosphopeptides enriched from each sample were used for DIA-MS
899 measurement on an Orbitrap Fusion Lumos Tribrid mass spectrometer (Thermo Scientific)
900 platform coupled to a nanoelectrospray ion source, as described previously (Mehnert et al.,
901 2019). DIA-MS data analyses were performed using Spectronaut v13 (Bruderer et al., 2017)
902 using default setting, by searching against a database of 6632 yeast open reading frames(Hebert
903 et al., 2014) and the Swiss-prot yeast proteome database. In particular, the PTM localization
904 option in Spectronaut v13 was enabled to locate phosphorylation sites (Bekker-Jensen et al.,
905 2020; Collins et al., 2017), with the probability score cutoff >0.75(7), resulting Class-I peptides
906 to be identified and quantified. Both peptide and protein FDR cutoff (Q value) were controlled at
907 1%, and the label-free protein quantification of proteome and phospho-proteome was performed
908 using the default settings in Spectronaut.

909 To identify peptides whose phosphorylation depended on *CDC5* or *CDC15*, we
910 calculated the ratio as well as the *p*-value of peptide intensities in *WT* versus *as1* samples. The *p*-
911 values were calculated using a two-sided Student's *t*-test and were adjusted for false discovery
912 rate (FDR) of multiple hypothesis testing using the linear step-up procedure (Benjamini-
913 Hochberg procedure). A threshold of ratio $R > 2$ and $p_{adj} < 0.05$ was used to identify hits.
914 Additional hits were also included for peptides that were not defected in the *as1* samples but
915 were detected in at least 5 out of 7 replicates (or 4 out of 6 replicates in the metaphase
916 experiment) of the *WT* samples. Peptides that were only detected in one replicate of the *as1*
917 samples but were detected in at least 5 out of 7 replicates (or 4 out of 6 replicates in the
918 metaphase experiment) of the *WT* samples with a ratio > 2 were also included. After we have
919 identified hits for peptides, we mapped the peptides and phosphorylation sites in those peptides

920 to proteins in the yeast proteome. For phosphorylation sites that were detected in multiple
921 peptides, peptides with a single phosphorylation were given priority. We marked a site as a
922 strong hit only when all single phosphorylation peptides for the specific site fit our selection
923 criteria. If a site was only detected in multi-phosphorylation peptides that fit our selection
924 criteria, we designated that site as a weak hit.
925
926 ***Plasmid shuffling***
927 To assess the genetic interactions between different *CFI1/NET1* phospho-mutants and FEAR
928 mutants (*slk19*Δ or *spo12*Δ), we constructed strains in the background of *slk19*Δ or *spo12*Δ with
929 *cfi1/net1*Δ carrying a *URA3*-based *CEN* plasmid expressing wild-type *CFI1/NET1* (pA2858) and
930 different *CFI1/NET1* phospho-mutants integrated at the *leu2* locus (A41645-A41654). Growing
931 these strains on plates with 5'-fluoroorotic acid (5-FOA) selects cells that are viable after losing
932 the *URA3* plasmid.
933
934 ***Data and Code Availability***
935 The mass spectrometry phosphoproteomics data have been deposited to the ProteomeXchange
936 Consortium via the PRIDE (Perez-Riverol et al., 2019) partner repository with the dataset
937 identifier PXD020369. Custom MATLAB scripts are available at https://github.com/snow-
938 zhou/Dbf2-Mob1.

REFERENCES

Anand, R., Memisoglu, G., and Haber, J. (2017). Cas9-mediated gene editing in Saccharomyces cerevisiae. Protoc. Exch.

Azzam, R. (2004). Phosphorylation by Cyclin B-Cdk Underlies Release of Mitotic Exit Activator Cdc14 from the Nucleolus. Science *305*, 516–519.

Bardin, A.J., Visintin, R., and Amon, A. (2000). A Mechanism for Coupling Exit from Mitosis to Partitioning of the Nucleus. Cell *102*, 21–31.

Bardin, A.J., Boselli, M.G., and Amon, A. (2003). Mitotic Exit Regulation through Distinct Domains within the Protein Kinase Cdc15. Mol. Cell. Biol. *23*, 5018–5030.

Bardwell, L. (2006). Mechanisms of MAPK signalling specificity. Biochem. Soc. Trans. *34*, 837–841.

Bekker-Jensen, D.B., Bernhardt, O.M., Hogrebe, A., Martinez-Val, A., Verbeke, L., Gandhi, T., Kelstrup, C.D., Reiter, L., and Olsen, J.V. (2020). Rapid and site-specific deep phosphoproteome profiling by data-independent acquisition without the need for spectral libraries. Nat. Commun. *11*, 787.

Bembenek, J., Kang, J., Kurischko, C., Li, B., Raab, J.R., Belanger, K.D., Luca, F.C., and Yu, H. (2005). Crm1-Mediated Nuclear Export of Cdc14 is Required for the Completion of Cytokinesis in Budding Yeast. Cell Cycle *4*, 961–971.

Bishop, A.C., Ubersax, J.A., Petsch, D.T., Matheos, D.P., Gray, N.S., Blethrow, J., Shimizu, E., Tsien, J.Z., Schultz, P.G., Rose, M.D., et al. (2000). A chemical switch for inhibitor-sensitive alleles of any protein kinase. Nature *407*, 395–401.

Branon, T.C., Bosch, J.A., Sanchez, A.D., Udeshi, N.D., Svinkina, T., Carr, S.A., Feldman, J.L., Perrimon, N., and Ting, A.Y. (2018). Efficient proximity labeling in living cells and organisms with TurboID. Nat. Biotechnol. *36*, 880–887.

Britschgi, A., Duss, S., Kim, S., Couto, J.P., Brinkhaus, H., Koren, S., De Silva, D., Mertz, K.D., Kaup, D., Varga, Z., et al. (2017). The Hippo kinases LATS1 and 2 control human breast cell fate via crosstalk with ERα. Nature *541*, 541–545.

Bruderer, R., Bernhardt, O.M., Gandhi, T., Xuan, Y., Sondermann, J., Schmidt, M., Gomez-Varela, D., and Reiter, L. (2017). Optimization of Experimental Parameters in Data-Independent Mass Spectrometry Significantly Increases Depth and Reproducibility of Results. Mol. Cell. Proteomics MCP *16*, 2296–2309.

Campbell, I.W., Zhou, X., and Amon, A. (2019). The Mitotic Exit Network integrates temporal and spatial signals by distributing regulation across multiple components. ELife *8*.

Cargnello, M., and Roux, P.P. (2011). Activation and Function of the MAPKs and Their Substrates, the MAPK-Activated Protein Kinases. Microbiol. Mol. Biol. Rev. *75*, 50–83.

Carpenter, K., Bell, R.B., Yunus, J., Amon, A., and Berchowitz, L.E. (2018). Phosphorylation-Mediated Clearance of Amyloid-like Assemblies in Meiosis. Dev. Cell *45*, 392-405.e6.

Cheng, L., Hunke, L., and Hardy, C.F.J. (1998). Cell Cycle Regulation of the Saccharomyces cerevisiae Polo-Like Kinase Cdc5p. Mol. Cell. Biol. *18*, 7360–7370.

Collins, B.C., Hunter, C.L., Liu, Y., Schilling, B., Rosenberger, G., Bader, S.L., Chan, D.W., Gibson, B.W., Gingras, A.-C., Held, J.M., et al. (2017). Multi-laboratory assessment of reproducibility, qualitative and quantitative performance of SWATH-mass spectrometry. Nat. Commun. *8*, 291.

D'Amours, D., Stegmeier, F., and Amon, A. (2004). Cdc14 and Condensin Control the Dissolution of Cohesin-Independent Chromosome Linkages at Repeated DNA. Cell *117*, 455–469.

D'Aquino, K.E., Monje-Casas, F., Paulson, J., Reiser, V., Charles, G.M., Lai, L., Shokat, K.M., and Amon, A. (2005). The Protein Kinase Kin4 Inhibits Exit from Mitosis in Response to Spindle Position Defects. Mol. Cell *19*, 223–234.

Elia, A.E.H., Rellos, P., Haire, L.F., Chao, J.W., Ivins, F.J., Hoepker, K., Mohammad, D., Cantley, L.C., Smerdon, S.J., and Yaffe, M.B. (2003). The Molecular Basis for Phosphodependent Substrate Targeting and Regulation of Plks by the Polo-Box Domain. Cell *115*, 83–95.

Fairhead, M., and Howarth, M. (2015). Site-specific biotinylation of purified proteins using BirA. Methods Mol. Biol. Clifton NJ *1266*, 171–184.

Feric, M., Vaidya, N., Harmon, T.S., Mitrea, D.M., Zhu, L., Richardson, T.M., Kriwacki, R.W., Pappu, R.V., and Brangwynne, C.P. (2016). Coexisting Liquid Phases Underlie Nucleolar Subcompartments. Cell *165*, 1686–1697.

Gao, Q., Zhu, H., Dong, L., Shi, W., Chen, R., Song, Z., Huang, C., Li, J., Dong, X., Zhou, Y., et al. (2019). Integrated Proteogenomic Characterization of HBV-Related Hepatocellular Carcinoma. Cell *179*, 1240.

Geymonat, M., Spanos, A., de Bettignies, G., and Sedgwick, S.G. (2009). Lte1 contributes to Bfa1 localization rather than stimulating nucleotide exchange by Tem1. J. Cell Biol. *187*, 497–511.

Good, M.C., Zalatan, J.G., and Lim, W.A. (2011). Scaffold proteins: hubs for controlling the flow of cellular information. Science *332*, 680–686.

Guertin, D.A., Trautmann, S., and McCollum, D. (2002). Cytokinesis in Eukaryotes. Microbiol. Mol. Biol. Rev. *66*, 155–178.

Hebert, A.S., Richards, A.L., Bailey, D.J., Ulbrich, A., Coughlin, E.E., Westphall, M.S., and Coon, J.J. (2014). The one hour yeast proteome. Mol. Cell. Proteomics MCP *13*, 339–347.

Hergovich, A., and Hemmings, B.A. (2012). Hippo signalling in the G2/M cell cycle phase: Lessons learned from the yeast MEN and SIN pathways. Semin. Cell Dev. Biol. *23*, 794–802.

Holt, L.J., Tuch, B.B., Villen, J., Johnson, A.D., Gygi, S.P., and Morgan, D.O. (2009). Global Analysis of Cdk1 Substrate Phosphorylation Sites Provides Insights into Evolution. Science *325*, 1682–1686.

Housley, M.P., Reischauer, S., Dieu, M., Raes, M., Stainier, D.Y.R., and Vanhollebeke, B. (2014). Translational profiling through biotinylation of tagged ribosomes in zebrafish. Development *141*, 3988–3993.

Jaspersen, S.L., and Morgan, D.O. (2000). Cdc14 activates Cdc15 to promote mitotic exit in budding yeast. Curr. Biol. *10*, 615–618.

Jost, A.P.-T., and Weiner, O.D. (2015). Probing Yeast Polarity with Acute, Reversible, Optogenetic Inhibition of Protein Function. ACS Synth. Biol. *4*, 1077–1085.

Kettenbach, A.N., Schweppe, D.K., Faherty, B.K., Pechenick, D., Pletnev, A.A., and Gerber, S.A. (2011). Quantitative Phosphoproteomics Identifies Substrates and Functional Modules of Aurora and Polo-Like Kinase Activities in Mitotic Cells. Sci. Signal. *4*, rs5–rs5.

Kırlı, K., Karaca, S., Dehne, H.J., Samwer, M., Pan, K.T., Lenz, C., Urlaub, H., and Görlich, D. (2015). A deep proteomics perspective on CRM1-mediated nuclear export and nucleocytoplasmic partitioning. ELife *4*, e11466.

Knockenhauer, K.E., and Schwartz, T.U. (2016). The Nuclear Pore Complex as a Flexible and Dynamic Gate. Cell *164*, 1162–1171.

König, C., Maekawa, H., and Schiebel, E. (2010). Mutual regulation of cyclin-dependent kinase and the mitotic exit network. J. Cell Biol. *188*, 351–368.

Kuilman, T., Maiolica, A., Godfrey, M., Scheidel, N., Aebersold, R., and Uhlmann, F. (2015). Identification of Cdk targets that control cytokinesis. EMBO J. *34*, 81–96.

Lee, K.S., Park, J.-E., Asano, S., and Park, C.J. (2005). Yeast polo-like kinases: functionally conserved multitask mitotic regulators. Oncogene *24*, 217–229.

Li, W., Cooper, J., Zhou, L., Yang, C., Erdjument-Bromage, H., Zagzag, D., Snuderl, M., Ladanyi, M., Hanemann, C.O., Zhou, P., et al. (2014). Merlin/NF2 loss-driven tumorigenesis linked to CRL4(DCAF1)-mediated inhibition of the hippo pathway kinases Lats1 and 2 in the nucleus. Cancer Cell *26*, 48–60.

Loughrey Chen, S., Huddleston, M.J., Shou, W., Deshaies, R.J., Annan, R.S., and Carr, S.A. (2002). Mass Spectrometry-based Methods for Phosphorylation Site Mapping of Hyperphosphorylated Proteins Applied to Net1, a Regulator of Exit from Mitosis in Yeast. Mol. Cell. Proteomics *1*, 186–196.

Lowery, D.M., Lim, D., and Yaffe, M.B. (2005). Structure and function of Polo-like kinases. Oncogene *24*, 248–259.

Mah, A.S., Jang, J., and Deshaies, R.J. (2001). Protein kinase Cdc15 activates the Dbf2-Mob1 kinase complex. Proc. Natl. Acad. Sci. *98*, 7325–7330.

Mah, A.S., Elia, A.E.H., Devgan, G., Ptacek, J., Schutkowski, M., Snyder, M., Yaffe, M.B., and Deshaies, R.J. (2005). Substrate specificity analysis of protein kinase complex Dbf2-Mob1 by peptide library and proteome array screening. BMC Biochem. *6*, 22.

Mehnert, M., Li, W., Wu, C., Salovska, B., and Liu, Y. (2019). Combining Rapid Data Independent Acquisition and CRISPR Gene Deletion for Studying Potential Protein Functions: A Case of HMGN1. Proteomics *19*, e1800438.

Meitinger, F., Boehm, M.E., Hofmann, A., Hub, B., Zentgraf, H., Lehmann, W.D., and Pereira, G. (2011). Phosphorylation-dependent regulation of the F-BAR protein Hof1 during cytokinesis. Genes Dev. *25*, 875–888.

Mohl, D.A., Huddleston, M.J., Collingwood, T.S., Annan, R.S., and Deshaies, R.J. (2009). Dbf2–Mob1 drives relocalization of protein phosphatase Cdc14 to the cytoplasm during exit from mitosis. J. Cell Biol. *184*, 527–539.

Murphy, L.O., Smith, S., Chen, R.-H., Fingar, D.C., and Blenis, J. (2002). Molecular interpretation of ERK signal duration by immediate early gene products. Nat. Cell Biol. *4*, 556–564.

Nakajima, H., Toyoshima-Morimoto, F., Taniguchi, E., and Nishida, E. (2003). Identification of a Consensus Motif for Plk (Polo-like Kinase) Phosphorylation Reveals Myt1 as a Plk1 Substrate*. J. Biol. Chem. *278*, 25277–25280.

Neville, M. (1999). The NES-Crm1p export pathway is not a major mRNA export route in Saccharomyces cerevisiae. EMBO J. *18*, 3746–3756.

Owen, I., and Shewmaker, F. (2019). The Role of Post-Translational Modifications in the Phase Transitions of Intrinsically Disordered Proteins. Int. J. Mol. Sci. *20*, 5501.

Pereira, G., Höfken, T., Grindlay, J., Manson, C., and Schiebel, E. (2000). The Bub2p Spindle Checkpoint Links Nuclear Migration with Mitotic Exit. Mol. Cell *6*, 1–10.

Perez-Riverol, Y., Csordas, A., Bai, J., Bernal-Llinares, M., Hewapathirana, S., Kundu, D.J., Inuganti, A., Griss, J., Mayer, G., Eisenacher, M., et al. (2019). The PRIDE database and related tools and resources in 2019: improving support for quantification data. Nucleic Acids Res. *47*, D442–D450.

Ptacek, J., Devgan, G., Michaud, G., Zhu, H., Zhu, X., Fasolo, J., Guo, H., Jona, G., Breitkreutz, A., Sopko, R., et al. (2005). Global analysis of protein phosphorylation in yeast. Nature *438*, 679–684.

Queralt, E., Lehane, C., Novak, B., and Uhlmann, F. (2006). Downregulation of PP2ACdc55 Phosphatase by Separase Initiates Mitotic Exit in Budding Yeast. Cell *125*, 719–732.

Ricicova, M., Hamidi, M., Quiring, A., Niemisto, A., Emberly, E., and Hansen, C.L. (2013). Dissecting genealogy and cell cycle as sources of cell-to-cell variability in MAPK signaling using high-throughput lineage tracking. Proc. Natl. Acad. Sci. *110*, 11403–11408.

Rock, J.M., and Amon, A. (2009). The FEAR network. Curr. Biol. CB *19*, R1063-1068.

Rock, J.M., and Amon, A. (2011). Cdc15 integrates Tem1 GTPase-mediated spatial signals with Polo kinase-mediated temporal cues to activate mitotic exit. Genes Dev. *25*, 1943–1954.

Rock, J.M., Lim, D., Stach, L., Ogrodowicz, R.W., Keck, J.M., Jones, M.H., Wong, C.C.L., Yates, J.R., Winey, M., Smerdon, S.J., et al. (2013). Activation of the Yeast Hippo Pathway by Phosphorylation-Dependent Assembly of Signaling Complexes. Science *340*, 871–875.

Romero, P., Obradovic, Z., Kissinger, C., Villafranca, J.E., and Dunker, A.K. (1997). Identifying disordered regions in proteins from amino acid sequence. In Proceedings of International Conference on Neural Networks (ICNN'97), (Houston, TX, USA: IEEE), pp. 90–95.

Sanchez, Y. (1999). Control of the DNA Damage Checkpoint by Chk1 and Rad53 Protein Kinases Through Distinct Mechanisms. Science *286*, 1166–1171.

Schindelin, J., Arganda-Carreras, I., Frise, E., Kaynig, V., Longair, M., Pietzsch, T., Preibisch, S., Rueden, C., Saalfeld, S., Schmid, B., et al. (2012). Fiji: an open-source platform for biological-image analysis. Nat. Methods *9*, 676–682.

Shcherbakova, D.M., and Verkhusha, V.V. (2013). Near-infrared fluorescent proteins for multicolor in vivo imaging. Nat. Methods *10*, 751–754.

Shin, Y., and Brangwynne, C.P. (2017). Liquid phase condensation in cell physiology and disease. Science *357*, eaaf4382.

Shou, W., Seol, J.H., Shevchenko, A., Baskerville, C., Moazed, D., Chen, Z.W.S., Jang, J., Shevchenko, A., Charbonneau, H., and Deshaies, R.J. (1999). Exit from Mitosis Is Triggered by Tem1-Dependent Release of the Protein Phosphatase Cdc14 from Nucleolar RENT Complex. Cell *97*, 233–244.

Shou, W., Azzam, R., Chen, S.L., Huddleston, M.J., Baskerville, C., Charbonneau, H., Annan, R.S., Carr, S.A., and Deshaies, R.J. (2002). Cdc5 influences phosphorylation of Net1 and disassembly of the RENT complex. BMC Mol. Biol. 14.

Stegmeier, F., and Amon, A. (2004). Closing Mitosis: The Functions of the Cdc14 Phosphatase and Its Regulation. Annu. Rev. Genet. *38*, 203–232.

Stegmeier, F., Visintin, R., and Amon, A. (2002). Separase, Polo Kinase, the Kinetochore Protein Slk19, and Spo12 Function in a Network that Controls Cdc14 Localization during Early Anaphase. Cell *108*, 207–220.

Stoepel, J., Ottey, M.A., Kurischko, C., Hieter, P., and Luca, F.C. (2005). The Mitotic Exit Network Mob1p-Dbf2p Kinase Complex Localizes to the Nucleus and Regulates Passenger Protein Localization□D □V. Mol. Biol. Cell *16*, 15.

Sullivan, M., Higuchi, T., Katis, V.L., and Uhlmann, F. (2004). Cdc14 Phosphatase Induces rDNA Condensation and Resolves Cohesin-Independent Cohesion during Budding Yeast Anaphase. Cell *117*, 471–482.

Swaney, D.L., Beltrao, P., Starita, L., Guo, A., Rush, J., Fields, S., Krogan, N.J., and Villén, J. (2013). Global analysis of phosphorylation and ubiquitylation cross-talk in protein degradation. Nat. Methods *10*, 676–682.

Torres-Rosell, J., Machín, F., Jarmuz, A., and Aragón, L. (2004). Nucleolar Segregation Lags Behind the Rest of the Genome and Requires Cdc14p Activation by the FEAR Network. Cell Cycle *3*, 494–500.

Villén, J., and Gygi, S.P. (2008). The SCX/IMAC enrichment approach for global phosphorylation analysis by mass spectrometry. Nat. Protoc. *3*, 1630–1638.

Visintin, R., and Amon, A. (2001). Regulation of the mitotic exit protein kinases Cdc15 and Dbf2. Mol. Biol. Cell *12*, 2961–2974.

Visintin, C., Tomson, B.N., Rahal, R., Paulson, J., Cohen, M., Taunton, J., Amon, A., and Visintin, R. (2008). APC/C-Cdh1-mediated degradation of the Polo kinase Cdc5 promotes the return of Cdc14 into the nucleolus. Genes Dev. *22*, 79–90.

Visintin, R., Hwang, E.S., and Amon, A. (1999). Cfi1 prevents premature exit from mitosis by anchoring Cdc14 phosphatase in the nucleolus. *398*, 6.

Yang, X., Jost, A.P.-T., Weiner, O.D., and Tang, C. (2013). A light-inducible organelle-targeting system for dynamically activating and inactivating signaling in budding yeast. Mol. Biol. Cell *24*, 2419–2430.

Yoshida, S., and Toh-e, A. (2002). Budding yeast Cdc5 phosphorylates Net1 and assists Cdc14 release from the nucleolus. Biochem. Biophys. Res. Commun. *294*, 687–691.

Yu, F.-X., and Guan, K.-L. (2013). The Hippo pathway: regulators and regulations. Genes Dev. *27*, 355–371.

Figure 1. Dbf2-Mob1 transiently localizes to the nucleolus in late anaphase.

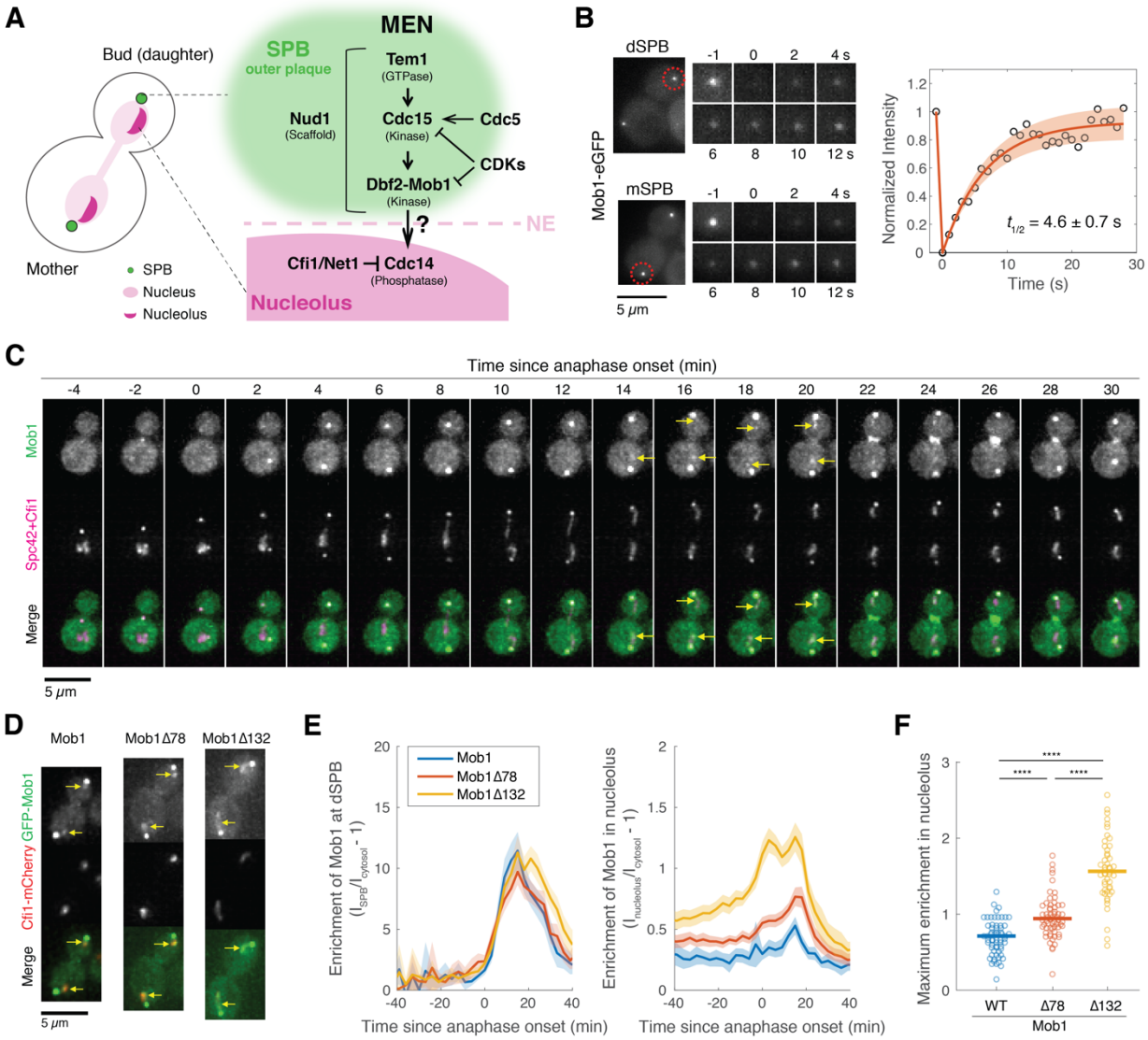

(**A**) Major components of the MEN and their subcellular localization.
(**B**) FRAP analysis of Mob1-eGFP (A39695). Red circles indicate the area of photo-bleaching. Cells were grown and imaged at room temperature in SC medium + 2% glucose. Graph to the right represents average measurements of double normalized fluorescence intensities (n = 6 cells) after correcting for photo-bleaching during acquisition. Red curve is the average fit and shaded area represents standard deviation (SD) of the fits. Half recovery time $t_{1/2}$ ± SD is indicated.
(**C**) Localization of Mob1 during the cell cycle. A40257 (with Mob1-eGFP, Cfi1-mCherry and Spc42-mCherry) cells were grown at room temperature in SC medium + 2% glucose and imaged every minute for 2 hours. Arrows highlight the nucleolar localization.
(**D**) Nucleolar localization of full-length (A39931) and N-terminally truncated (A39933 and A39935) Mob1. Cells were grown at room temperature in SC medium + 2% glucose and imaged every 3 minutes for 4 hours. Arrows highlight the nucleolar localization.

(**E**) Enrichment of Mob1 (A41211, *n* = 62 cells), Mob1Δ78 (A41212, *n* = 60 cells) and Mob1Δ132 (A41213, *n* = 48 cells) at the dSPB (left) and in the nucleolus (right) as a function of cell cycle progression. Cells were grown at 25°C in SC medium + 2% glucose and imaged every 3 minutes for 4 hours. Single cell traces were aligned based on anaphase onset, as defined as spindle length > 3 μm (Figure1-figure supplement 1F, measured based on SPB marker Spc42-mCherry), and averaged. Solid lines represent the average, shaded areas represent 95% confidence intervals.
(**F**) Maximum enrichment of full-length Mob1 (WT) and truncated Mob1 (Mob1Δ78 and Mob1Δ132) in the nucleolus in anaphase of cells in (E). Solid lines represent the median. ****$P < 0.0001$ by two-sided Wilcoxon rank sum test.

Figure 2. Dbf2-Mob1 localizes to the nucleolus through interacting with Cfi1/Net1.

A

# of peptides detected		Bait (TurboID tagged)				
		Mob1	Dbf2	Tem1	Cdc15	Untagged
Hits	Cfi1	84	45	0	0	0
	Dbf2/Dbf20	16	9	2	5	1
	Mob1	12	4	0	0	0
	Nud1	5	2	2	2	0

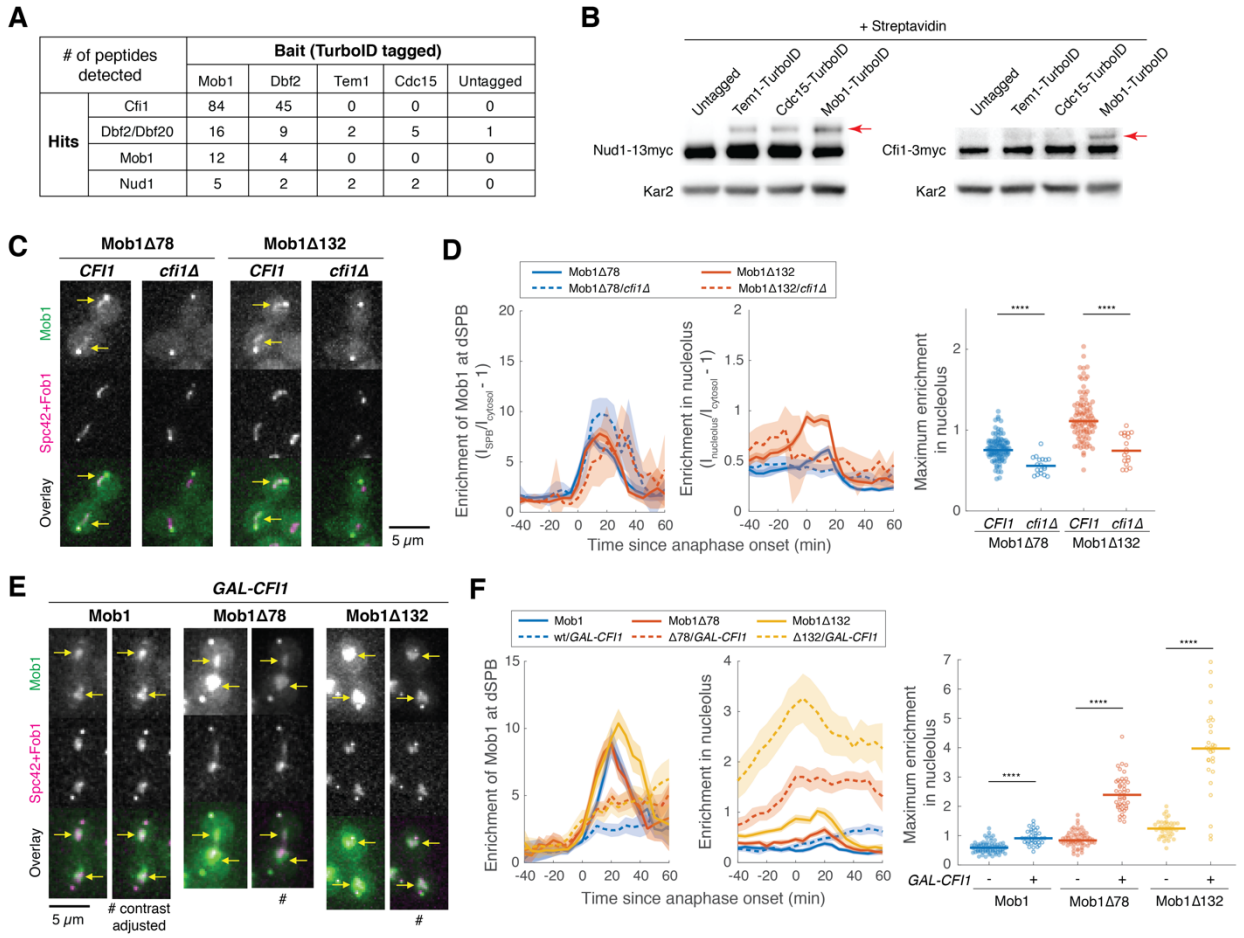

(**A**) Results of proximity-based biotinylation with TurboID for MEN proteins (A41367, A41370, A41368, A41369 and A2588). Cells were grown at room temperature in YEP + 2% glucose + 50 μM biotin.

(**B**) Streptavidin gel-shift assays to probe the interactions of TurboID-labeled MEN proteins with the MEN scaffold Nud1 (left, A11869, A41381, A41382 and A41380) or Cfi1/Net1 (right, A1638, A41406, A41407 and A41372). Cells were grown at room temperature in YEP + 2% glucose and lysates were treated with streptavidin and immunoblotted as indicated. Red arrows highlight biotinylated proteins.

(**C** and **D**) Representative images (C) and quantification (D) of Mob1Δ78 localization in wild-type *CFI1/NET1* (A41344, n = 106 cells) or *cfi1/net1Δ* (A41347, n = 18 cells) cells and Mob1Δ132 localization in *CFI1/NET1* (A41345, n = 95 cells) or *cfi1/net1Δ* (A41348, n = 18 cells) cells. Cells were grown at 25°C in SC medium + 2% glucose and imaged every 5 minutes for 4 hours. Arrows highlight nucleolar localization.

(**E** and **F**) Representative images (E) and quantification (F) of Mob1 localization in wild-type (A41343, n = 110 cells) or *GAL-CFI1/NET1* expressing cells (A41340, n = 71 cells), Mob1Δ78 localization in wild-type (A41344, n = 103 cells) or *GAL-CFI1/NET1* expressing cells (A41341,

n = 68 cells), and Mob1Δ132 localization in wild-type (A41345, *n* = 71 cells) or cells expressing *GAL-CFI1/NET1* (A41342, *n* = 53 cells). # denotes that the image was linearly contrast adjusted to avoid over-saturation for Mob1Δ78 and Mob1Δ132. Cells were first grown at room temperature in SC medium + 2% raffinose. Cells were then mounted onto agarose pads made with SC medium + 1% raffinose + 1% galactose and imaged every 5 minutes for 5 hours at 25°C. Arrows highlight nucleolar localization. Solid lines represent the average of single cell traces aligned to anaphase onset while shaded areas represent 95% confidence intervals. For maximum enrichment, each dot represents a single cell. The solid lines represent the median. ****$P < 0.0001$ by two-sided Wilcoxon rank sum test.

Figure 3. *CDC15* regulates nuclear access of Dbf2-Mob1.

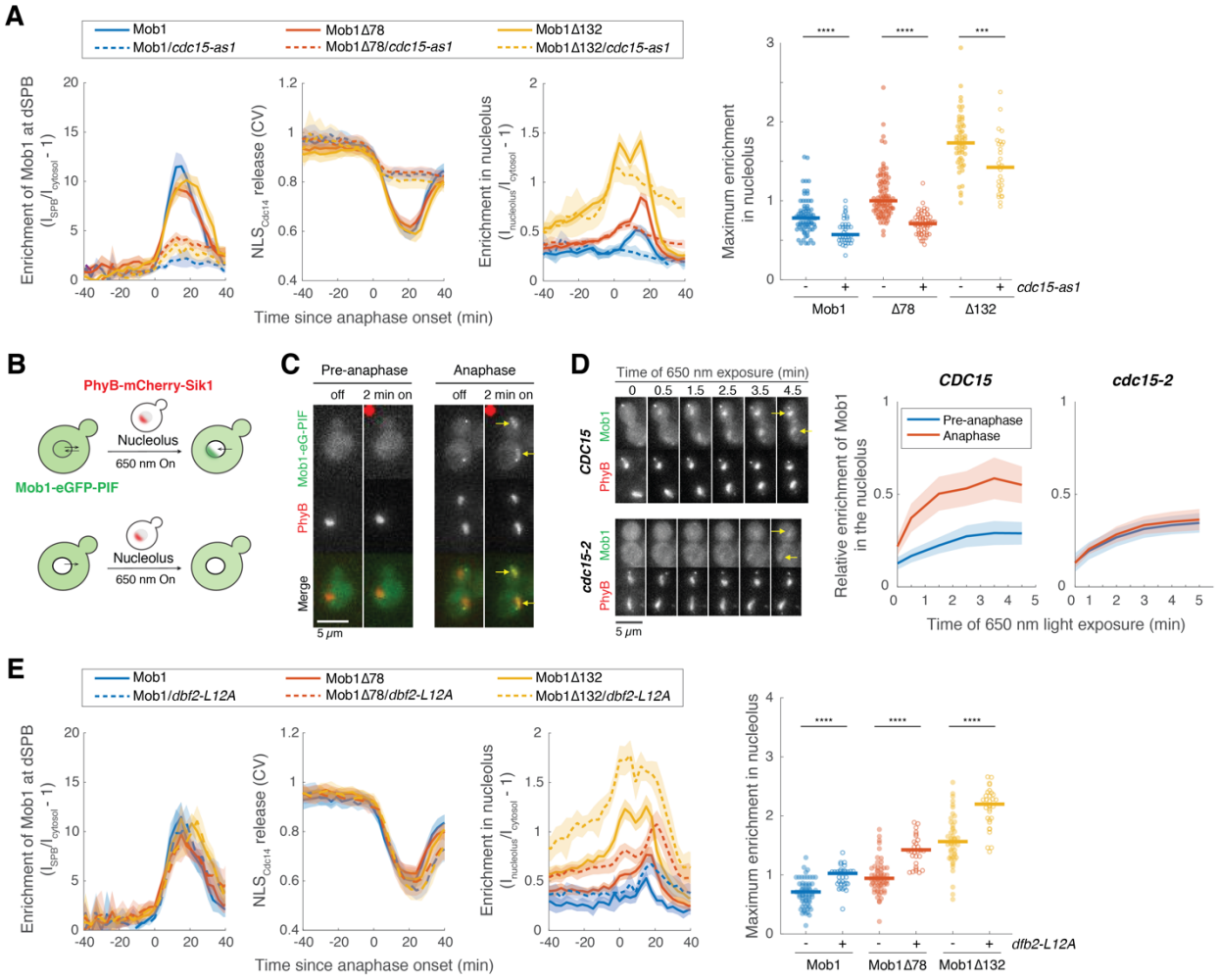

(**A**) Enrichment of Mob1 at the dSPB, in the nucleolus, and Dbf2-Mob1's kinase activity were determined in cells going through anaphase in *CDC15* (A41211, A41212, and A41213; n = 74, 94, and 55 cells respectively) or *cdc15-as1* (A41214, A41215, and A41216; n = 37, 63, and 30 cells respectively) cells. Cells were grown at 25°C in SC medium + 2% glucose and 10 μM 1-NA-PP1 and imaged every 3 minutes for 4 hours.

(**B**) Probing Dbf2-Mob1's nuclear access by recruiting Mob1 to the nucleolus with the PhyB-PIF optogenetics system. By anchoring PhyB to the nucleolus, diffuse nuclear Dbf2-Mob1, if present, can be visualized by recruiting Mob1-eGFP-PIF to the nucleolus.

(**C**) Recruiting Mob1 to the nucleolus at different cell cycle stages. A40260 cells were grown at 25°C in SC medium + 2% glucose, imaged after a 2-hour incubation with 12.5 μM PCB in the dark. Red dot denotes the frame where 650 nm light was applied to activate PhyB. Yellow arrows highlight the light-induced recruitment.

(**D**) Recruitment of Mob1 to the nucleolus in *CDC15* (A41360) or *cdc15-2* (A41361) cells. Quantifications of Mob1's enrichment in the nucleolus as a function of PhyB activation time in *CDC15* (A41360, n = 27 and 16 cells for pre-anaphase and anaphase respectively) or *cdc15-2*

(A41361, n = 14 and 36 cells for pre-anaphase and anaphase respectively) cells. Cells were grown at room temperature in SC medium + 2% glucose, incubated with 12.5 μM PCB for 2 hours in the dark, and shifted to 34 °C for 50 minutes before imaging.
(**E**) Nucleolar enrichment of wild-type and truncated Mob1 in wild-type and *dbf2-L12A* cells (A41394, A41395 and A41396; n = 32, 28 and 31 cells respectively). Wild-type traces for comparison were the same as in Fig. 1E. Cells were grown similarly as in Fig. 1E.
For graphs in (A) and (E), solid lines represent the average of single cell traces aligned to anaphase onset. Shaded areas represent 95% confidence intervals. For maximum enrichment, each dot represents a single cell. Solid lines represent the median. ****$P < 0.0001$; ***$P < 0.001$ by two-sided Wilcoxon rank sum test.

Figure 4. Nucleolar localization of Dbf2-Mob1 is regulated by *CDC5* independently of *CDC15*.

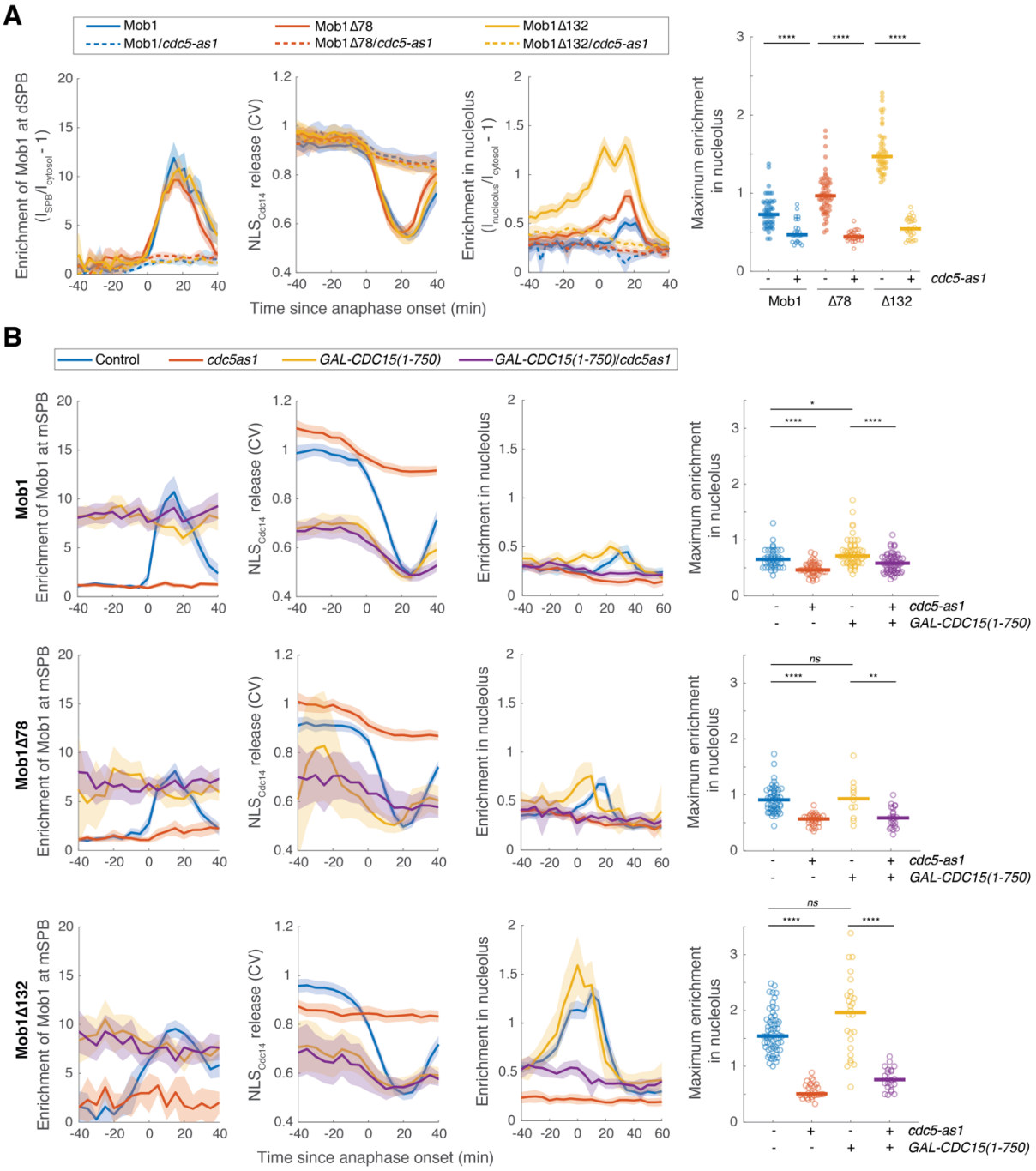

(**A**) Enrichment of Mob1 at the dSPB, in the nucleolus, and Dbf2-Mob1's kinase activity in cells wild-type for *CDC5* (A41211, A41212, and A41213; *n* = 49, 60 and 47 cells respectively) or harboring a *cdc5-as1* allele (A41334, A41335, and A41336; *n* = 23, 30 and 28 cells respectively). Cells were grown at 25°C in SC medium + 2% glucose and 5 µM CMK and imaged every 3 minutes for 4 hours.

(**B**) Cells harboring *GAL-CDC15(1-750)* and *cdc5-as1* either containing *eGFP-MOB1* (A41211, A41334, A41376 and A41337; n = 44, 41, 58 and 61 cells respectively), or *eGFP-MOB1Δ78* (A41212, A41335, A41377, and A41338; n = 54, 30, 12 and 22 cells respectively), or *eGFP-MOB1Δ132* (A41213, A41336, A41378 and A41339; n = 62, 28, 26 and 22 cells respectively) were analyzed to determine Mob1 localization. Localization to the mSPB instead of dSPB was quantified here because cells expressing *GAL-CDC15(1-750)* often exit from mitosis in the mother (without movement of a SPB into the bud). For cells exited with two SPBs in the mother cell, maximum intensities of the two SPBs were used. Cells were grown at 25°C in SC medium + 1% raffinose, 1% galactose and 5 μM CMK and imaged every 5 minutes for 5 hours. Solid lines represent the average of single cell traces aligned to anaphase onset. Shaded areas represent 95% confidence intervals. For maximum enrichment, each dot represents a single cell. Solid lines represent the median. ****$P < 0.0001$; **$P < 0.01$; *$P < 0.05$ by two-sided Wilcoxon rank sum test.

Figure 5. Cdc5 promotes Dbf2-Mob1's nucleolar localization by phosphorylating Cfi1/Net1.

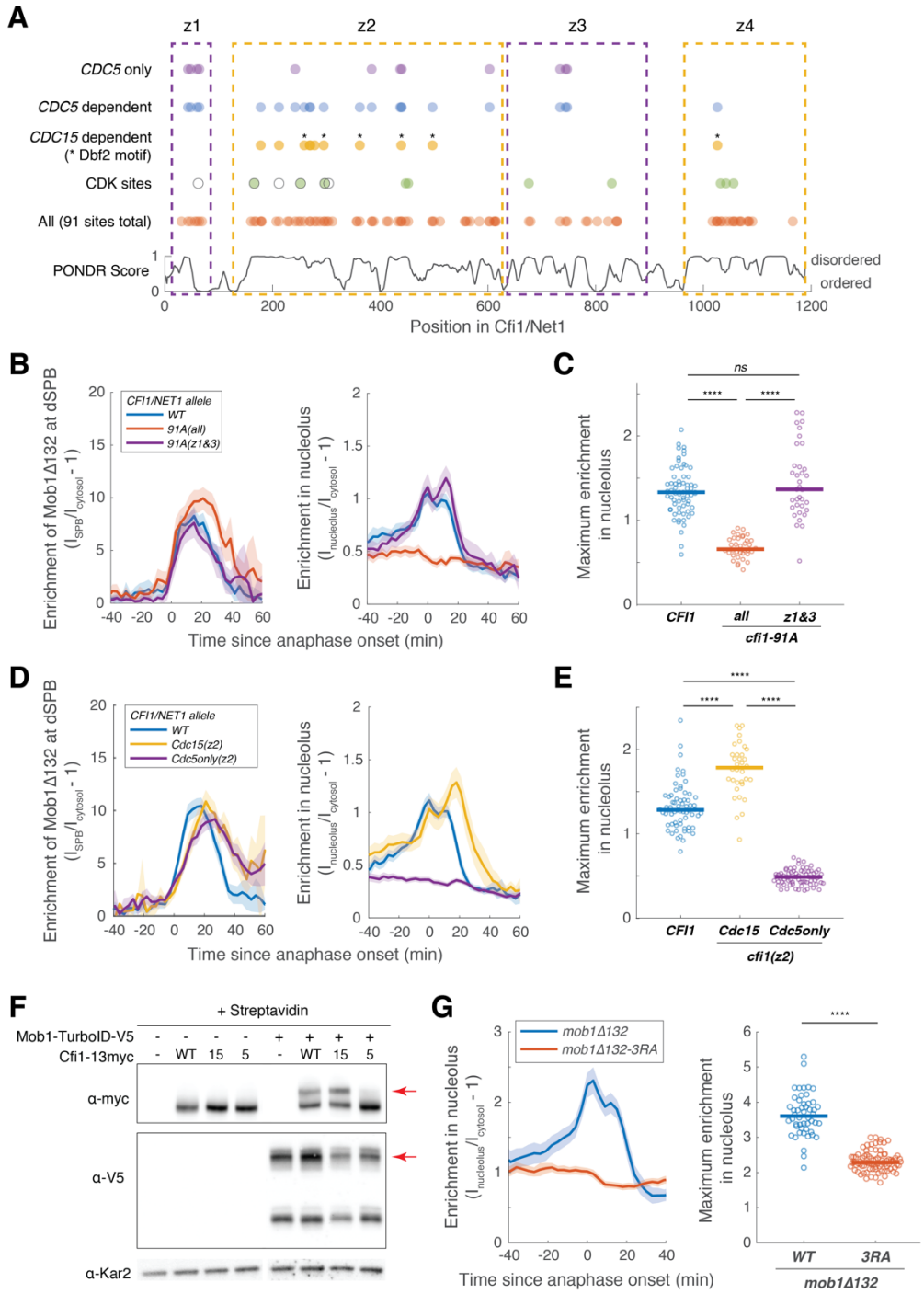

(**A**) Distribution of all, CDK sites, *CDC15*- and *CDC5*-dependent phosphorylation sites (Table S4) and disordered regions in Cfi1/Net1. For CDK sites, open circles represent sites identified and mutated in Azzam et al. 2004 (*cfi1*/*net1-6Cdk*) and filled circles represent sites identified in Holt et al. 2009. Dashed boxes denote the four zones.

(**B-E**) Localization of Mob1Δ132 in *CFI1/NET1* (A41411, *n* = 67 cells for B-C and 66 cells for D-E), *cfi1-91A* mutants (A41412 and A41413, *n* = 36 and 35 cells), *cfi1-Cdc15(z2)* (A41593, *n* = 34 cells) or *cfi1-Cdc5only(z2)* (A41594, *n* = 69 cells). Cells were grown at 25°C in SC medium + 2% glucose and imaged every 3 minutes for 4 hours.
(**F**) Streptavidin gel-shift assays to probe the interactions between TurboID-tagged Mob1 and different *CFI1/NET1* alleles (from left to right: A2587, A41596, A41597, A41598, A41379, A41611, A41612, A41613). -, not tagged; WT, wild-type Cfi1-13myc; 15, Cfi1-Cdc15(z2)-13myc; 5, Cfi1-Cdc5only(z2)-13myc. Cells were grown at room temperature in YEP + 2% glucose and lysates were treated with streptavidin and immunoblotted as indicated. Red arrows highlight biotinylated proteins.
(**G**) Enrichment of Mob1Δ132 (A41664, *n* = 50 cells) or Mob1Δ132-3RA (A41665, *n* = 85 cells) in the nucleolus. Cells were grown at 25°C in SC medium + 2% glucose and imaged every 3 minutes for 4 hours.
For graphs in (B-E and G), solid lines represent the average of single cell traces aligned to anaphase onset. Shaded areas represent 95% confidence intervals. For maximum enrichment, each dot represents a single cell. Solid lines represent the median. ****$P < 0.0001$ by two-sided Wilcoxon rank sum test.

Figure 6. MEN and Cdc5 promote release of Cdc14 from the nucleolus by phosphorylating Cfi1/Net1.

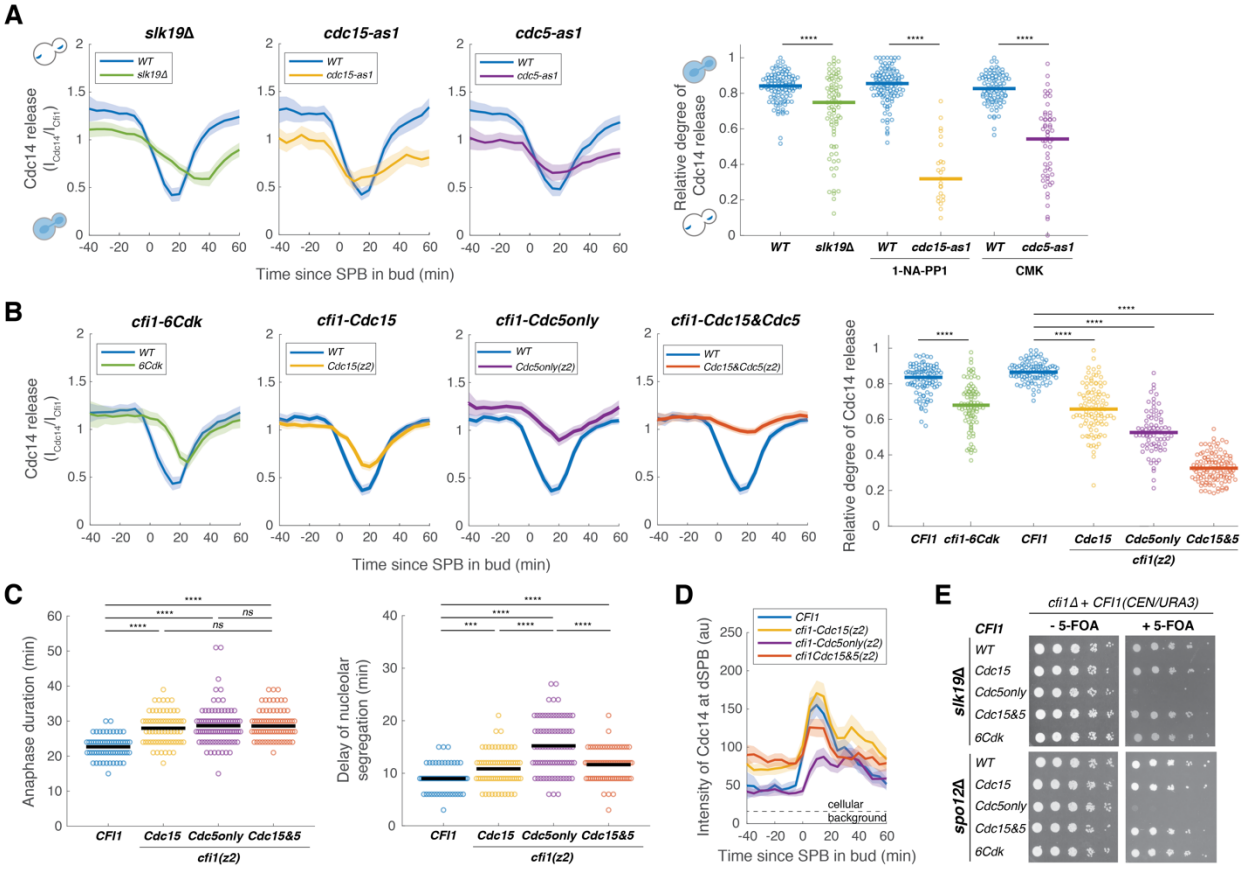

(**A**) Cdc14 nucleolar release kinetics in wild-type (A41387, n = 134, 123 and 96 cells for each condition), *slk19*Δ (A41410, n = 86 cells), *cdc15-as1* (A41408, n = 38 cells) or *cdc5-as1* mutant (A41409, n = 61 cells). Cells were grown at 25°C in SC medium + 2% glucose with corresponding inhibitors and imaged every 5 minutes for 5 hours. Release of Cdc14 from the nucleolus was quantified as the ratio of fluorescence intensity of Cdc14-eGFP to Cfi1/Net1-mScarlet in the nucleolus (I_{Cdc14}/I_{Cfi1}). Relative degree of Cdc14 release from the nucleolus was calculated as the normalized minimal Cdc14 level in the nucleolus: $(I_{Cdc14}(t_{min})/I_{Cfi1}(t_{min}))/(I_{Cdc14}(t_{-20})/I_{Cfi1}(t_{-20}))$ where t_{min} represents the frame with minimal Cdc14 level in the nucleolus and t_{-20} represent 20 min before movement of the SPB into bud.

(**B**) Cdc14 nucleolar release kinetics in cells harboring wild-type *CFI1/NET1* (A41387, n = 102 and 114 cells) or *CFI1/NET1* phospho-mutants for CDK sites (A41420, n = 95 cells), Cdc15 sites (A41587, n = 104 cells), Cdc5 sites (A441588, n = 86 cells), and Cdc15&Cdc5 sites (A41589, n = 131 cells). Cells were grown at 25°C in SC medium + 2% glucose and imaged every 5 minutes for 5 hours.

(**C**) Distribution of anaphase duration and relative delay of nucleolar segregation for different *CFI1/NET1* phospho-mutants (A41436, A41590, A41591 and A41592; n = 76, 85, 99, 92 cells respectively) measured using the SPB marker Spc42-eGFP and the nucleolar marker Cfi1/Net1-

mScarlet- I (see Figure 6-figure supplement 3 for details). Cells were grown at 25°C in SC medium + 2% glucose and imaged every 3 minutes for 4 hours.
(**D**) Intensities of Cdc14-eGFP at dSPBs in different *CFI1/NET1* phospho-mutant cells (A41387, A41587, A441588 and A41589; n = 80, 82, 77 and 89 cells respectively). Cells were grown and imaged as in (B).
(**E**) Genetic interactions between different *CFI1/NET1* phospho-mutants and *slk19*Δ (A41645, A41646, A41647, A41648, A41649) or *spo12*Δ (A41650, A41651, A41652, A41653, A41654) analyzed by plasmid shuffling (see Methods for details). 5-fold serial dilutions were spotted onto plates with or without 5'-fluoroorotic acid (5-FOA) and incubated at 25°C for 2 to 3 days. The presence of 5-FOA selects cells that are viable after losing the *CFI1(URA3/CEN)* plasmid.
For all graphs, single cell traces were aligned to the frame where the dSPB entered the bud and averaged. Solid lines represent the average. Shaded areas represent 95% confidence intervals. For distributions, each dot represents a single cell. Solid lines represent the median for (A-B) and the mean for (C). ****$P < 0.0001$; ***$P < 0.001$; **$P < 0.01$; *$P < 0.05$ by two-sided Wilcoxon rank sum test.

Figure 7. Phosphorylation of Cfi1/Net1 by Cdc5 and Dbf2-Mob1 promotes mitotic exit.

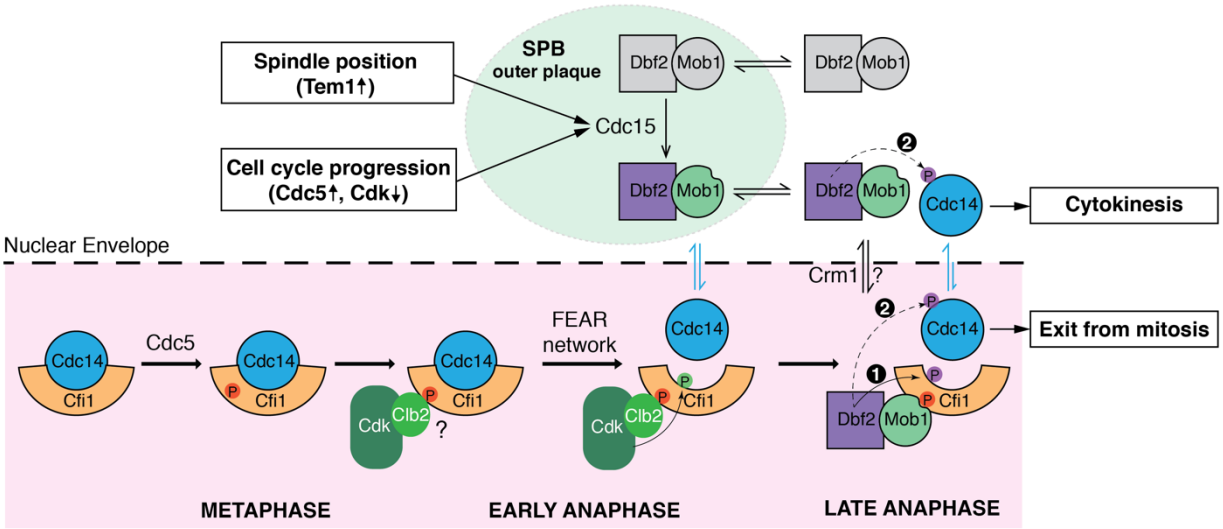

A model for Cdc14 activation. In metaphase, Cdc5 phosphorylates Cfi1/Net1 in the nucleolus to prepare for Cdc14 release/activation in anaphase. Upon anaphase onset, the FEAR network promotes phosphorylation of Cfi1/Net1 by Clb2-Cdk1 which results in transient release of Cdc14 from the nucleolus. In the meantime, the MEN kinase Cdc15 is activated integrating inputs from both spindle position (via Tem1) and cell cycle progression (via Cdc5 and CDK activities). Activated (SPB-localized) Cdc15 phosphorylates the SPB outer plaque protein Nud1 which creates a dynamic docking site for the MEN terminal kinase complex Dbf2-Mob1 and facilitates phosphorylation and activation of Dbf2-Mob1 by Cdc15. Activated Dbf2-Mob1 gains access to the nucleus and is targeted to the nucleolus by interacting with Cdc5-primed Cfi1/Net1. Nucleolar Dbf2-Mob1 then phosphorylates Cfi1/Net1, keeping Cdc14 dissociated from its nucleolar inhibitor to trigger exit from mitosis. In addition, active Dbf2-Mob1 in the nucleolus and/or cytoplasm phosphorylates Cdc14 at its NLS resulting in cytoplasmic retention of Cdc14 to facilitate cytokinesis.

Figure 1–figure supplement 1: N-terminally truncated Mob1 is hyperactive.

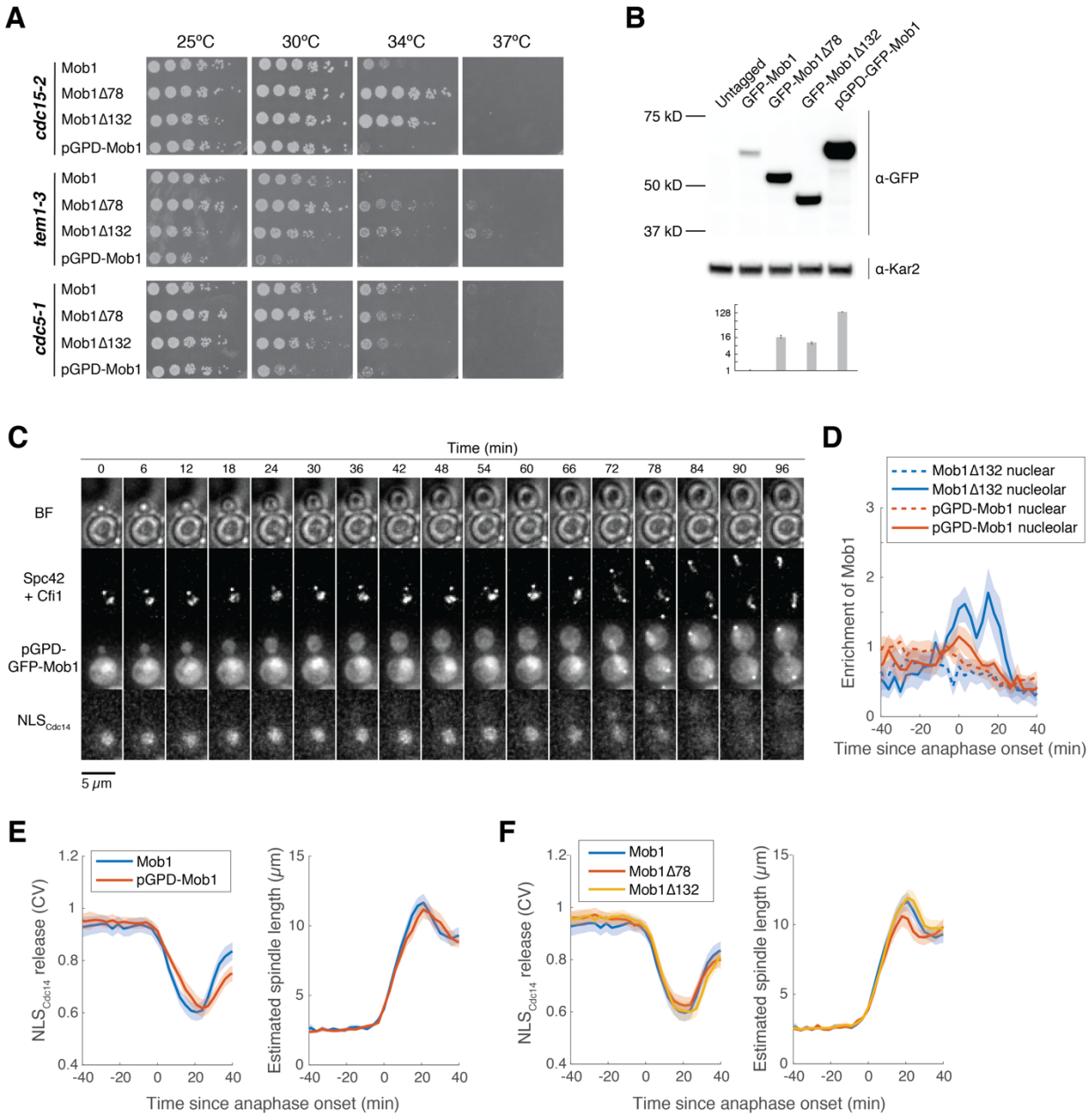

(**A**) 5-fold serial dilutions of *cdc15-2* (A41424, A41425, A41426, A41427), *tem1-3* (A41429, A41430, A41431, A41428) and *cdc5-1* (A41432, A41433, A41434, A41435) harboring the indicated *MOB1* constructs in YEP + 2% glucose at the indicated temperatures.
(**B**) Immunoblot (top) and quantification (bottom) of untagged (A2587), full-length (A41351) and truncated GFP-Mob1 (A41352, A41353) as well as full-length GFP-Mob1 expressed from the *pGPD*/*TDH3* promoter (A41350).
(**C**) Localization of GFP-Mob1 expressed under the control of *pGPD* promoter (A41595) during the cell cycle. Cells were grown and imaged as in Figure 1E. Increased nuclear but not nucleolar localization of Mob1 was observed.

(**D**) Enrichment of Mob1Δ132 (A41213, *n* = 14 cells) and pGPD-Mob1 (A41595, *n* = 17 cells) in the nucleolus (solid lines) compared to the nucleus (dashed lines) as a function of cell cycle progression. Cells were grown and imaged as in Figure 1E.
(**E**) Kinetics of MEN activation as measured by the release of NLS_{Cdc14} reporter from the nucleus (see Figure 1-figure supplement 2) and anaphase progression as indicated by spindle length for cells harboring Mob1 (A41213, *n* = 62 cells) or pGPD-Mob1 (A41595, *n* = 43 cells). pGPD-Mob1 slightly delays MEN activation and exit from mitosis.
(**F**) Kinetics of MEN activation and anaphase progression for experiments shown in Figure 1E. Mob1Δ78 slightly accelerated mitotic exit.
For graphs in (D-F), single cell traces were aligned based on anaphase onset and averaged. Solid lines represent the average, shaded areas represent 95% confidence intervals.

Figure 1–figure supplement 2: Mob1's nucleolar localization correlates with MEN activation and Cdc14 release from the nucleolus.

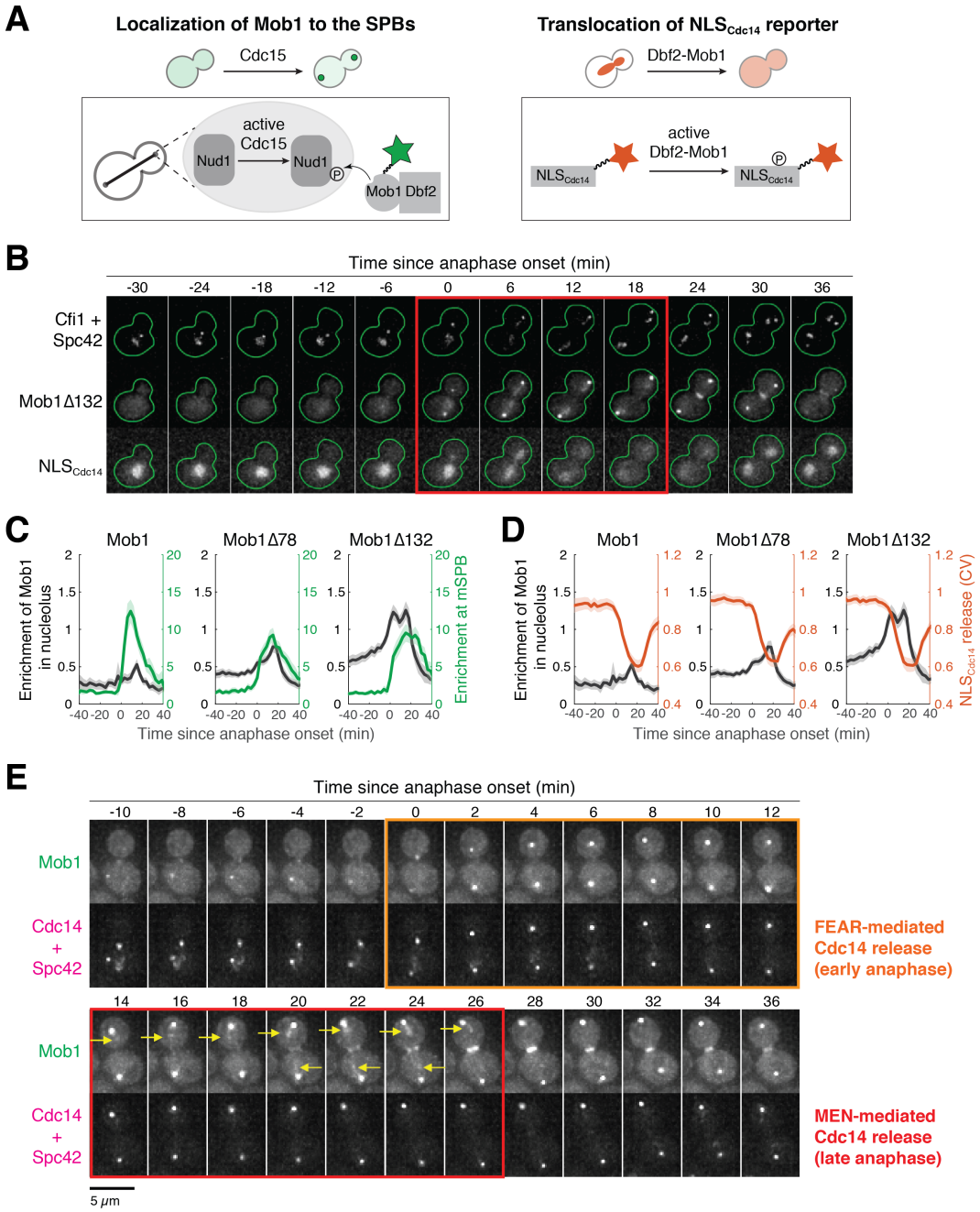

(**A**) Illustration of Mob1's SPB localization and translocation of NLS_{Cdc14} reporter in response to MEN activation.

(**B**) Localization of Mob1Δ132 and the MEN activity reporter NLS_{Cdc14} during the cell cycle. A41213 (*GFP-MOB1Δ132*, *CFI1/NET1-mCherry*, *SPC42-mCherry* and *NLS_{Cdc14}-ymiRFP670*) cells were grown as in Figure 1E. Red square indicates anaphase.

(**C**) Relative timing of nucleolar localization of Mob1 (black) and SPB localization of Mob1 (green) in cells harboring the indicated *MOB1* alleles.
(**D**) Relative timing of nucleolar localization of Mob1 (black) and release of the NLS_{Cdc14} reporter from the nucleus (red) in cells harboring the indicated *MOB1* alleles.
(**E**) Localization of Mob1 and Cdc14 during the cell cycle. A40314 (*MOB1-eGFP*, *SPC42-mCherry* and *CDC14-mCherry*) cells were grown at room temperature in SC medium + 2% glucose and imaged every 2 minutes for 4 hours. The colored squares indicate the frames where Cdc14 is released from the nucleolus mediated by either the FEAR network or the MEN. Yellow arrows highlight localization of Mob1 in the nucleolus.

Figure 2–figure supplement 1: TurboID identified interaction between Dbf2-Mob1 and Cfi1/Net1.

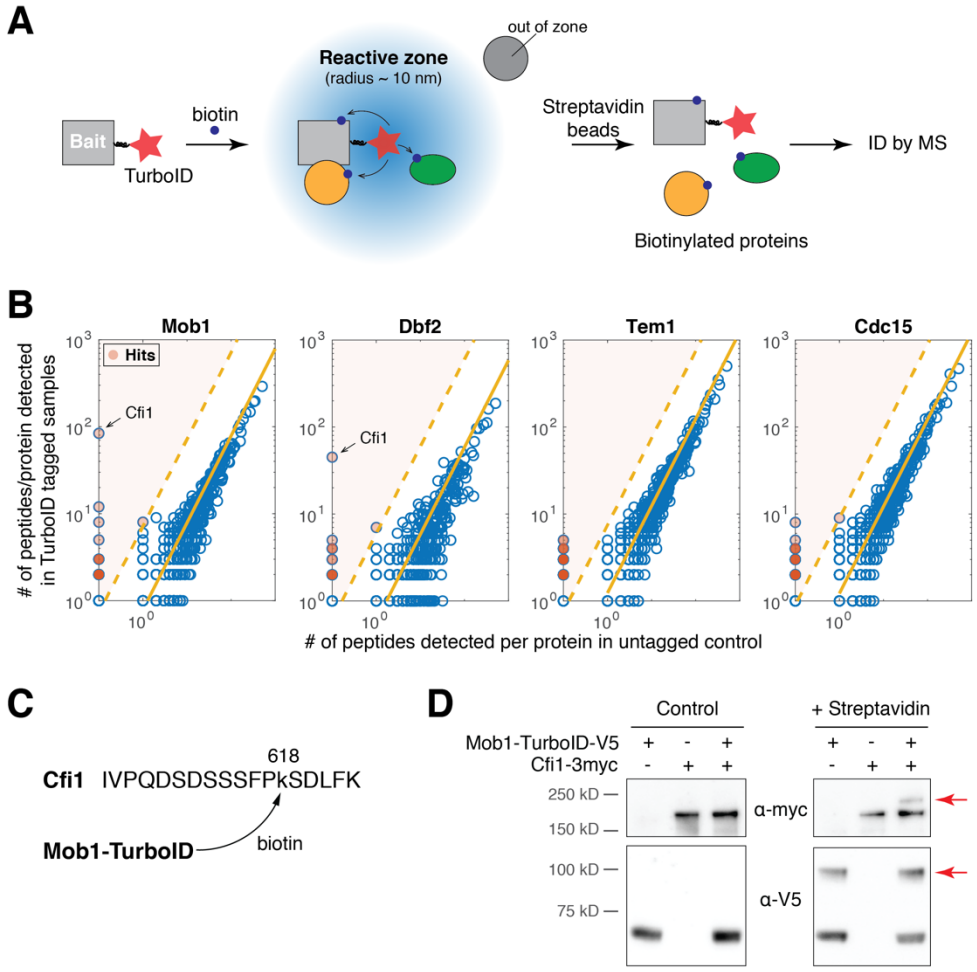

(**A**) Overview of TurboID proximity-based biotinylation to identify interaction partners of a target protein.
(**B**) Number of total peptides detected for MS-identified proteins in cells with TurboID tagged baits relative to untagged control cells (source data for Figure 2A). Shaded red dots represent proteins (hits) identified as interaction partners of the bait protein. Solid yellow lines denote the mean ratio of total peptide detected for all proteins. Dashed lines denote the threshold used for identifying hits (10 standard derivations above the mean).
(**C**) Biotinaylated peptide of Cfi1/Net1 detected in cells harboring Mob1-TurboID.
(**D**) Streptavidin gel-shift assay to probe the interaction between Mob1 and Cfi1/Net1. Lysates of A41379, A1638, and A41372 cells with or without streptavidin treatment were immunoblotted as indicated. Red arrows highlight biotinylated proteins.

Figure 3–figure supplement 1: Examining nuclear access of Dbf2-Mob1 by optogenetics.

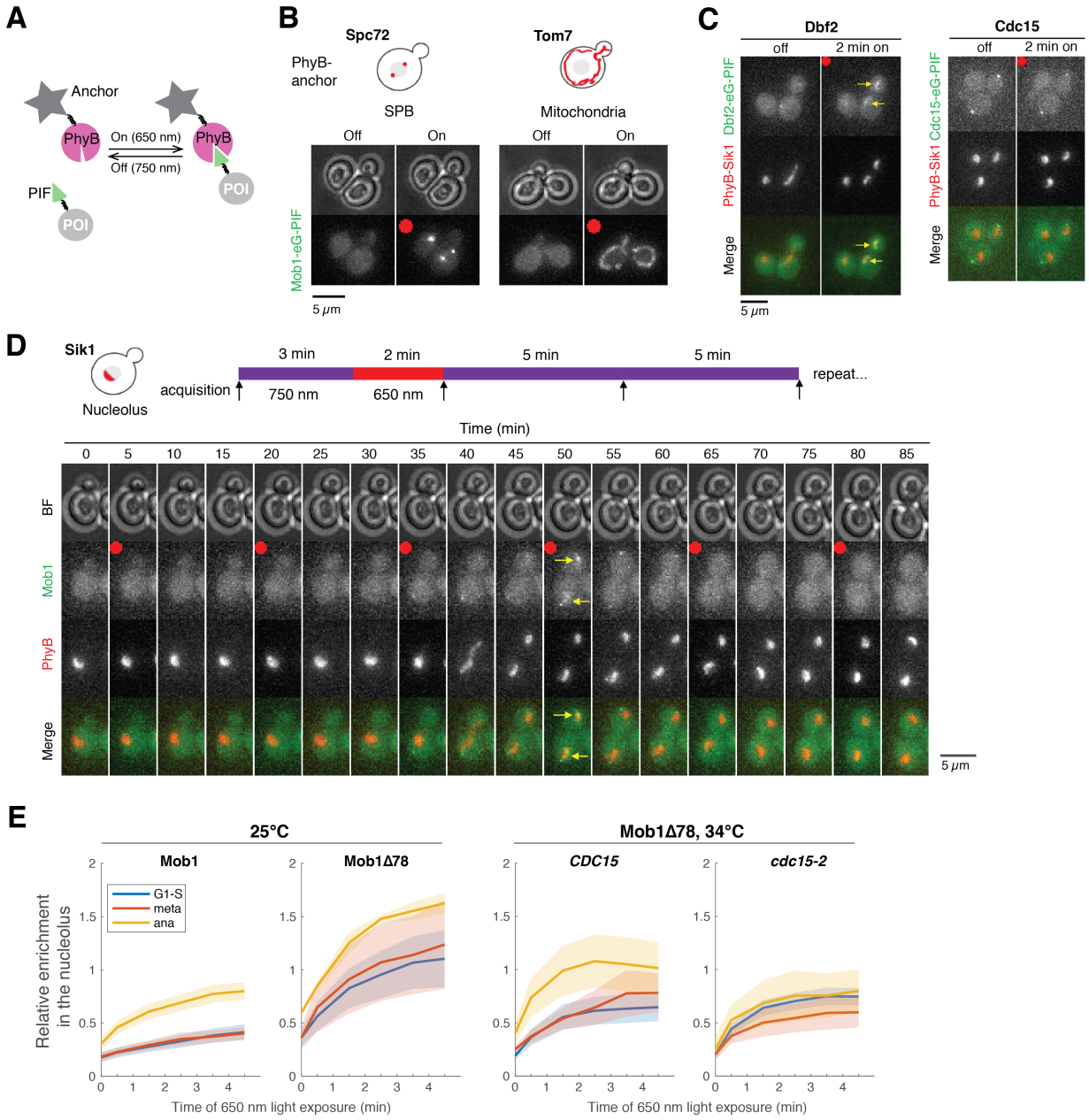

(**A**) The PhyB-PIF based light-inducible organelle targeting system. When exposed to 650 nm light, anchored PhyB interacts with PIF and thus targets protein of interest (POI) to designated subcellular regions. This interaction is reversed with exposure to 750 nm light.
(**B**) Recruiting Mob1 to SPBs (A40346) or the mitochondrial surface (A40354) with the PhyB-PIF optogenetics system. Cells were grown at room temperature in SC medium + 2% glucose, incubated with 12.5 μM PCB for 2 hours in the dark prior to imaging. Red dots indicate application of red light (650 nm) for 5 minutes to activate PhyB.

(**C**) Recruiting Dbf2 (A40262) or Cdc15 (A40258) to the nucleolus with PhyB-Sik1. Cells were grown similarly to (B). Yellow arrows highlight the light-induced recruitment.
(**D**) Probing Mob1's nuclear access during the cell cycle with PhyB-Sik1. A40260 cells were grown similarly to (B) and imaged every 5 minutes while the red light (650 nm) was applied for 2 minutes every 15 minutes. Red dots denote frames where 650 nm light was applied to activate PhyB prior to imaging as indicated in the cartoon above. Yellow arrows highlight the light-induced recruitment.
(**E**) Quantifications of enrichment of Mob1 in the nucleolus as a function of PhyB activation time for wild-type Mob1 (A41360; n = 22, 14, and 21 cells for G1-S, metaphase and anaphase respectively), Mob1Δ78 (A41366; n = 11, 6, and 2 cells for G1-S, metaphase and anaphase respectively) at 25°C and for Mob1Δ78 in *CDC15* (A41366; n = 25, 4, and 9 cells for G1-S, metaphase and anaphase respectively) or *cdc15-2* cells (A41365; n = 39, 9, and 10 cells for G1-S, metaphase and anaphase respectively) at 34°C. Cells were grown similarly to (B).

Figure 3–figure supplement 2: Identification of a functional NES in Dbf2.

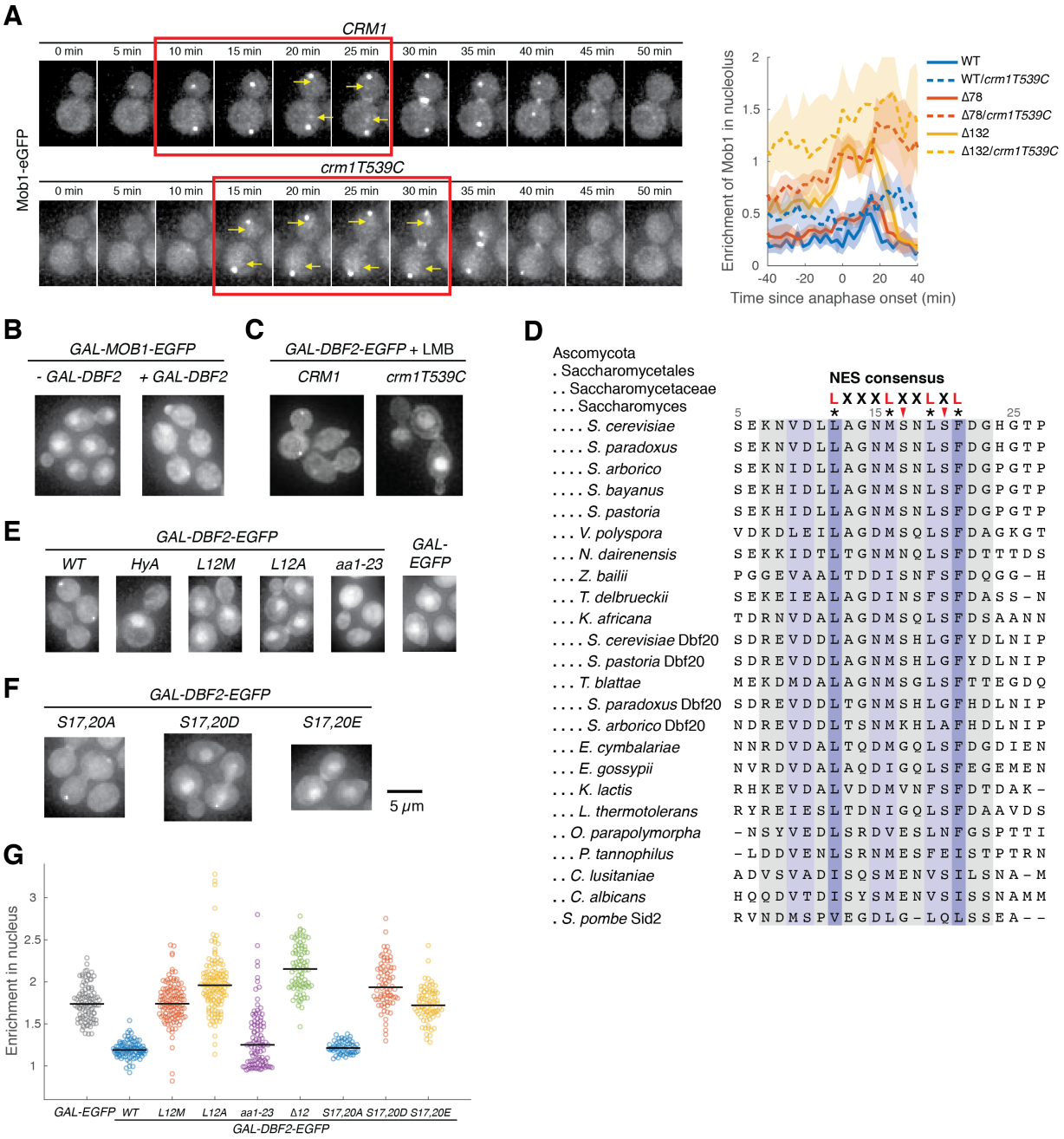

(**A**) Mob1's cellular localization when nuclear export is inhibited. Left, cells (A39893, A41349) were grown at room temperature in SC medium + 2% glucose and leptomycin B. Red box indicates anaphase and yellow arrows highlight increased nuclear and nucleolar localization. Right, comparison of nucleolar enrichment of Mob1 in *CRM1* (A41211, A41212 and A41213; n = 12, 18 and 11 cells respectively) and *crm1T539C* cells (A41373, A41374 and A41375; n = 13, 9 and 16 cells respectively). Cells were grown at 25°C in SC medium + 2% glucose with 100 ng/ml LMB and imaged every 3 minutes for 4 hours.

(**B**) Localization of overexpressed Mob1-eGFP from the *GAL1-10* promoter with (A41363) or without (A41364) co-overexpressing Dbf2 from the same promoter. Cells were grown in SC medium + 2% raffinose and mounted onto agarose pads made with SC medium + 1% raffinose and 1% galactose.
(**C**) Localization of overexpressed Dbf2-eGFP with (A41383) or without (A41384) inhibiting Crm1 with LMB. Cells were grown in SC medium + 2% raffinose and mounted onto agarose pad made with SC medium + 1% raffinose, 1% galactose and 100 ng/ml LMB.
(**D**) Alignment of Dbf2 homologs in *Saccharomycetes* and *S. pombe*.
(**E-G**) Localization of various Dbf2-eGFP mutants expressed from the *GAL1-10* promoter (A41388, A41389, A41386, A41390, A41391, A41392, A41393, A41440, A41441 and A41442; n = 97, 98, 123, 135, 120, 88, 58, 76 and 79 cells respectively). Cells were grown as in (B) and analyzed after 5 hours of growth in galactose containing medium.

Figure 3–figure supplement 3: Phosphorylation of Dbf2's NES partially regulates Dbf2-Mob1's nuclear access.

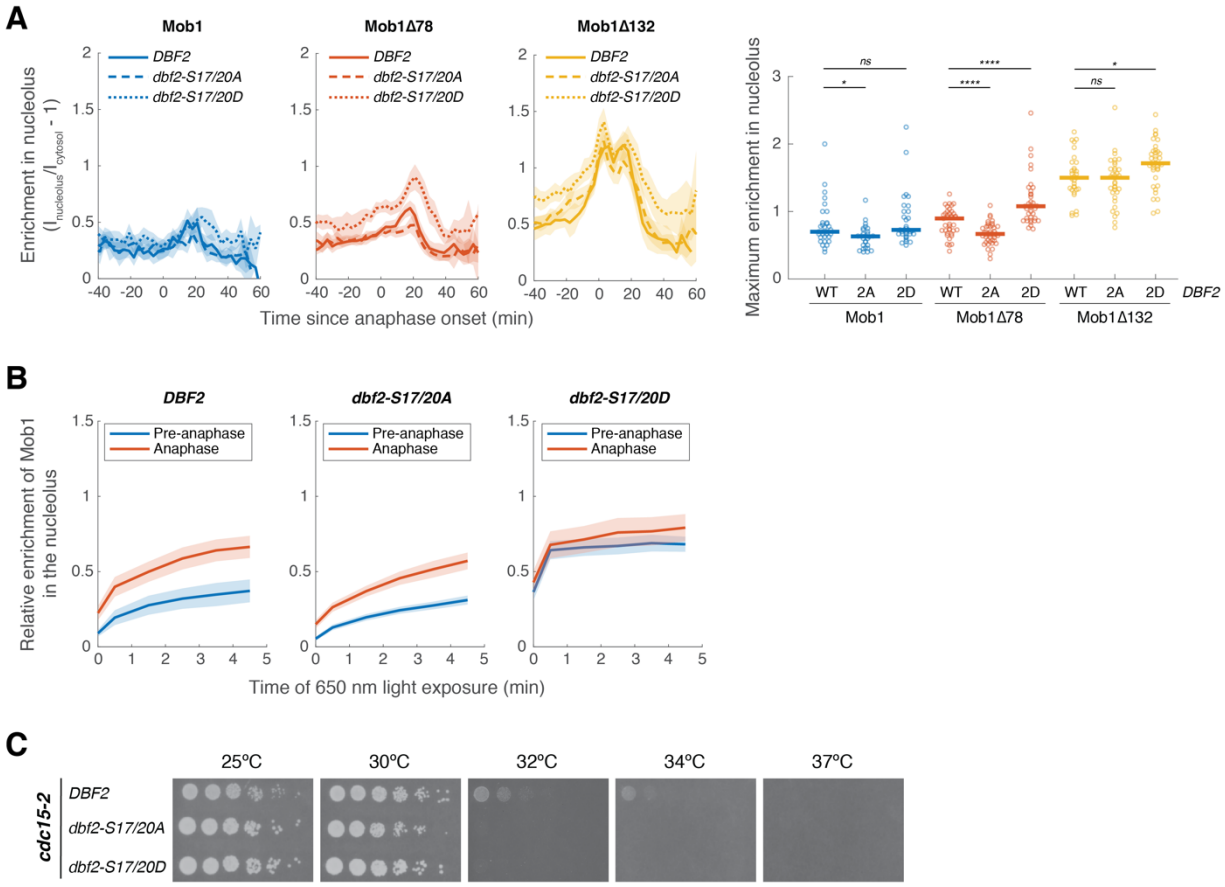

(**A**) Nucleolar enrichment of wild-type and truncated Mob1 in wild-type, *dbf2-S17/20A* or *dbf2-S17/20D* cells (A41614, A41617, A41620, A41615, A41618, A41621, A41616, A41619, A41622; n = 32, 28, 33,39, 43, 37, 31, 35 and 37 cells respectively). Cells were grown and imaged as in Figure 1E. Solid lines represent the average; shaded areas represent 95% confidence intervals. For maximum enrichment, each dot represents a single cell. Solid lines represent the median. ****$P < 0.0001$; *$P < 0.05$ by two-sided Wilcoxon rank sum test.
(**B**) Quantifications of enrichment of Mob1 in the nucleolus as a function of PhyB activation time for wild-type *DBF2* (A41608; n = 42 and 24 cells for pre-anaphase and anaphase, respectively), *dbf2-S17/20A* (A41609; n = 55 and 41 cells for pre-anaphase and anaphase, respectively) and *dbf2-S17/20D* (A41610; n = 58 and 28 cells for pre-anaphase and anaphase, respectively). Cells were grown as in Figure3-figure supplement 1.
(**C**) 5-fold serial dilutions of *cdc15-2* cells harboring wild-type *DBF2* (A41624), *dbf2-S17/20A* (A41625) or *dbf2-S17/20D* (A41626) in YEP + 2% glucose at the indicated temperatures.

Figure 4–figure supplement 1: Nucleolar localization of Dbf2-Mob1 does not depend on the FEAR network.

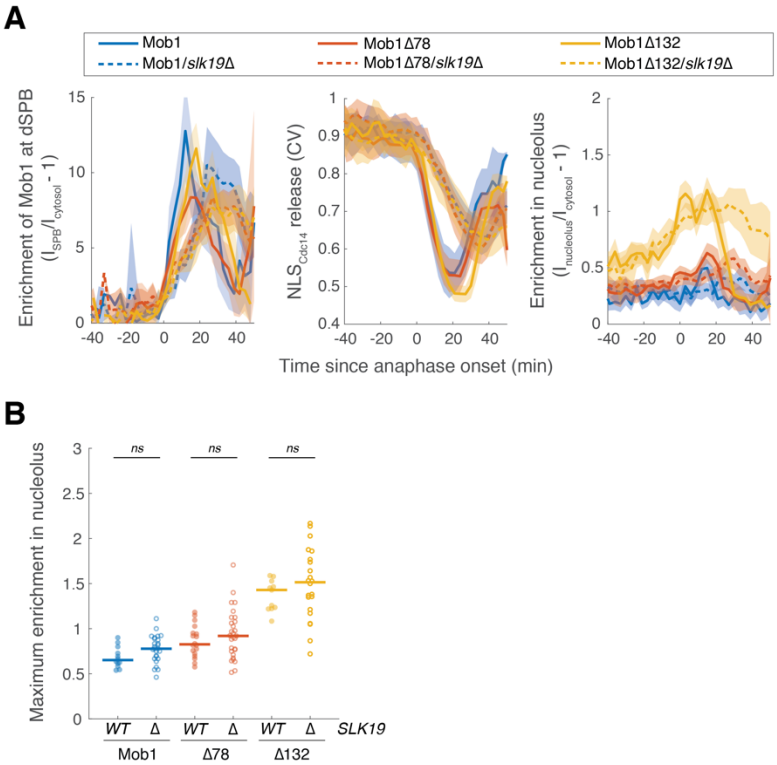

(**A**) Enrichment of Mob1 at the dSPB, in the nucleolus, and Dbf2-Mob1's kinase activity in wild-type (A41211, A41212 and A41213; n = 12, 18, 11) or *slk19*Δ (A41357, A41358, A41359; n = 26, 29, 22 cells) cells. Cells were grown at 25°C in SC medium + 2% glucose and imaged every 3 minutes for 4 hours. Solid lines represent the average of single cell traces aligned to anaphase onset. Shaded areas represent 95% confidence intervals.
(**B**) Maximum enrichment of Mob1 in the nucleolus. Each dot represents a single cell. The solid lines represent the median. *ns*, not significant ($P > 0.05$) by two-sided Wilcoxon rank sum test.

Figure 5–figure supplement 1: Phosphoproteomics identifies *CDC15* (MEN) and *CDC5* dependent phosphorylation in anaphase.

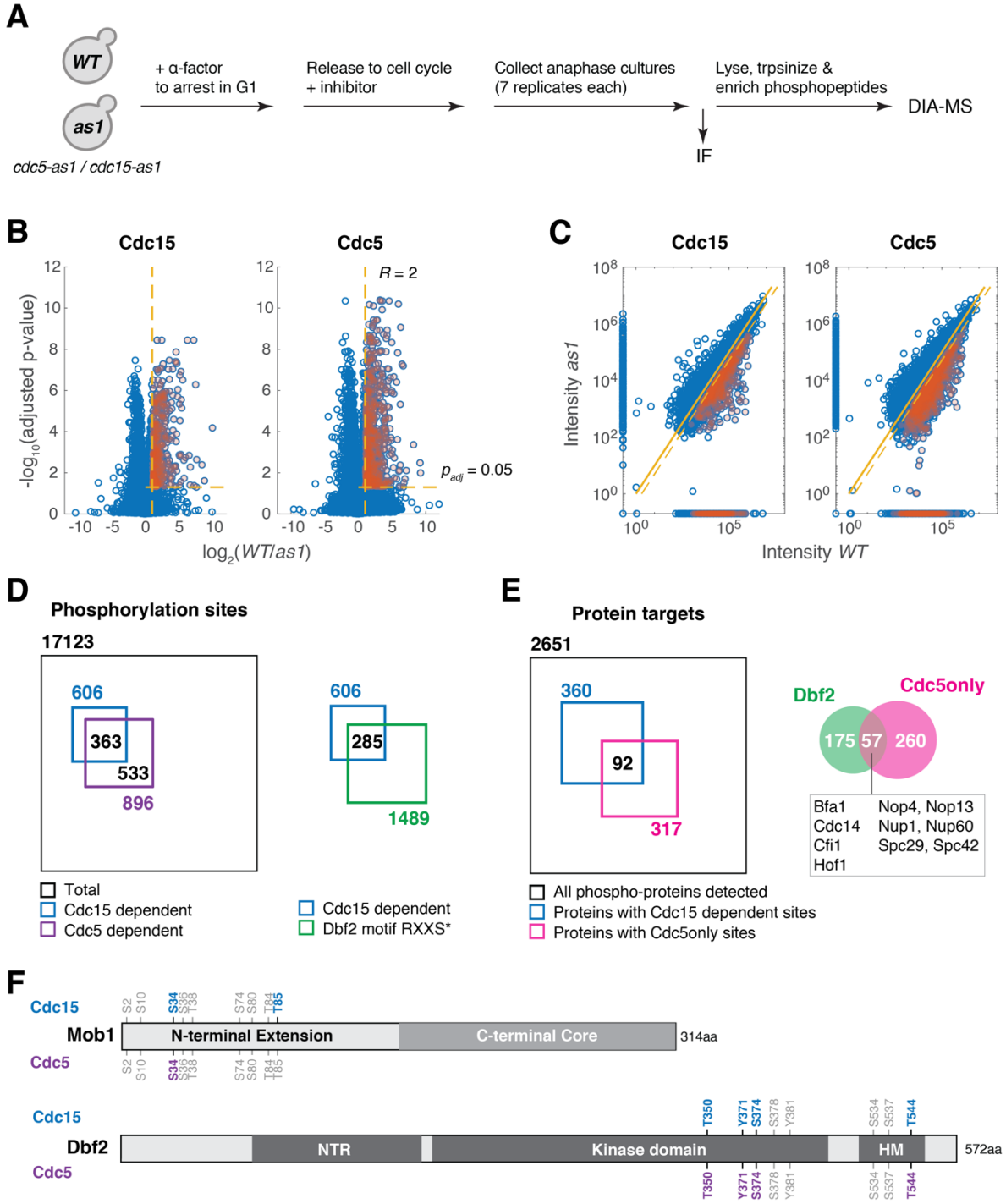

(**A**) Overview of the sample preparation for phosphoproteomics analysis to map *CDC15* (MEN) and *CDC5* dependent phosphorylation in anaphase. Paired wild-type (*WT*, A2587) and *cdc15-as1* (A10991) or paired wild-type and *cdc5-as1* (A40903) cultures were synchronized in G1 with α-factor (5 µg/ml). After 150 minutes cells were released into fresh medium with the

corresponding inhibitors in the absence of pheromone at room temperature. After ~100 minutes cells were harvested to extract proteins and processed for data-independent acquisition mass spectrometry (DIA-MS) analysis with 7 technical replicates for each sample. Immuno-fluorescence (IF) using an anti-tubulin antibody was performed on the collected cells to determine the percentage of cells with anaphase spindle (~70% for wild-type cells and ~95% for cdc5-as1 and cdc15-as1 cells).

(**B**) Volcano plots of $-\log_{10}$ transformed FDR adjusted *P*-value versus $\log_2$(fold change or ratio) of intensities measured for peptides identified in anaphase cells with *WT* or analog-sensitive (*as1*) alleles of *CDC15* or *CDC5*. Yellow dashed lines indicate the cutoff ($R > 2$ and $p_{adj} < 0.05$) used to identify peptides whose phosphorylation depends on the corresponding kinase as marked with red shaded dots.

(**C**) Correlations of peptide intensity in *WT* and *as1* samples for Cdc15 and Cdc5 inhibition in anaphase. Data points on the axis represent peptides that were only detected in one sample but not the other. Red shaded dots denote hits for *CDC15* or *CDC5*-dependent phosphopeptides identified based on the cutoff described in (B) and for peptides that were detected in at least 5 out of 7 replicates in *WT* samples but were missing in *as1* samples (thus no fold change could be calculated).

(**D-E**) Summary of phosphorylation sites (D) and phospho-proteins (E) determined as *CDC15*- or *CDC5*-dependent. Potential Dbf2-Mob1 targets were identified as *CDC15*-dependent and to fit the Dbf2 phosphorylation consensus motif RXXS*, where * denotes the site of phosphorylation. Cdc5-only sites are sites that are *CDC5*-dependent but not *CDC15*-dependent.

(**F**) *CDC15*- and *CDC5*-dependent sites in Mob1 and Dbf2. Light gray sites represent sites that were detected but were not determined as either *CDC15*- or *CDC5*-dependent.

Figure 5–figure supplement 2: Phosphorylation of Cfi1/Net1 modulates Dbf2-Mob1's nucleolar localization.

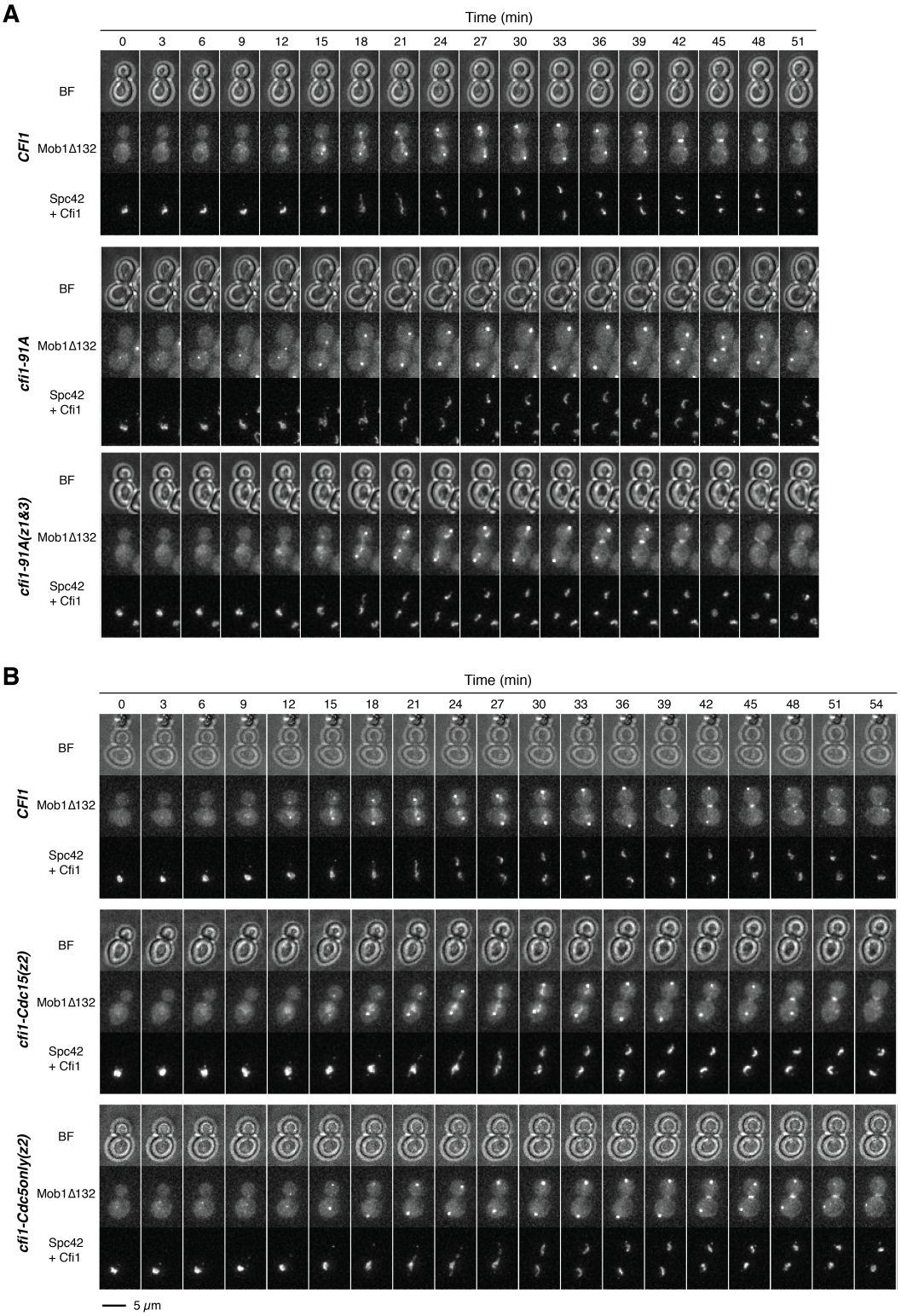

(**A-B**) Representative images of Mob1Δ132 localization in *CFI1/NET1* (A41411), *cfi1-91A* (A41412 and A41413), *cfi1-Cdc15(z2)* (A41593) or *cfi1-Cdc5only(z2)* (A41594) cells.

Figure 5–figure supplement 3: Identification of *CDC5*-dependent phosphorylation sites in metaphase.

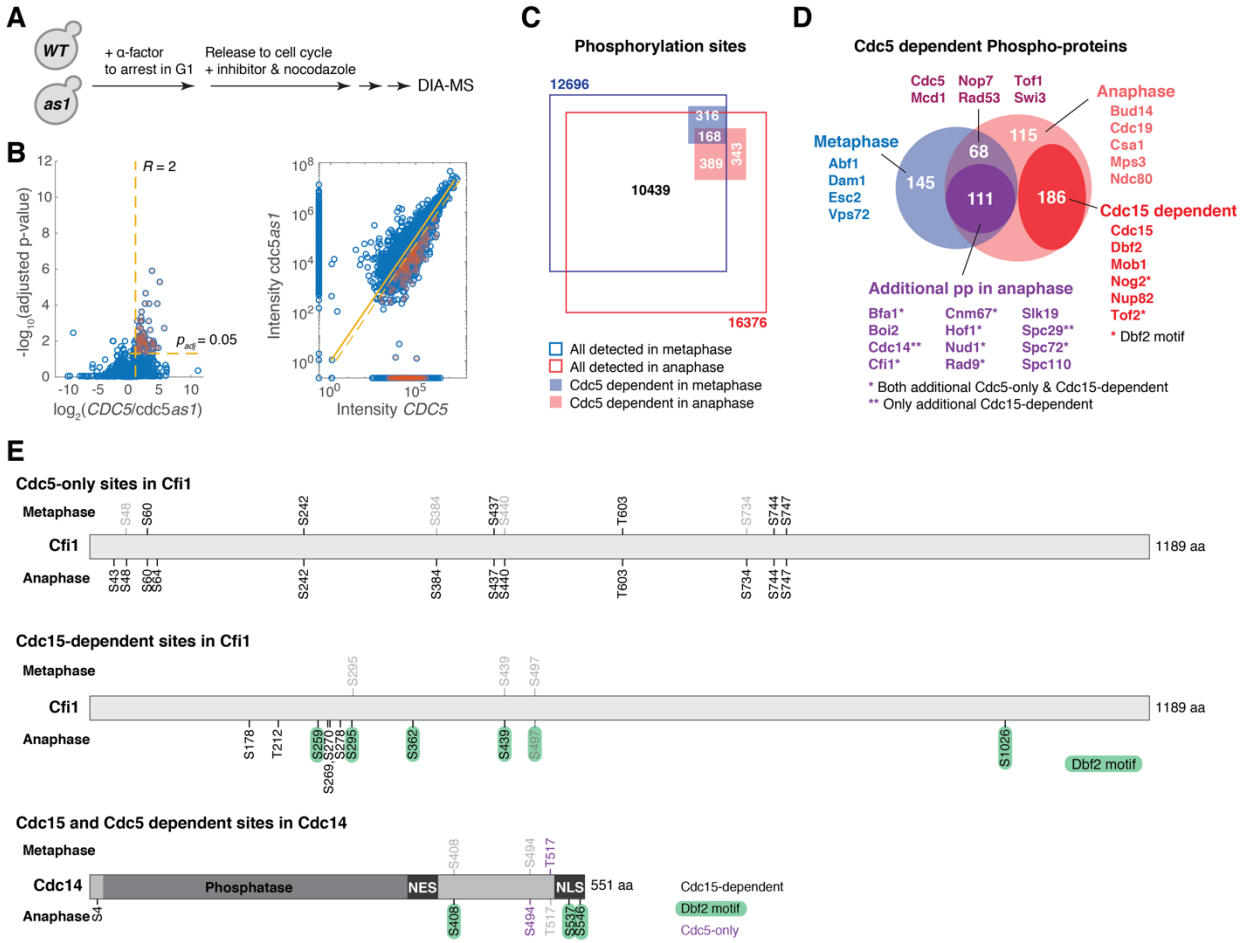

(**A**) Overview of the sample preparation for phosphoproteomics analysis to map *CDC5*-dependent phosphorylation sites in metaphase. Same procedures were followed as in Figure S8A except that following release of cells from the G1 arrest, cells were resuspended in medium containing the inhibitor CMK (5 µM) and nocodazole (15 µg/ml).

(**B**) Volcano plot and correlation of peptide intensities with and without inhibition of Cdc5 (*cdc5-as1* or *WT*) in metaphase. Yellow dashed lines indicate the cutoff ($R > 2$ and $P_{adj} < 0.05$, or detected in at least 4 out of 6 replicates in *WT* sample but missing in *cdc5as1* sample) used to identify peptides whose phosphorylation depends on *CDC5* as marked with red shaded dots.

(**C-D**) Summary and comparison of phosphorylation sites (C) and phospho-proteins (D) detected in metaphase and anaphase.

(**E**) *CDC5*-only and *CDC15*-dependent sites in Cfi1/Net1 and Cdc14 mapped in metaphase and anaphase. Light gray sites in metaphase/anaphase represent phosphorylation sites that were detected but were not determined as *CDC5*-dependent.

Figure 5–figure supplement 4: Cdc5 interacts with Cfi1/Net1 *in vivo*.

A

# of peptides detected		Bait (TurboID tagged)	
		Cdc5	Untagged
Hits	Cfi1	164	6
	Boi2	21	0
	Mps3	20	0
	Csa1	17	0

B

618
Cfi1 IVPQDSDSSSFPkSDLFK
↑
biotin

623
Cfi1 IVPQDSDSSSFPKSDLFkMIEGDDTDLPQWFK
↑
biotin

C

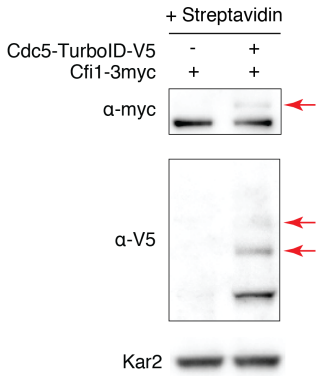

(**A**) Results of TurboID proximity-based biotinylation for Cdc5 (A41385 and A2588).
(**B**) Biotinaylated peptides of Cfi1/Net1 detected in cells with Cdc5-TurboID.
(**C**) Streptavidin gel-shift assay to probe the interaction between Cdc5-TurboID and Cfi1/Net1 (A1638 and A41418). Cells were grown at room temperature in YPED. Lysates were treated with streptavidin and immunoblotted as indicated. Red arrows highlight biotinylated proteins.

Figure 5–figure supplement 5: Dbf2-Mob1 localizes to the nucleolus via Mob1's phosphoserine-threonine binding domain.

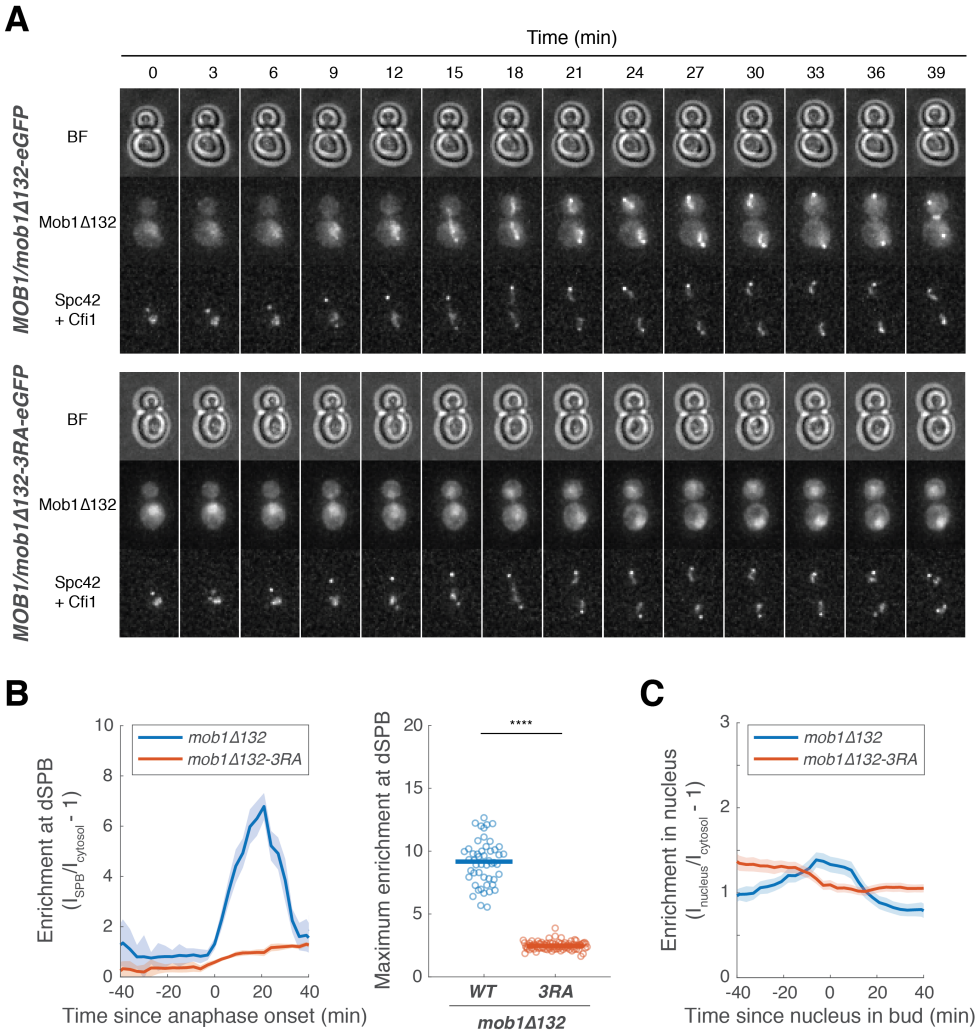

(**A**) Representative images of Mob1Δ132 (A41664) and Mob1Δ132-3RA (A41665) localization.
(**B**) Enrichment of Mob1Δ132 (A41664, n = 50 cells) or Mob1Δ132-3RA (A41665, n = 85 cells) at the dSPB. Cells were grown like in Figure 5G. Solid lines represent the average of single cell traces aligned to anaphase onset. Shaded areas represent 95% confidence intervals. For maximum enrichment, each dot represents a single cell. Solid lines represent the median. ****P < 0.0001 by two-sided Wilcoxon rank sum test.
(**C**) Enrichment of Mob1Δ132 (A41666, n = 54 cells) or Mob1Δ132-3RA (A41667, n = 77 cells) in the nucleus. Cells were grown at 25°C in SC medium + 2% glucose and imaged every 3 minutes for 4 hours. Solid lines represent the average of single cell traces aligned to anaphase onset. Shaded areas represent 95% confidence intervals.

Figure 6–figure supplement 1: Phosphorylation in zone 2 of Cfi1/Net1 regulates Cdc14 release from the nucleolus.

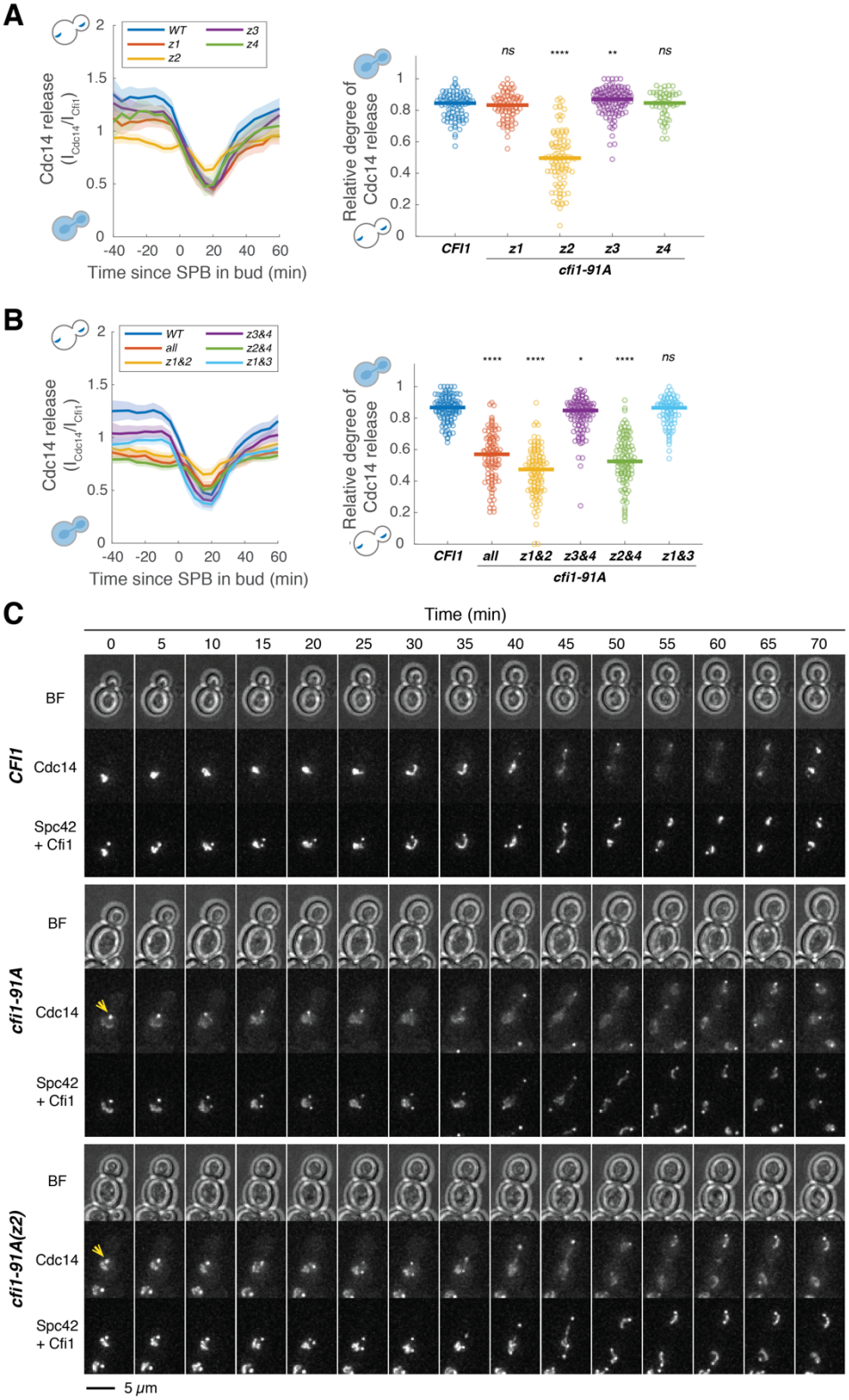

(**A-B**) Kinetics of Cdc14 release from the nucleolus in cells harboring wild-type *CFI1/NET1* (A41387, n = 103 cells for A, n = 130 cells for B) or different *CFI1/NET1* phospho-null mutants (A41398, A41399, A41400, A41401, A41404, A41405, A41397, A41402 and A41403; n = 95, 103, 146, 59, 102, 113, 128, 114 and 102 cells respectively). Cells were grown at 25°C in SC medium + 2% glucose and imaged every 5 minutes for 5 hours. Release of Cdc14 from the nucleolus was quantified as the ratio of fluorescence intensity of Cdc14-eGFP to Cfi1/Net1-mScarlet in the nucleolus (I_{Cdc14}/I_{Cfi1}). Relative degree of Cdc14 release from the nucleolus was calculated as the normalized minimal Cdc14 level in the nucleolus: $(I_{Cdc14}(t_{min})/I_{Cfi1}(t_{min}))/(I_{Cdc14}(t_{-20})/I_{Cfi1}(t_{-20}))$ where t_{min} represents the frame with minimal Cdc14 levels in the nucleolus and t_{-20} represent 20 min before movement of the SPB into bud. Each dot represents a single cell and the solid lines represent the median. ****$P < 0.0001$; **$P < 0.01$; *$P < 0.05$ by two-sided Wilcoxon rank sum test.
(**C**) Representative images showing Cdc14 nucleolar release kinetics for cells harboring wild-type *CFI1/NET1* (A41387) or *CFI1/NET1* phospho-mutants with all 91 sites (A41404) or only sites in zone 2 (A41399) mutated to alanine. Yellow arrows highlight localization of Cdc14 at dSPB prior to anaphase.

Figure 6–figure supplement 2: The MEN and *CDC5* promote release of Cdc14 from the nucleolus by phosphorylating Cfi1/Net1.

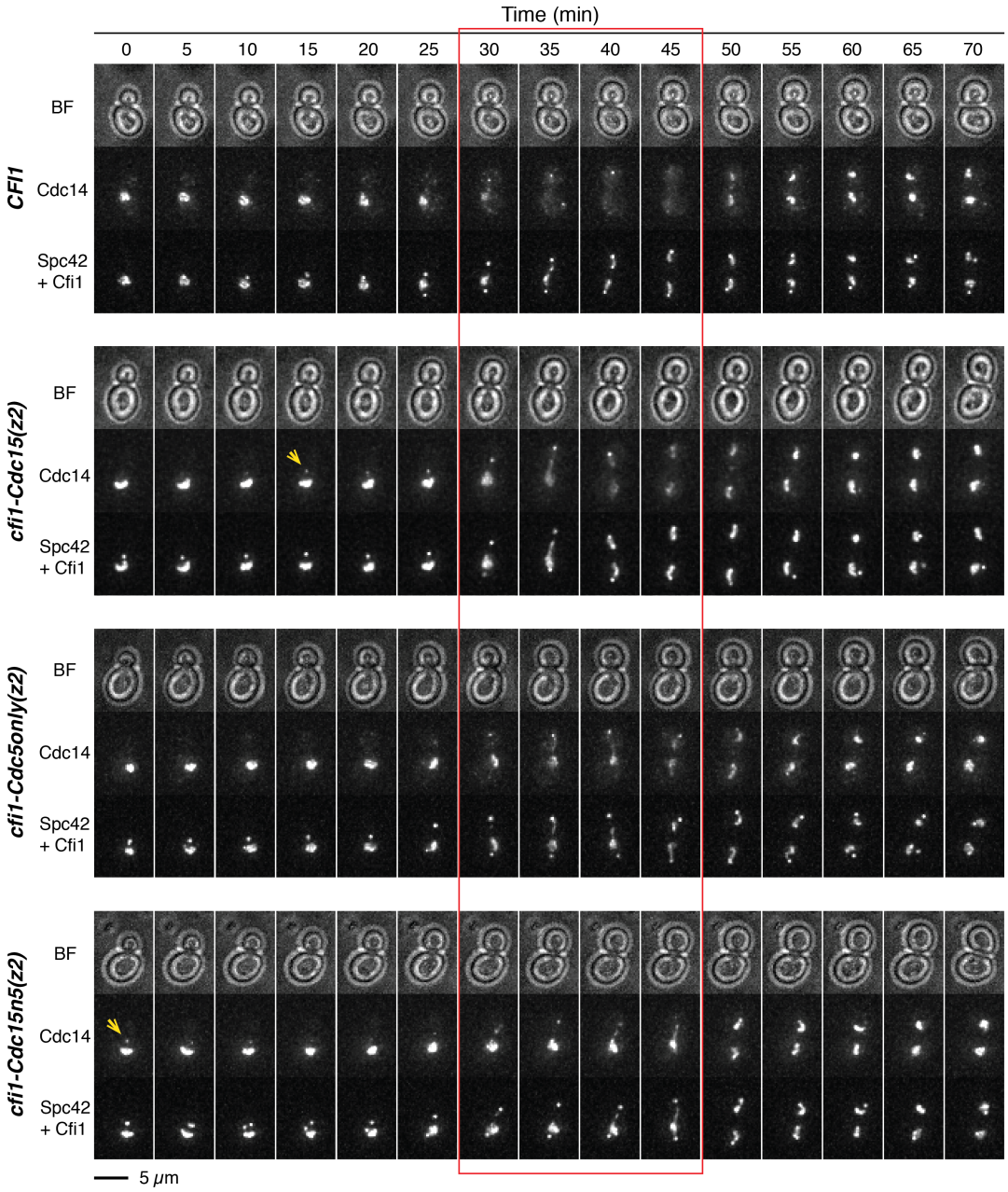

Representative images showing Cdc14 nucleolar release kinetics for cells harboring wild-type *CFI1/NET1* (A41387) or *CFI1/NET1* phospho-mutants for Cdc15 sites (A41587), Cdc5 sites (A441588), and Cdc15&Cdc5 sites (A41589). Red box highlights anaphase when Cdc14 is fully released in WT cells. Yellow arrows highlight localization of Cdc14 at dSPB prior to anaphase.

Figure 6–figure supplement 3: Cfi1/Net1 phospho-mutants delay mitotic exit and nucleolar segregation.

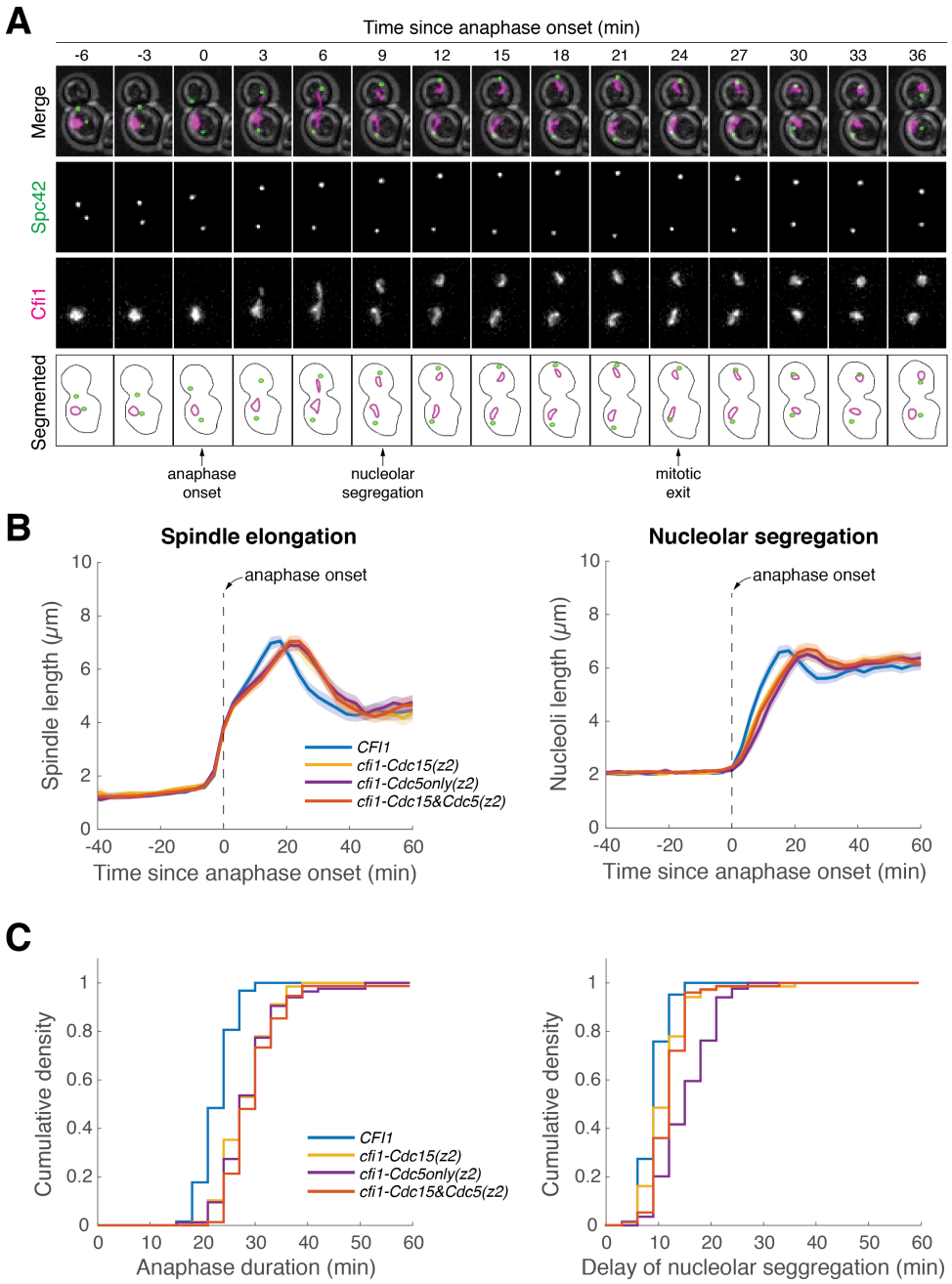

(**A**) Tracking anaphase progression and nucleolar segregation using Spc42-eGFP and Cfi1/Net1-mScarlet-I as markers, respectively. A41436 cells were grown at 25°C in SC medium + 2% glucose and imaged every 3 minutes for 4 hours.

(**B**) Quantification of spindle elongation (spindle length was estimated by measuring the distance between the two SPBs) and nucleolar segregation (nucleoli length was estimated by measuring the length of the major axis of the nucleolar mass) for *CFI1/NET1* mutants using the SPB marker Spc42-eGFP and the nucleolar marker Cfi1/Net1-mScarlet-I (A41436, A41590, A41591 and

A41592; same dataset as in Figure 6C). Single cell traces were aligned to anaphase onset (spindle length > 3 μm) and averaged. Solid lines represent the average. Shaded areas represent 95% confidence intervals.

(**C**) Cumulative density of anaphase duration (left) and delay of nucleolar segregation (right) for cells in (B). Anaphase duration was defined as the time from anaphase onset (spindle length > 3 μm) to mitotic exit (spindle breakdown, determined as relaxation of the distance between SPBs). Delay of nucleolar segregation was defined as the time of nucleolar segregation (clear separation of two nucleolar masses) relative to anaphase onset.

Figure 6–figure supplement 4: Phosphorylation of the Cdc14 NLS does not play a major role in promoting mitotic exit.

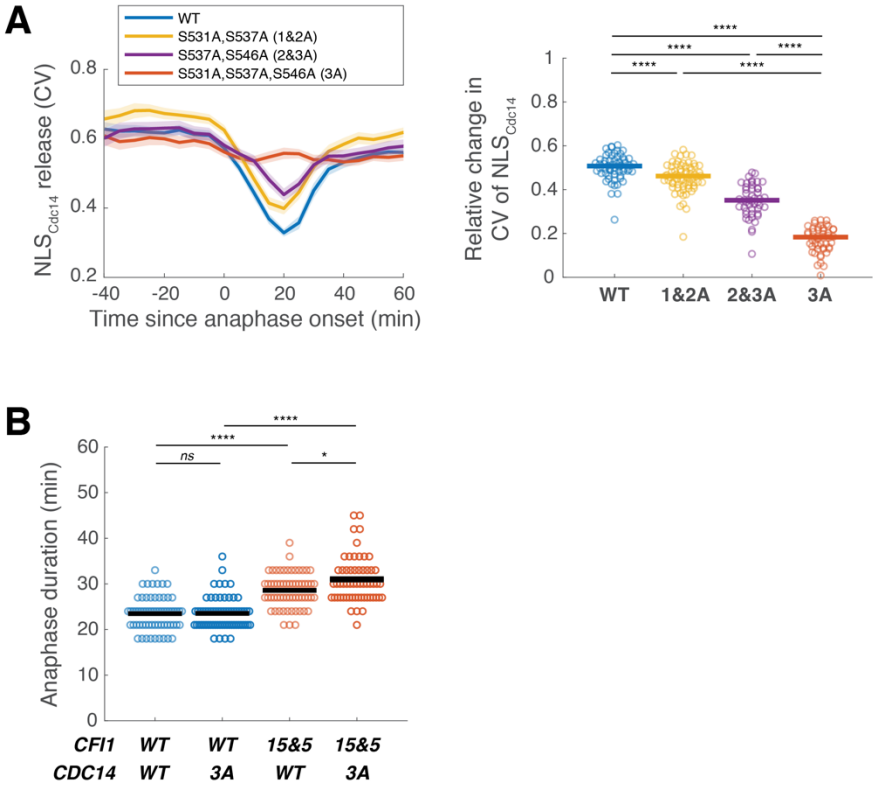

(**A**) Profiles (left) and relative degrees (right) of nuclear release of wild-type (A41584, n = 69 cells) and mutant NLS_{Cdc14} reporters where all three potential Dbf2-Mob1 (MEN) target sites (A41585, n = 59 cells) or only two out of three sites (A41586 and A41623, n = 77 and 55 cells) were mutated to alanine. Cells were grown at 25°C in SC medium + 2% glucose and imaged every 5 minutes for 4 hours. Solid lines (right) represent the median.
(**B**) Distribution of anaphase duration for *CDC14* phospho-mutants in combination with *CFI1* or *cfi1-Cdc15&5* measured using the SPB marker Spc42-eGFP (A41436, A41707, A41592 and A41708; n = 64, 65, 61 and 58 cells, respectively). Cells were grown at 25°C in SC medium + 2% glucose and imaged every 3 minutes for 4 hours. Anaphase duration was defined as the time from anaphase onset (spindle length > 3 µm) to mitotic exit (spindle breakdown). Solid lines represent the mean. ****$P < 0.0001$; *$P < 0.05$; *ns*, not significant ($P > 0.05$) by two-sided Wilcoxon rank sum test.

Figure 6–figure supplement 5: Mutating both CDK and Cdc5 sites in Cfi1/Net1 results in severe delays in exit from mitosis and nucleolar segregation.

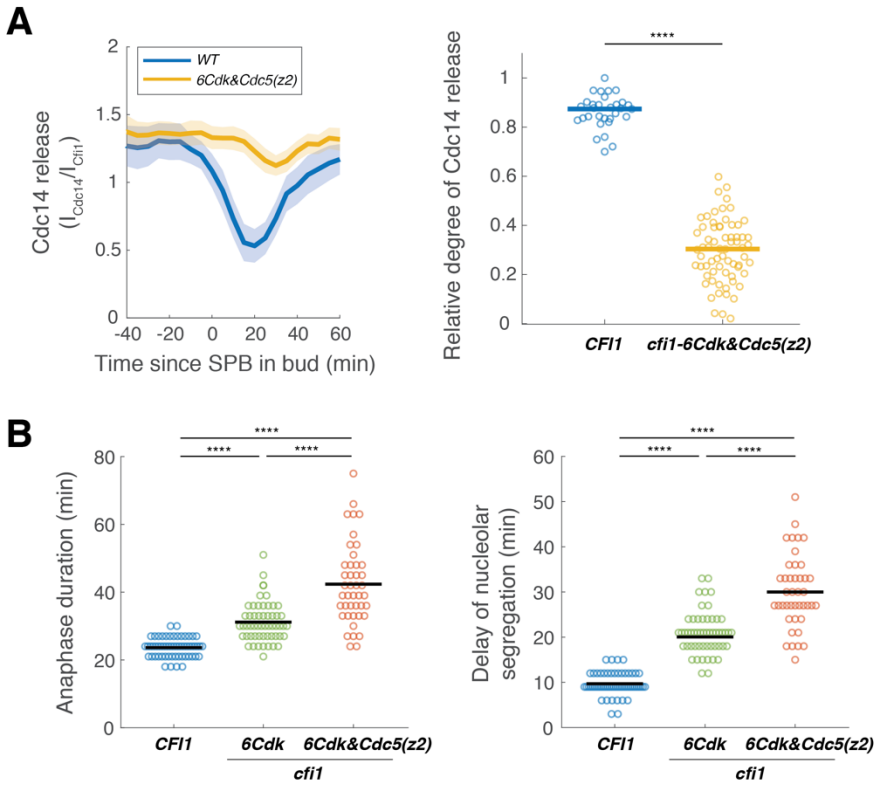

(**A**) Cdc14 nucleolar release kinetics in cells harboring wild-type *CFI1/NET1* (A41387, $n = 39$ cells) or *CFI1/NET1* phospho-mutants for CDK sites combined with Cdc5 sites in zone 2 (A41691, $n = 79$ cells). Cells were grown at 25°C in SC medium + 2% glucose and imaged every 5 minutes for 5 hours. Single cell traces were aligned to the frame where the dSPB entered the bud and averaged. Solid lines represent the average. Shaded areas represent 95% confidence intervals. Each dot represents a single cell. Solid lines represent the median. ****$P < 0.0001$ by two-sided Wilcoxon rank sum test.

(**B**) Distribution of anaphase duration and relative delay of nucleolar segregation for different *CFI1/NET1* phospho-mutants (A41436, A41692 and A41694; $n = 58, 55, 44$ cells respectively) measured using the SPB marker Spc42-eGFP and the nucleolar marker Cfi1/Net1-mScarlet-I. Cells were grown at 25°C in SC medium + 2% glucose and imaged every 3 minutes for 4 hours. Each dot represents a single cell. Solid lines represent the median. ****$P < 0.0001$ by two-sided Wilcoxon rank sum test.

Supplementary tables and datasets

Table S1. Yeast strains used in this study.

Table S2. Plasmids used in this study.

Table S3. Summary of TurboID labeling experiments.

Table S4. Phosphorylation of Cfi1/Net1.

Dataset S1. Summary of phospho-proteomics results for inhibiting Cdc15 and Cdc5 in anaphase cells and Cdc5 in metaphase cells.

Dataset S2. Complete list of phosphopeptides for each phosphorylation site detected in the DIA-MS experiments.